DP-1526

SAVANNAH RIVER LABORATORY ENVIRONMENTAL TRANSPORT AND EFFECTS RESEARCH

ANNUAL REPORT — 1978

E. I. du Pont de Nemours & Co. (Inc.)
Savannah River Laboratory
Aiken, South Carolina 29801

PREPARED FOR THE U. S. DEPARTMENT OF ENERGY UNDER CONTRACT DE-AC09-76SR00001

Printed in the United States of America

Available from

National Technical Information Service
U. S. Department of Commerce
5285 Port Royal Road
Springfield, Virginia 22161

Price: Printed Copy A11; Microfiche A01

DP-1526

Distribution Category UC-11

SAVANNAH RIVER LABORATORY ENVIRONMENTAL TRANSPORT AND EFFECTS RESEARCH

ANNUAL REPORT — 1978

T. V. Crawford, Compiler

Approved by:

T. V. Crawford, Research Manager
Environmental Transport Division
Savannah River Laboratory

Publication Date: November 1979

E. I. du Pont de Nemours & Co. (Inc.)
Savannah River Laboratory
Aiken, South Carolina 29801

PREPARED FOR THE U. S. DEPARTMENT OF ENERGY UNDER CONTRACT DE-AC09-76SR00001

CONTRIBUTING AUTHORS

SAVANNAH RIVER LABORATORY

Environmental Transport Division

C. E. Bailey
R. E. Cooper
J. C. Corey
A. H. Dexter
C. B. Fliermans
S. J. Fritz
D. W. Hayes
J. H. Horton
D. L. Kiser
C. W. Krapp
C. E. Murphy, Jr.
M. M. Pendergast
D. W. Pepper
R. W. Root, Jr.
J. F. Schubert
D. E. Stephenson
J. E. Suich
J. R. Watts
A. H. Weber
E. W. Wilde

Environmental Effects Division

T. J. Anderson
W. W. Bowman
S. M. Sanders

Computer Applications Division

M. R. Buckner

Nuclear Physics Division

F. Beranek

Health Protection Department

N. O. Johnson

Savannah River Ecology Laboratory
University of Georgia

D. C. Adriano
J. C. Luvall
J. E. Pinder

Wake Forest University
Winston-Salem, North Carolina

G. W. Esch
R. W. Gordon
T. C. Hazen
M. L. Rotec

University of Tennessee
Knoxville, Tennessee

A. J. Baker***

Renssalaer Polytechnic Inst.
Troy, New York

D. H. Pope**
D. L. Tison*

Skidaway Inst. of Oceanography
Savannah, Georgia
(Under Contract EY-77-5-09-1025
with the U.S. Department of Energy)

J. O. Blanton

Clemson University
Clemson, South Carolina

T. R. Fawcett*

University of South Carolina
Columbia, South Carolina

D. C. Brown*

Terra Tek, Inc.
Salt Lake City, Utah

H. R. Pratt

Georgia Institute of Technology
Atlanta, Georgia

S. Kaplan*

* Graduate Research Participant.

**National Environmental Research Park collaborator.

***Consultant to SRL

726179

ABSTRACT

Research in the environmental sciences by the Savannah River Laboratory during 1978 is described in 43 articles. These articles are in the fields of terrestrial ecology, geologic studies, aquatic transport, aquatic ecology, atmospheric transport, emergency response, computer methods development, ocean program, and fuel cycle program.

FOREWORD

This report is the fifth in a series of annual reports prepared by the Savannah River Laboratory (SRL) on environmental transport and effects research. This report covers research performed during calendar year 1978. The general objective of the environmental sciences research at SRL, particularly within the Environmental Transport Division, is to develop (or adapt), test, modify, and apply models for calculating transport, dispersion, and effects of various materials moving through environmental systems such as the atmosphere, streams, ponds, rivers, estuaries, ocean, ground water, soil, and plants. That part of the research with specific applicability to the operation of the Savannah River Plant (SRP) is funded by the U.S. Department of Energy (DOE) divisions supporting that operation. That part of the effort with general applicability to the energy industry of the southeastern United States is funded by the Office of Health and Environmental Research (OHER). Studies related to the geologic storage of radioactive waste were funded by the Department of Energy through the Office of Waste Isolation of Union Carbide Corporation.

The OHER-funded environmental science research programs are centered in the Environmental Transport Divison (ETD), but with heavy collaboration with the Environmental Effects Division (EED), and with support from other SRL divisions. Many of these programs involve direct collaboration with other groups on and off the Savannah River site, through coordination by the Savannah River Operations Office of DOE. For instance, the SRL research on transuranics in terrestrial ecosystems was in collaboration with a separately funded program at the Savannah River Ecology Laboratory (operated by the University of Georgia), the Environmental Monitoring Group of the Health Protection Department of SRP, and the Savannah River Forest Stations (U.S. Forest Service) on the Savannah River site. Marine science programs are in collaboration with the Skidaway Institute of Oceanography, with the National Oceanic and Atmospheric Administration (NOAA) marine laboratories at Beaufort, North Carolina, and with other DOE-funded oceanographic groups in the southeastern United States. Measurements of environmental ^{85}Kr are being interpreted in collaboration with the Air Resources Laboratories of NOAA at Silver Spring, MD.

Other environmental efforts performed by Du Pont personnel at the site, such as the large effort of the SRP Health Protection Department in environmental monitoring and the portion of the National Uranium Resource Evaluation (NURE) program being conducted by SRL, are reported elsewhere.

CONTENTS

Well Data Computer File - C. W. Krapp and J. E. Suich 219

A computer file is currently being developed to provide a centralized access to pertinent data for SRP wells.

Earthquake Damage to Underground Facilities - D. E. Stephenson and H. R. Pratt 223

A recently completed literature study shows that earthquakes of equal intensity damage underground facilities significantly less than surface facilities.

Comparison of Earthquake Parameters Derived from Empirical Relationships - D. E. Stephenson 227

A review was made of southeastern seismicity to illustrate the effects of attenuating, recurrence, and intensity-acceleration relationships on seismic design.

ATMOSPHERIC STUDIES

THE EFFECT OF SPATIAL VARIABILITY OF METEOROLOGICAL DATA ON ANNUAL AVERAGE AIR CONCENTRATIONS

M. M. Pendergast

The significance of spatial variability of meteorological data was evaluated using calculated and observed annual average air concentrations. The joint frequency distribution of wind velocity and stability measured at eight locations was used in a simple diffusion model recommended by the Nuclear Regulatory Commission to predict annual average air concentrations at SRP. The model caused an overprediction of about a factor of three with a variability of about 50% among the eight locations examined. The linear correlation coefficients between calculated and observed concentration range between 0.73 and 0.96 depending upon tower location. The magnitude of the correlation coefficient showed no relationship between distance from the source release point and the amount of meteorological data used to represent the annual frequency distribution of wind and stability.

METHOD

Meteorologists are frequently asked to perform annual average diffusion calculations for a proposed site based upon data from the nearest available source. The meteorologist does not know how well these data represent the proposed site. This uncertainty reduces the reliability of his calculations.

The variability of meteorological data is evaluated using annual average air concentrations of ^{85}Kr calculated from data at the 62-m level of 8 meteorological towers at SRP. These calculated air concentrations are compared with observed concentrations of ^{85}Kr measured downwind from a source near the center of the plant (Figure 1).

The source of ^{85}Kr is between towers labeled F and H. The procedure was to 1) assume wind data at each tower applies at the ^{85}Kr source location, 2) calculate relative concentration using the computer code developed by Sagendorf and Goll (1977) for each of 13 ^{85}Kr sampling sites,* 3) compare calculated relative concentrations at 13 sampling sites with observed relative concentrations, and 4) repeat using data from other towers.

* Input meteorological data were similar for all calculations: wind speed and direction at 62-m level, and stability determined from measured values of standard deviation of wind azimuth according to USAEC (1972).

RESULTS

Table 1 lists the calculated relative ^{85}Kr concentrations for 1976 at each of the 13 sites.

The estimates for each site are generally within 20% of one another; however, variations of as much as a factor of two occur. Calculated values consistently overpredict relative concentrations when compared with the observed relative concentrations listed in the far right column.

Table 2 summarizes the data to show how well the various estimates agree with the observed values. Neither the distance from the ^{85}Kr source at which concentrations are measured, nor the amount of data used affects how well the calculated and observed concentrations agree with one another.

CONCLUSIONS

The effects of spatial variability of meteorological data on annual average air concentrations were examined for distances from the source ranging from 2 to 21 km. Annual average relative air concentrations varied by about 50% for the stations examined. This variation appeared to be random with respect to distance from the source release point. This study also showed that annual average concentrations obtained with a simple wind rose model, although overpredicting by a factor of three, are not particularly sensitive to the amount of meteorological data used to represent the frequency distribution of wind and stability (within the range of 35 to 70% of the possible 15-min average data).

REFERENCES

Safety Guide Number 23: **Safety Guides for Water Cooled Nuclear Power Plants.** USAEC, Division of Reactor Standards. Onsite Meteorological Programs (1972).

J. F. Sagendorf and J. T. Goll. **XOQDOQ Program for the Meteorological Evaluation of Routine Effluent Releases at Nuclear Power Stations (DRAFT).** NUREG-0324, Nuclear Regulatory Commission (1977).

TABLE 1

A Comparison of Calculated and Observed Relative Concentrations at 13 ^{85}Kr Monitoring Sites Using Meteorological Data Collected at Eight Source Locations Near SRP*

^{85}Kr Site No.	$(X/Q)_{CALC}$ for Eight Towers								$(X/Q)_{OBS}$
	T	D	P	A	K	C	F	H	
2	10.0	11.0	9.1	6.6	10.0	7.8	9.5	6.8	1.3
3	11.0	22.0	15.0	8.4	41.0	13.0	17.0	12.0	4.6
4	9.9	33.0	37.0	13.0	25.0	27.0	49.0	20.0	6.2
5	4.7	9.6	6.7	6.0	5.5	6.1	5.1	8.1	2.5
6	8.4	13.0	6.3	9.5	7.5	8.9	9.6	16.0	3.6
7	15.0	25.0	21.0	19.0	19.0	22.0	23.0	33.0	8.0
8	31.0	50.0	41.0	36.0	37.0	45.0	45.0	68.0	20.0
9	15.0	24.0	23.0	20.0	23.0	21.0	25.0	29.0	29.0
10	33.0	38.0	48.0	45.0	39.0	36.0	44.0	57.0	29.0
11	14.0	16.0	21.0	20.0	18.0	16.0	19.0	25.0	9.6
12	11.0	21.0	21.0	15.0	16.0	20.0	22.0	17.0	4.7
13	8.7	9.9	13.0	12.0	11.0	9.9	12.0	16.0	4.3
14	45.0	49.0	44.0	42.0	45.0	37.0	41.0	37.0	18.0

* All X/Q values are in units of 1×10^{-10} sec/m^3.

TABLE 2

Summary of the Effect of Spatial Variability of Meteorological Data on Annual Average Air Concentrations

Data Source	T	D	P	A	K	C	F	H
Average of ratio $\frac{(X/Q)_{CALC}}{(X/Q)_{OBS}}$	2.3	3.6	3.2	2.5	3.3	2.8	3.4	3.3
Linear correlation coefficient between $(X/Q)_{CALC}$ and $(X/Q)_{OBS}$	0.86	0.80	0.87	0.96	0.73	0.85	0.75	0.91
Percentage of possible 15-min average wind data	76	51	70	35	62	67	57	65
Distance from ^{85}Kr release point, km	21	12	10	10	9	4	2	2

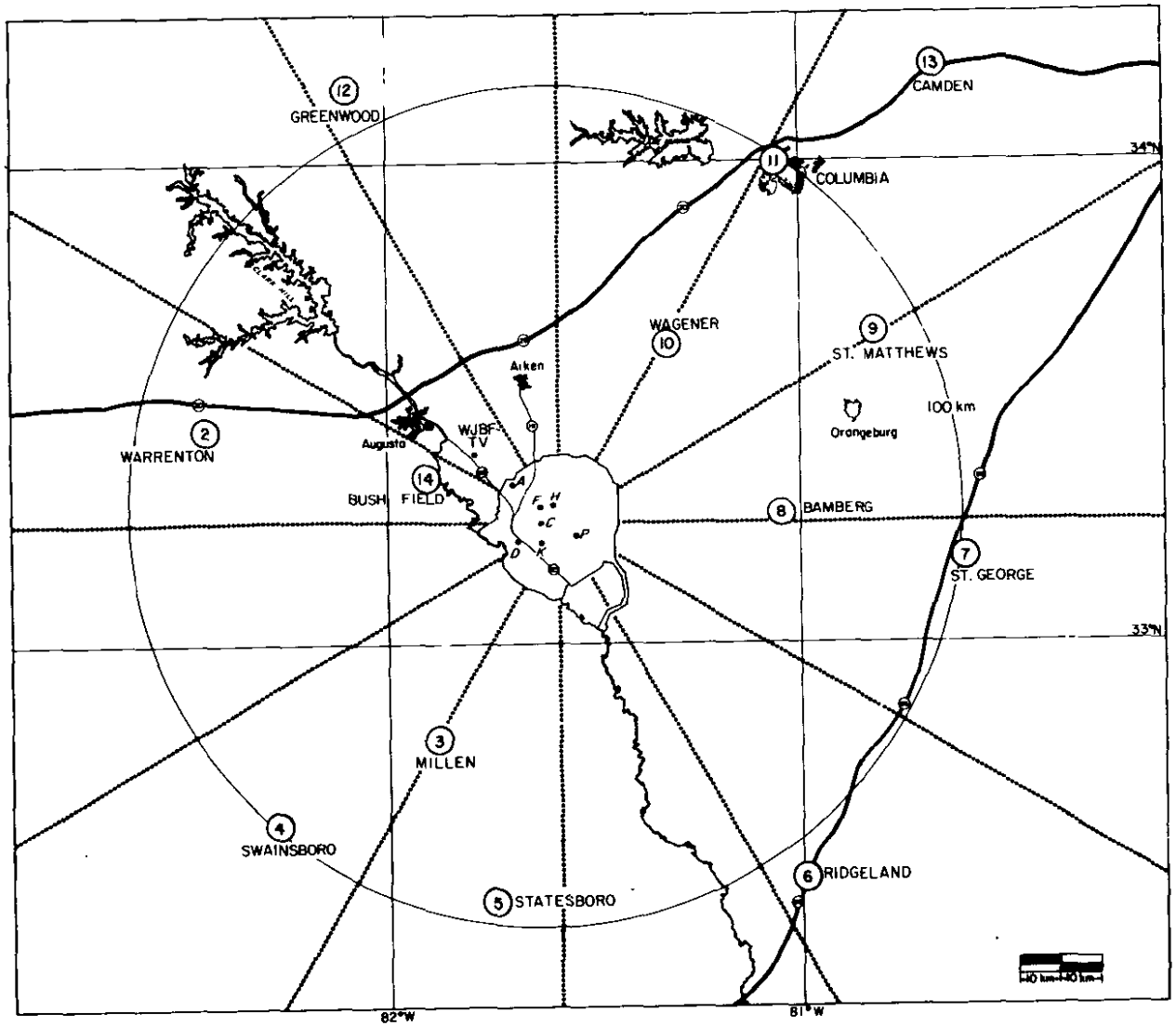

FIGURE 1. Location of ^{85}Kr Observation Sites 2-14 and Eight Meteorological Towers (T, A, C, D, F, H, K, P)

SOURCE TERM ESTIMATIONS OF THE RUTHENIUM RELEASE ON NOVEMBER 6, 1978

M. M. Pendergast and A. H. Weber

On November 6, 1978, an undetermined amount of ^{106}Ru was released in a 2-hour period to the atmosphere from F Area. The amount released could not be determined by measurement within the process or by monitoring within the stack. Using measurements of meteorology and ^{106}Ru in the environment and different atmospheric dispersion models, the amount released was determined to range between 24 and 52 Ci, with an average of about 32 Ci.

PROCEDURE

SRP air monitoring data, from stations located at and beyond the plant boundary (Figure 1), provided measurements of ruthenium in air. Four separate estimates of the release rate were made using a Gaussian plume model. Two estimates were based upon ground level air concentrations at plume centerline at distances corresponding to the two arcs of air monitoring samplers. Two other estimates were based upon the crosswind integrated concentrations at the two arcs.

A deposition velocity of 0.028 m/sec was used to account for the depletion of material (Crawford, 1970). The effects of deposition were calculated through use of a suspension ratio. The suspension ratio is the fraction of the original source remaining suspended in the air at a particular distance downwind (Van der Hoven, 1968).

The Gaussian plume model for an elevated continuous point source adjusted for deposition through use of the suspension ratio gives the true release rate Q_o as

$$Q_o = \bar{\chi}\, \pi\sigma_y\sigma_z\, \bar{u}\, \exp\left(\frac{1}{2}\frac{H^2}{\sigma_z^2}\right)\Big/(Q'/Q_o) \qquad (1)$$

where $\bar{\chi}$ is the average ground level concentration at the plume centerline,

σ_y and σ_z are the horizontal and vertical diffusion coefficients,

Q'/Q_o is the suspension ratio,

H is the height of release, and

$\bar{u}$ is the mean wind speed.

The magnitudes of σ_y and σ_z were evaluated using the BNL method (Smith, 1968).

Because the path of the plume could not be predicted exactly, the plume is assumed to have passed directly over East Talatha (at distance x = 17 km, and air concentration $\overline{X}$ = 11.1 pCi/m^3 for a 24-hr average) and Langley (x = 33 km, $\overline{X}$ = 1.8 pCi/m^3 for a 24-hr average). Using the meteorological data averaged over the two-hour release period and suspension ratios of 0.69 and 0.62, respectively, the release estimates of $\int Q_o dt$ are 52 Ci based on data obtained 17 km from the release point and 25 Ci based on data obtained 33 km from the release point.

The crosswind integrated method of estimation has the advantage of smoothing the crosswind distributions which would otherwise yield fluctuating estimates of the amount released. The true release rate, Q_o, is given by

$$Q_o = \frac{\chi_{CWI}\sigma_z\bar{u}}{\sqrt{2/\pi}} \exp\left(H^2/2\sigma_z^2\right)/(Q'/Q_o) \qquad (2)$$

where the crosswind integrated concentration, χ_{CWI}, was estimated using air concentration data in Figure 1 along arcs assumed to be centered at distances of 12 and 31 km from the release point, respectively. The σ values and suspension ratios of 0.60 and 0.44 for the inner and outer arcs (Willis, 1978), respectively, yield values of $\int Q_o dt$ equal to 29 and 24 Ci. These values are in reasonable agreement with those of 52 Ci and 25 Ci using the plume centerline concentrations.

INDEPENDENT EVALUATION OF SOURCE TERM ESTIMATES

Vegetation Samples

Grass samples were collected and analyzed for ^{106}Ru out to about 35 km in a NE direction toward Langley (Figure 2). Although these grass samples were collected primarily to indicate the path of the release, they can be used to evaluate the true release rate estimates. To make these evaluations, the deposition per unit area, D, at plume centerline was calculated as a function of distance using

$$D = Ft = \chi v_d t \qquad (3)$$

where t = release time (two hours),

F = the flux of ruthenium to the ground assumed to be equal to χv_d,

χ = the ground level centerline air concentration,

v_d = the ruthenium deposition velocity (0.028 m/sec).

In order to compare deposition, D, with grass concentrations, the average areal density of grass at SRP of 8.0 kg/m^2 was assumed to apply (U.S.F.S).

The curves in Figure 2 show calculations of centerline concentration of Ru in grass, as a function of distance. Good agreement was found between observed and calculated values considering the nonuniform sampling and the use of a constant conversion factor for the areal density of grass. It is of particular interest that the calculated distance to the peak concentration agrees with observations within the accuracy of the Gaussian plume model. The decrease in concentration with distance is consistent with the deposition velocity of 0.028 m/sec used in these calculations.

Ground Survey Data

Due to the sampling pattern used to make the F-Area ground survey, only sector average values were compared with the models (Figure 3). The Thyac G-M counter readings were expressed in units of pCi/m^2. The calculations using the peak centerline method were based upon a source of 38 Ci and a deposition velocity of 0.028 m/sec. The plume was assumed to be uniformly distributed over a 90° sector.

The calculation of deposition for the crosswind integrated method was based on calculated suspension ratios. All material lost from the plume was spread uniformly over the area of the arc.

The results (Table 1) show good agreement between the two methods, and results agree fairly well with the observations although the calculated values are uniformly higher than the measured values. This agreement is viewed as additional independent validation of the estimates of source terms and deposition velocity used to make the assessment.

REFERENCES

T. V. Crawford. **Long-Range Travel and Diffusion of the Buggy Cloud.** Report UCRL-50806, Lawrence Livermore Laboratory (1970).

I. Van der Hoven. "Deposition of Particles and Gases." **Meteorology and Atomic Energy,** 202-208 (1968).

M. E. Smith (Ed.). "Recommended Guide for the Prediction of the Dispersion of Airborne Effluents." **Am. Soc. of Mech. Engineers 85,** (1968).

G. E. Willis and J. W. Deardorff. "A Laboratory Study of Dispersion from an Elevated Source Within a Modeled Convective Planetary Boundary Layer." **Atmos. Environ. 12,** 1305-1311 (1978).

Southern Forestry Smoke Management Guidebook. USDA Report SE-10 Southeastern Forest Experiment Station. U.S. Forest Service, Asheville, NC (1976).

TABLE 1

Comparisons of Calculated Sector-Averaged Deposition of ^{106}Ru with Ground Survey Data

Downwind Distance	Calculated Deposition Peak Centerline Method, pCi/m^2	Calculated Deposition Crosswind Integrated Method, pCi/m^2	Observed Deposition, pCi/m^2
0.85 km	1.9×10^6	0.8×10^6	0.8×10^6
1.17	1.4	1.50	0.3
1.49	1.0	0.9	0.2
1.71	0.8	0.4	0.08

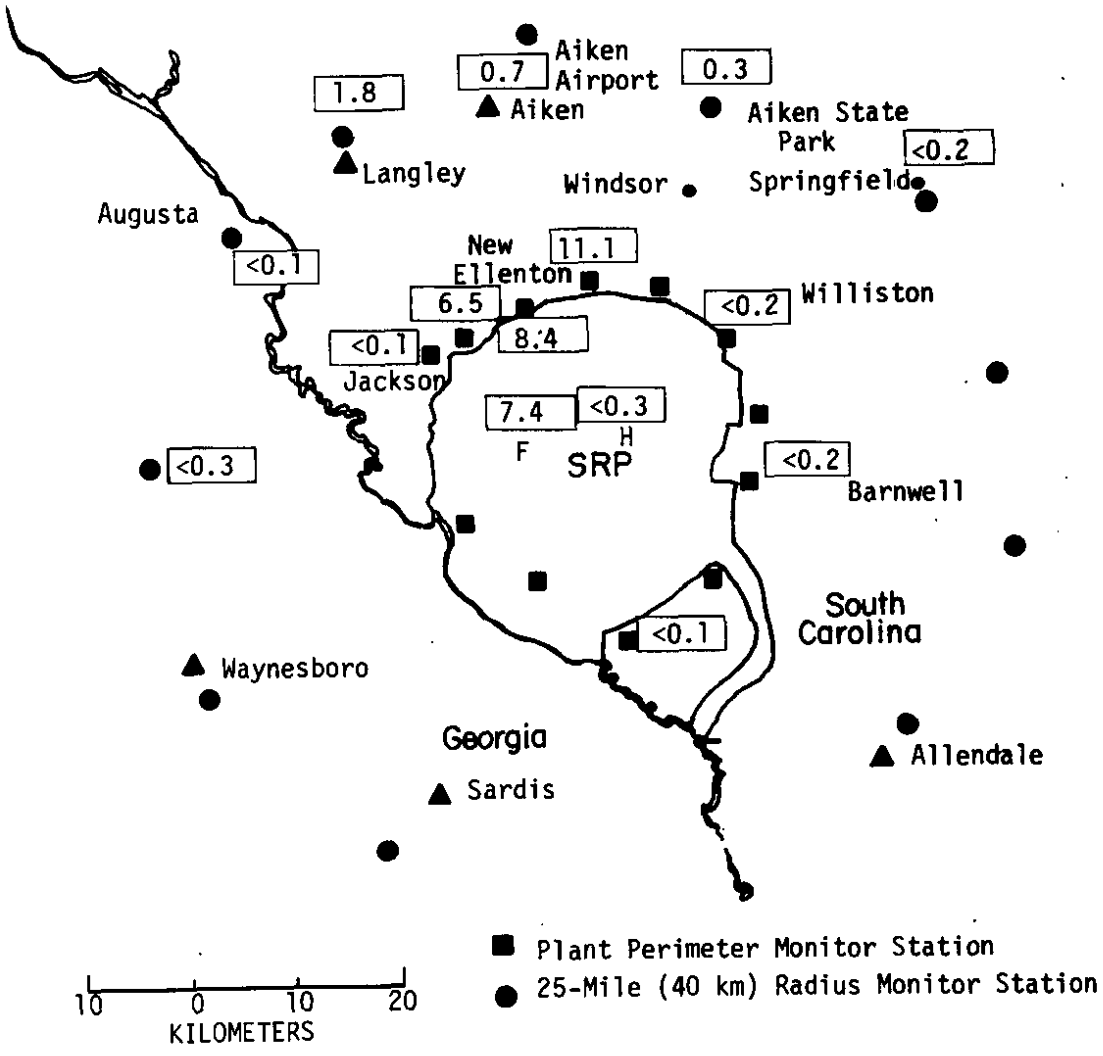

FIGURE 1. Map Showing 24-hr Concentrations of Ruthenium at Various Locations

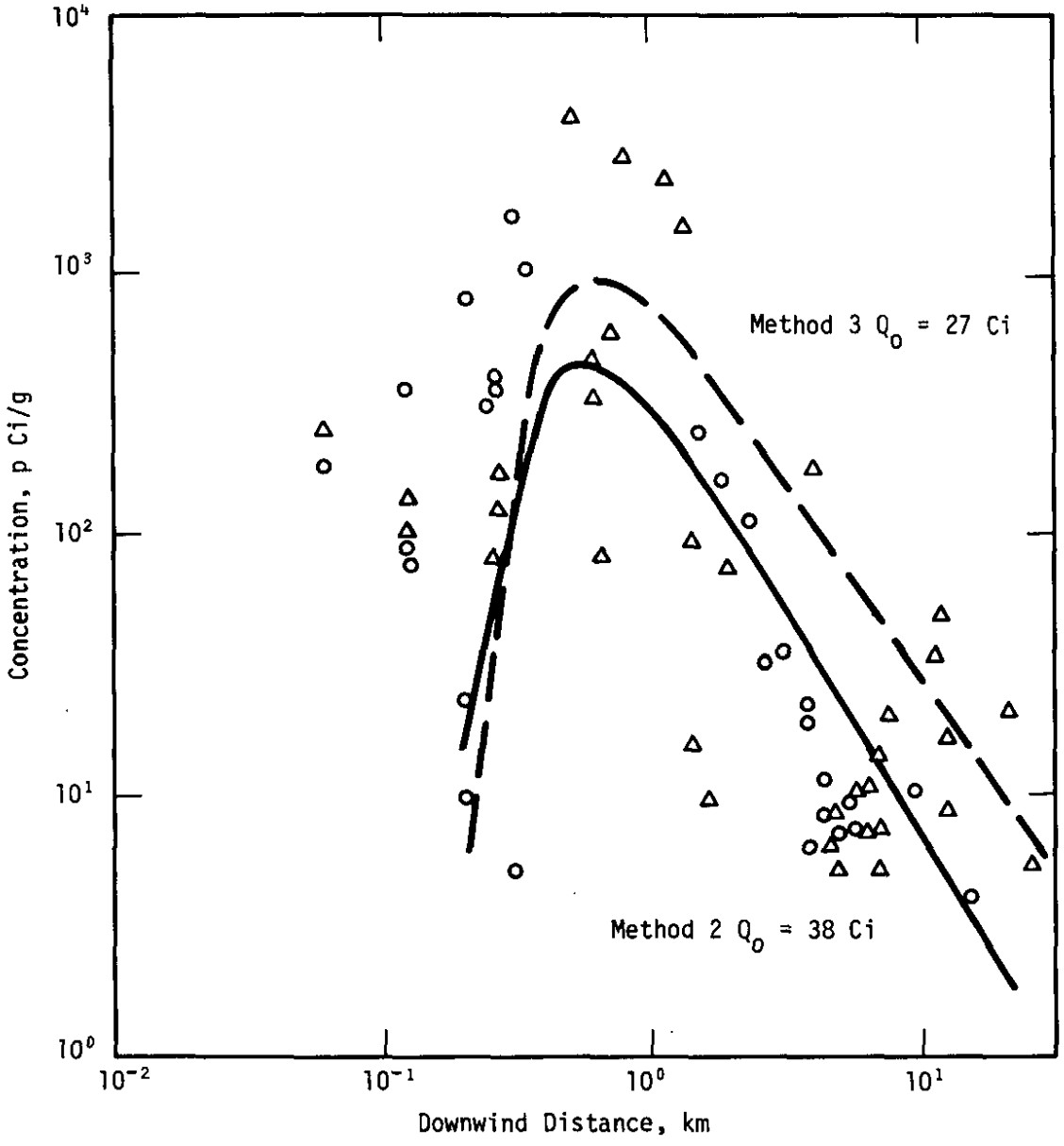

FIGURE 2. Calculated and Observed Grass Concentration

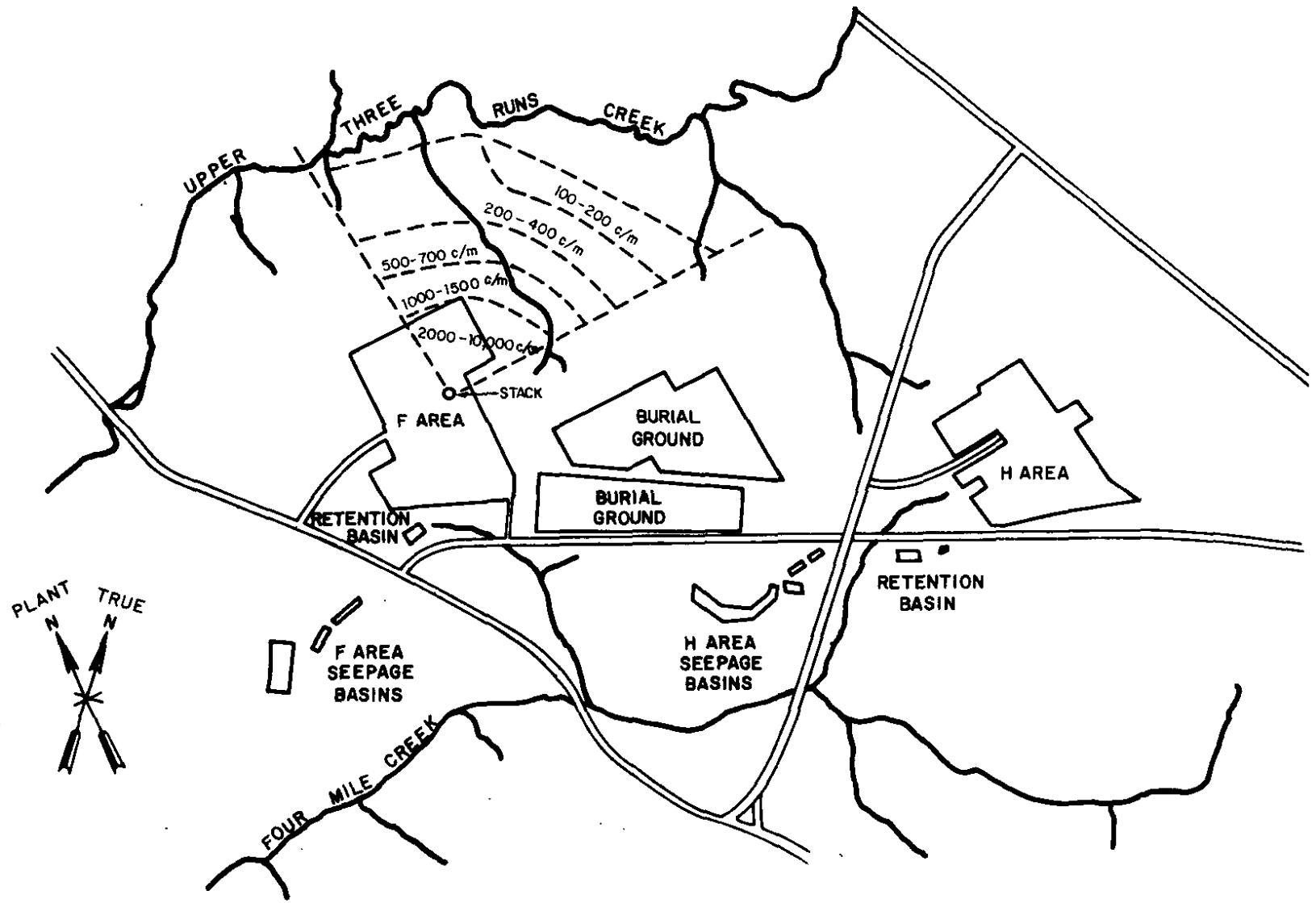

FIGURE 3. Ground Survey of ^{106}Ru. Readings are in counts per minute.

MODEL EVALUATION FOR TRAVEL DISTANCES OF 30-140 km

M. M. Pendergast

Krypton-85 released as the result of routine operations at SRP has been used to evaluate how well two different models predict 10-hour average concentrations at travel distances of 30-140 km. The segmented plume model is almost twice as accurate as the wind rose model in evaluating transport of a short-term (10-hr) release, while it is only slightly more accurate over larger averaging times. Adding hourly varying stability only slightly improves the segmented plume model when assuming neutral stability for all times.

MODELS

The wind rose model assumes that a pollutant released at a point with source strength Q travels in a straight line for all time. The pollutant is assumed to be uniformly mixed in the vertical direction up to the mixing depth and in the horizontal direction within the 30-degree sector determined by the wind direction at the time of release.

The segmented plume model (Kern, 1975) utilizes a gridded wind field to transport material released from the ^{85}Kr source near the center of the SRP. Wind fields are calculated at hourly intervals using an objective analysis routine (Fleming, 1969; Kern, 1974). The analysis scheme applies a method of successive corrections to a first guess wind field. A variable scan radius, dependent on the distribution of observed values, is used to weigh the influence of observations on grid point values.

PROCEDURE

Each model was evaluated by comparing observed concentration (OBS) and calculated concentrations (CAL) for all sites. The following information was tabulated:

n_b = number of times when OBS and CAL were both at or below background.

n = number of times when either OBS or CAL exceeded background. The data were used to evaluate the diffusion portion of the models.

Hits = number of times when both OBS and CAL exceed background. (These data were used to evaluate the transport portion of the model.)

The transport portion of the model was evaluated by calculating the percentage of Hits excluding background values, H, given by:

$$H = \left(\frac{\text{Hits}}{n}\right) 100 \tag{1}$$

and by also calculating the percentage of Hits including as a hit those times when OBS and CAL were background, HB, given by:

$$HB = \left(\frac{\text{Hits} + n_b}{n + n_b}\right) 100 \tag{2}$$

Note values of H and HB give no measure of how well observed and calculated values agree; they show if the trajectory is in the correct direction. The diffusion portion of the model (which also includes error due to transport) was evaluated by calculating the ratio of OBS/CAL for those periods when OBS or CAL exceeded background. These data were used to define a Goodness Factor, G, given by:

$$G = \sum_{i=1}^{n} \log_{10} \left|(\text{OBS/CAL})_i\right| \Big/ n \tag{3}$$

A value of G = 0 corresponds to a perfect forecast; a value of G = 1 implies that the ratio of OBS/CAL is either 10 or 0.1.

Table 1 presents a summary of results for all models tested with the ^{85}Kr data. The results indicate that the segmented plume model produces a significant improvement over the wind rose model in evaluating transport with the segmented plume model producing about 40% hits and the wind rose model producing only about 25% hits. The overall results as measured by the Goodness Factor suggest that the segmented plume models are slightly better than the wind rose models. The segmented plume model produced results that agreed to within a factor of 2.7 with observations and the wind rose model produced results that agreed to within a factor of 3.2 with observations. The use of hourly stability leads to only slight improvement over calculations obtained by assuming neutral conditions for all time.

REFERENCES

T. V. Crawford, et al. "A Computer for Objective Analysis and Display of Meteorological Fields," **Savannah River Laboratory Environmental Transport and Effects Research, Annual Report FY-1974.** Report DP-1374, E. I. du Pont de Nemours and Company, Savannah River Laboratory, Aiken, SC (1974).

T. V. Crawford, et al. "A Weather Information and Display System for Research and Emergency Response," **Savannah River Laboratory Environmental Transport and Effects Research, Annual Report FY-1975.** Report DP-1412, E. I. du Pont de Nemours and Company, Savannah River Laboratory, Aiken, SC (1975).

R. J. Fleming. **AFGWC Fine-Mesh Upper Air Analysis Model.** AFGWC Report TM69-2. Available through Federal Clearing House under AD 710203 (1969).

TABLE 1

Evaluation of Meteorological Models Using 10-HR ^{85}Kr Data

Run No.	Model	Stability Typing Schemes	σ_y and σ_z Relationship	n_b	n	Percent Within Factor of 2	Percent Within Factor of 10	G	H, %	HB, %
1	Wind rose with gridded winds[a]	neutral	BNL[b]	167	146	42(73)[c]	79(90)[c]	.57	26	66
2	Wind rose with Bush Field winds	neutral	BNL	168	145	49(76)	86(94)	.46	23	65
3	Segmented plume NWS[d] winds	neutral	BNL	145	161	48(83)	73(91)	.49	37	67
4	Segmented plume NWS and SRP tower winds	neutral	BNL	146	160	51(74)	87(93)	.46	41	69
5	Segmented plume NWS and towers	Turner[d]	BNL	153	153	55(78)	88(94)	.44	37	68
6	Segmented plume NWS and towers	Turner	Briggs	153	153	55(78)	88(94)	.44	37	68

a. Hourly winds obtained for the source location obtained from the objective analysis scheme.
b. Brookhaven National Laboratory
c. Values in parenthases include periods when observed and calculated were at background.
d. National Weather Service
e. Turner method uses meteorological data from Bush Field airport, Augusta, GA.

MONTHLY MEAN WIND FIELDS FOR THE SOUTH ATLANTIC BIGHT*

A. H. Weber

Computer analysis of meteorological observations taken aboard ships passing through the area of the South Atlantic bight (Figure 1) yielded a spatially and temporally consistent wind field.** The wind observations for both a 10-year period (1963-1973) and an 18-year period (1945-1963) show essentially the same results.

WIND FIELDS IN WINTER

The winter pattern (Figure 2) persists throughout the months of November through February. In November, the flow is characterized by northwesterlies over the North Carolina continental shelf, and increasingly northerly flows over the shelf regions of South Carolina, Georgia, and the northern Florida peninsula. The shelf area east of the southern Florida peninsula is characterized by northeasterly flow. Throughout December, January, and February, the northwesterlies progress toward more southerly latitudes.

WIND FIELDS IN SPRING

The first changes in the low-level circulation occur in March, as evidenced by easterlies or northeasterlies becoming more southerly to the seaward side of the bight area off the south Florida coast. In addition, westerlies or southwesterlies appear along the landward side of the bight from north Florida to Charleston.

---

* A bight is an open bay formed by a bend in a coast.

** Wind fields are spatially consistent in that, at any particular time, the calculated wind vector in a particular grid cell fits into a reasonable pattern with respect to vectors in adjoining cells. Wind fields are temporally consistent in that all the wind vectors form a reasonable pattern from month to month.

In April, westerly and southwesterly flows develop off the landward side of the bight off the two Carolinas. Easterlies set in off southern Florida. In other areas, the flow tends to be somewhat chaotic.

The May flow pattern (Figure 3) is easterly off most of Florida and southeasterly off the landward side of northern Florida to Georgia. The winds are quite random in other areas of the bight.

WIND FIELDS IN SUMMER

In June, easterly and southeasterly flows dominate the southern half of the bight. The wind flow is southerly off the coast of South Carolina. A small transition zone from Cape Romain to Cape Lookout is bordered by a southwesterly flow off North Carolina.

July (Figure 4) is dominated by easterlies off south Florida, southerlies off north Florida and Georgia, and southwesterlies off the two Carolinas. From north Florida to Cape Hatteras, the wind is remarkably alongshore over the mid- to outer-continental margin.

WIND FIELDS DURING TRANSITION TO FALL

Breakdown of the summer flow occurs in August, according to the 1945-1963 data (Figure 5). The flow is generally disorganized except for the seaward side of the zone. On the other hand, the 1963-1973 data indicate that the summer wind flow persists longer into August, but at much lower speeds than in July (not shown).

WIND FIELDS DURING "MARINER'S FALL"*

This season can be inferred from some of the published climatologies (Meserve, 1974; Naval Weather Service, 1975,1976). The wind pattern in September and October is quite different from the summer pattern, and is consistent over the entire area. During September (Figure 6), flow is northeasterly over the entire

* *No suitable term to describe this fifth season seems to be* available in either the published climatologies or oceanographic journals. Therefore, the author has tentatively designated the months of September and October as "Mariner's Fall" to be analogous to "Indian Summer."

region except off southern Florida and in the inner shelf region from northern Florida to Charleston, SC, where a thin bank of easterlies is evident.

In October, there are northeasterlies over the entire bight. Most of the wind vectors shift counterclockwise to become more northerly than in September. Average monthly wind speeds for the entire year are highest in October.

REFERENCES

J. M. Meserve. **U.S. Navy Marine Climatic Atlas of the World, Vol. I, North Atlantic Ocean.** U.S. Department of Commerce Report NAVAIR 50-1C-528, U.S. Government Printing Office, Washington, DC 20402 (1974).

Naval Weather Service Detachment. **Climatic Study of the Near Coastal Zone; East Coast of the United States.** Director, Naval Oceanography and Meteorology, Asheville, NC (1976).

Summary of Synoptic Meteorological Observations, Vol. 3. U.S. Naval Weather Service Command, Climatic Center, Asheville, NC (1975).

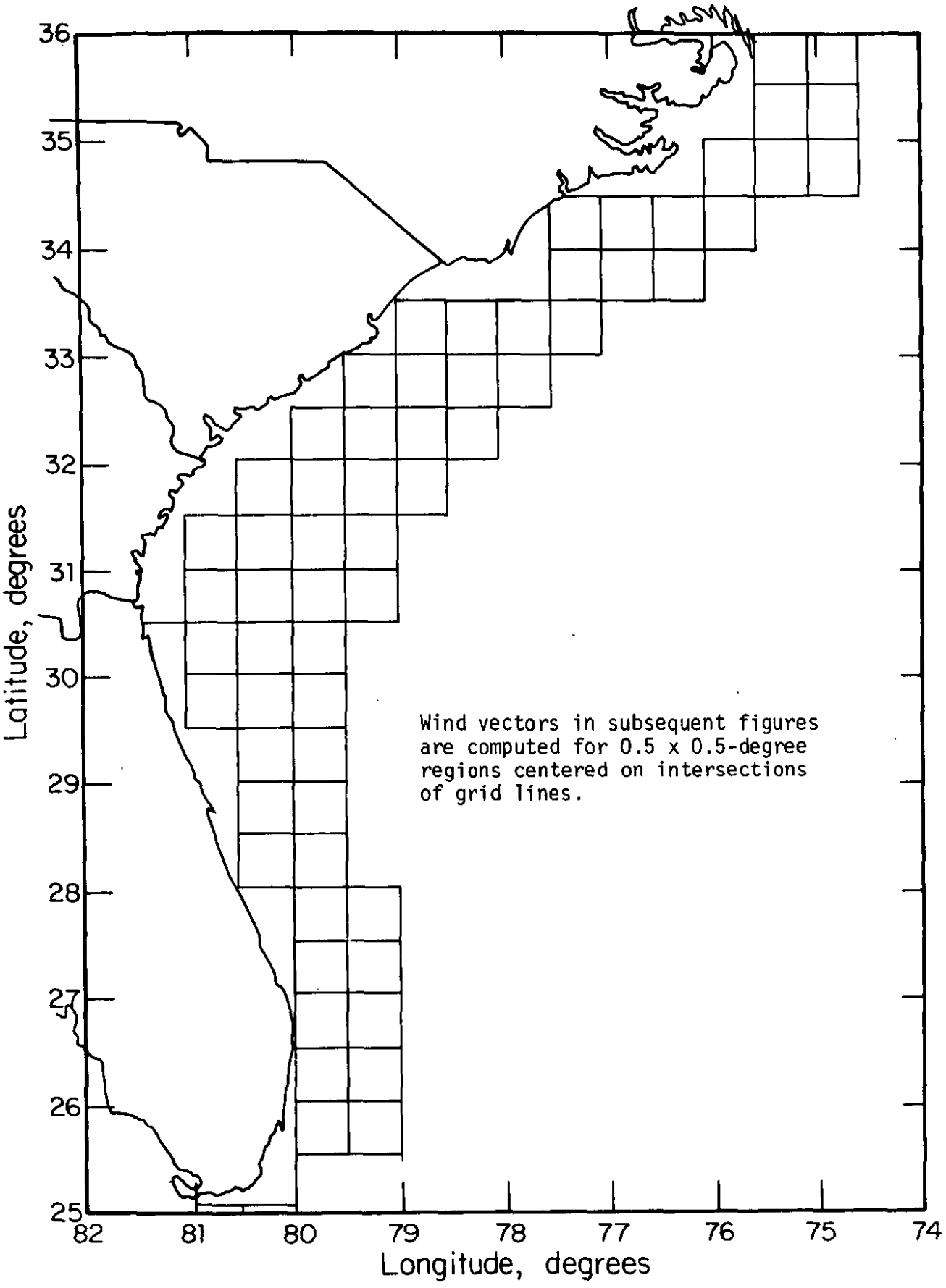

FIGURE 1. Area of Shipboard Meteorological Observations in South Atlantic Bight, 1945-1973, with Superimposed Computational Grid

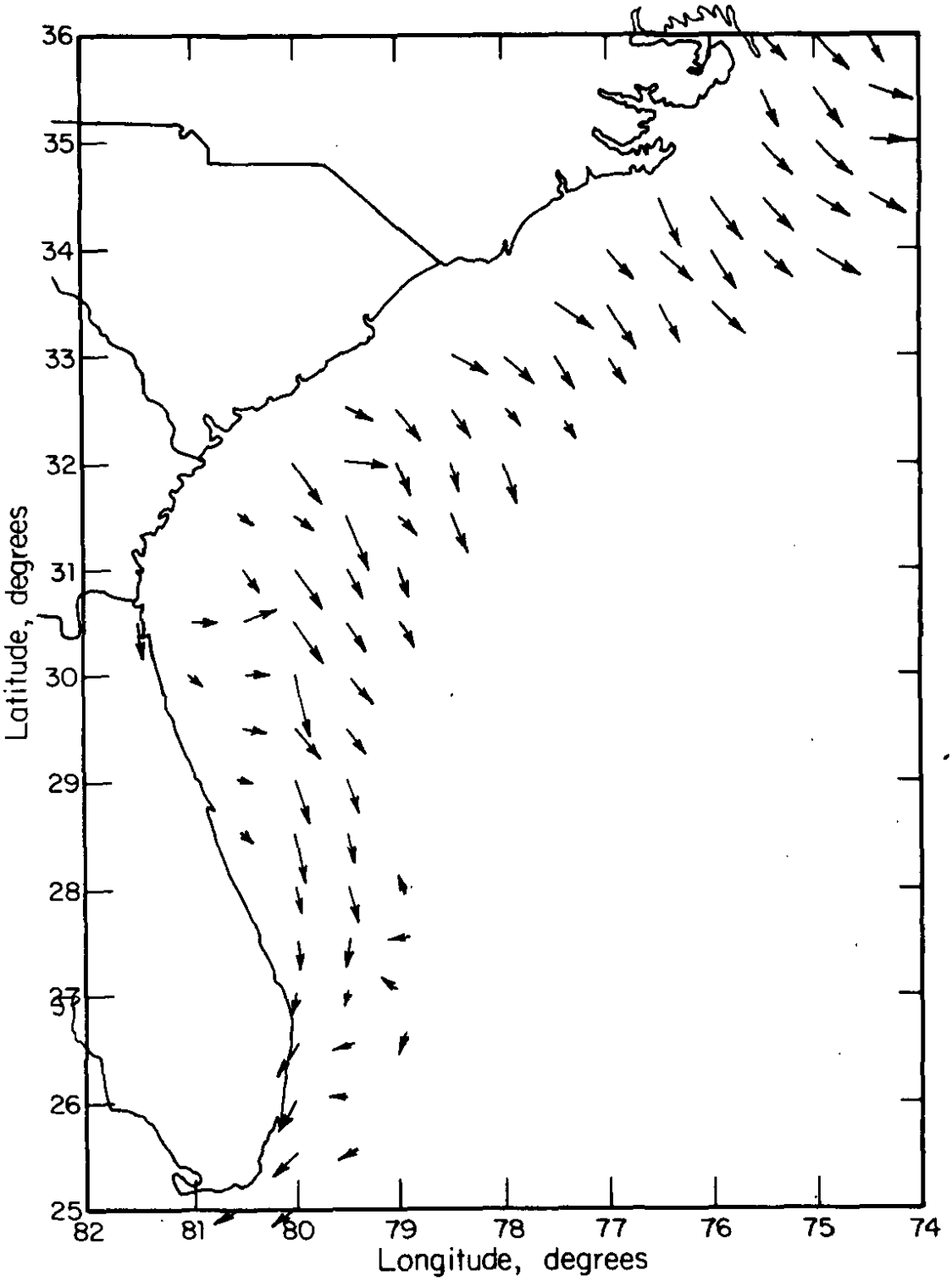

FIGURE 2. Mean Monthly Wind Vectors for January 1945-1963

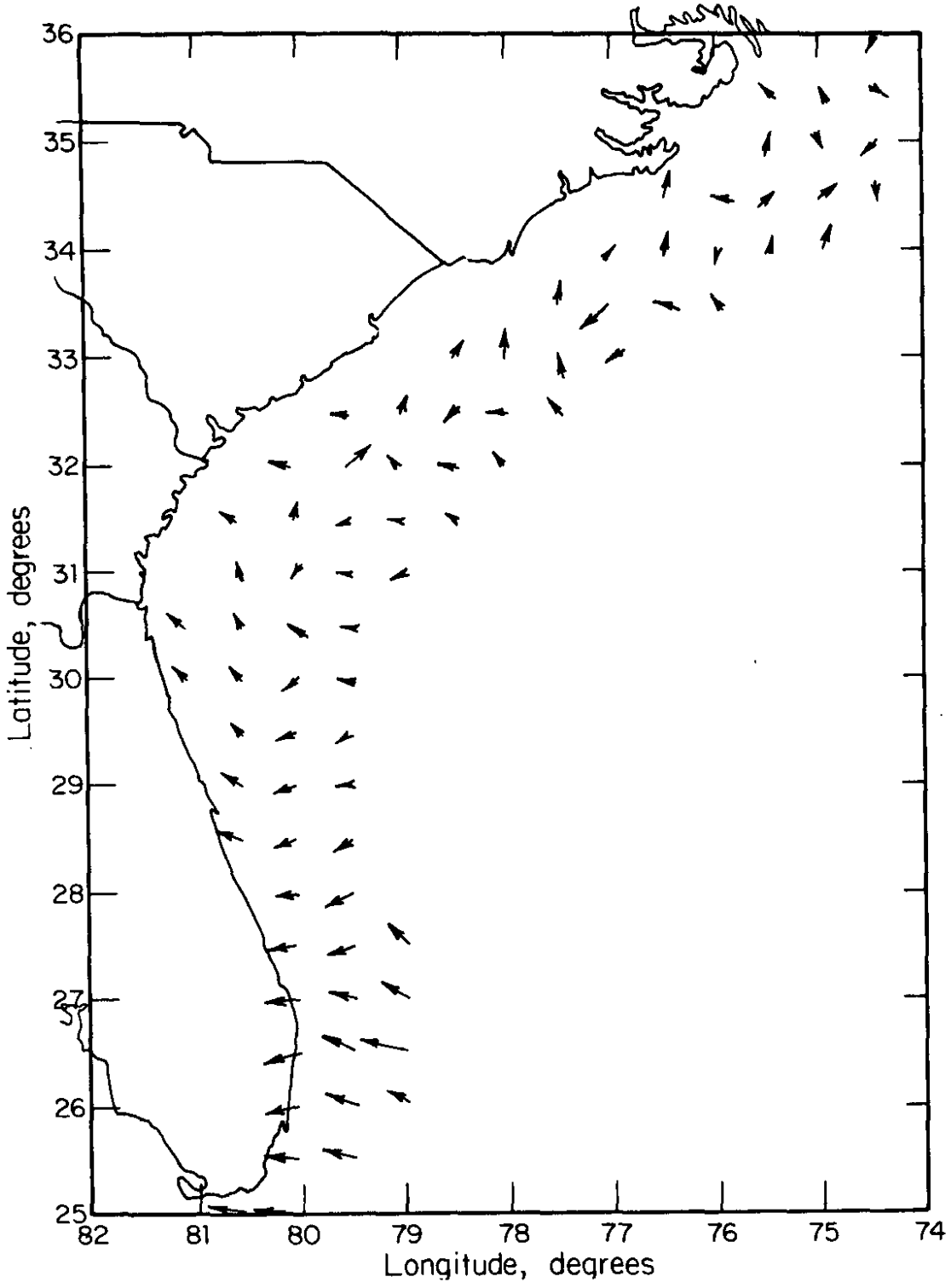

FIGURE 3. Mean Monthly Wind Vectors for May 1945-1963

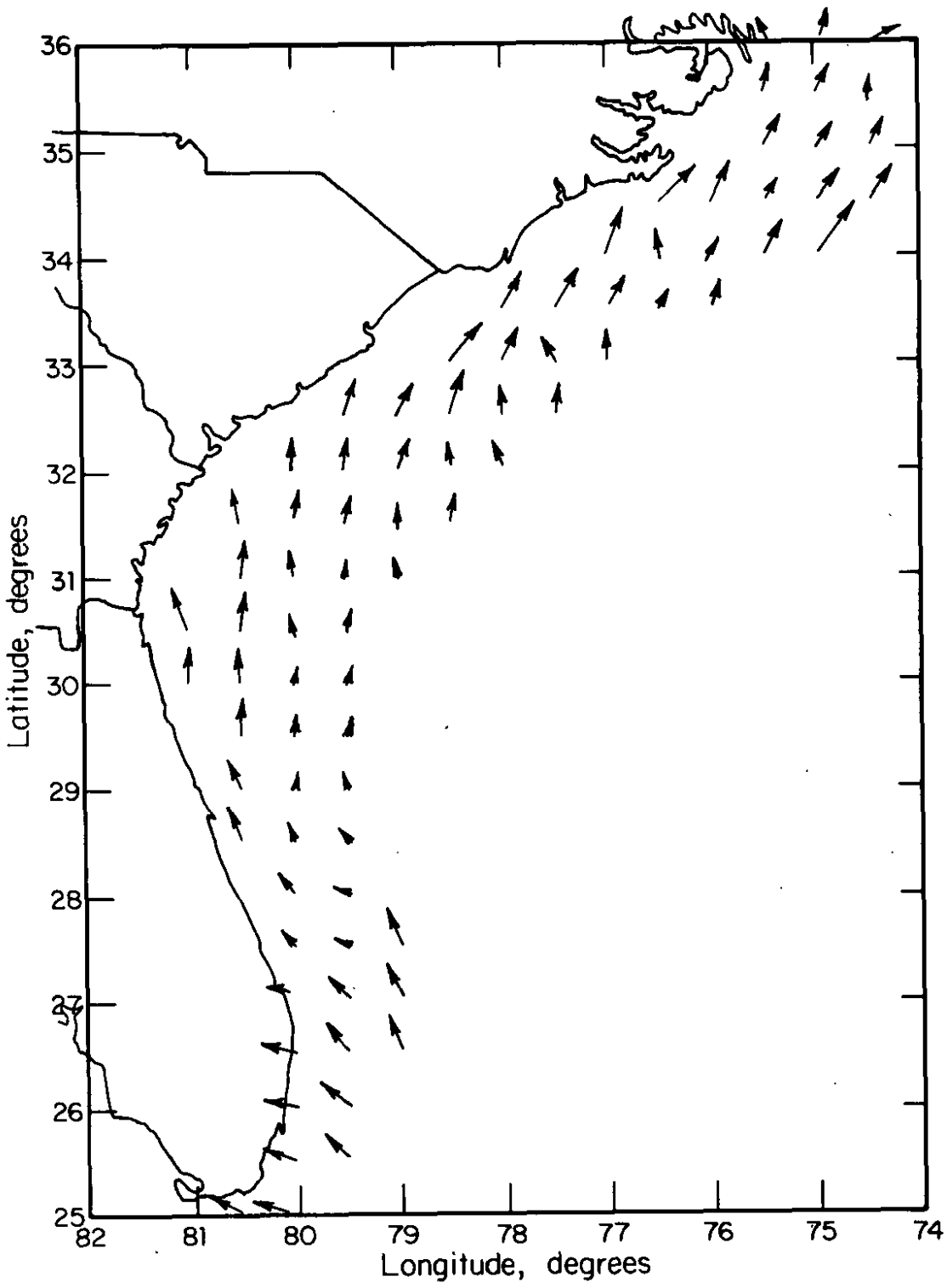

FIGURE 4. Mean Monthly Wind Vectors for July 1945-1963

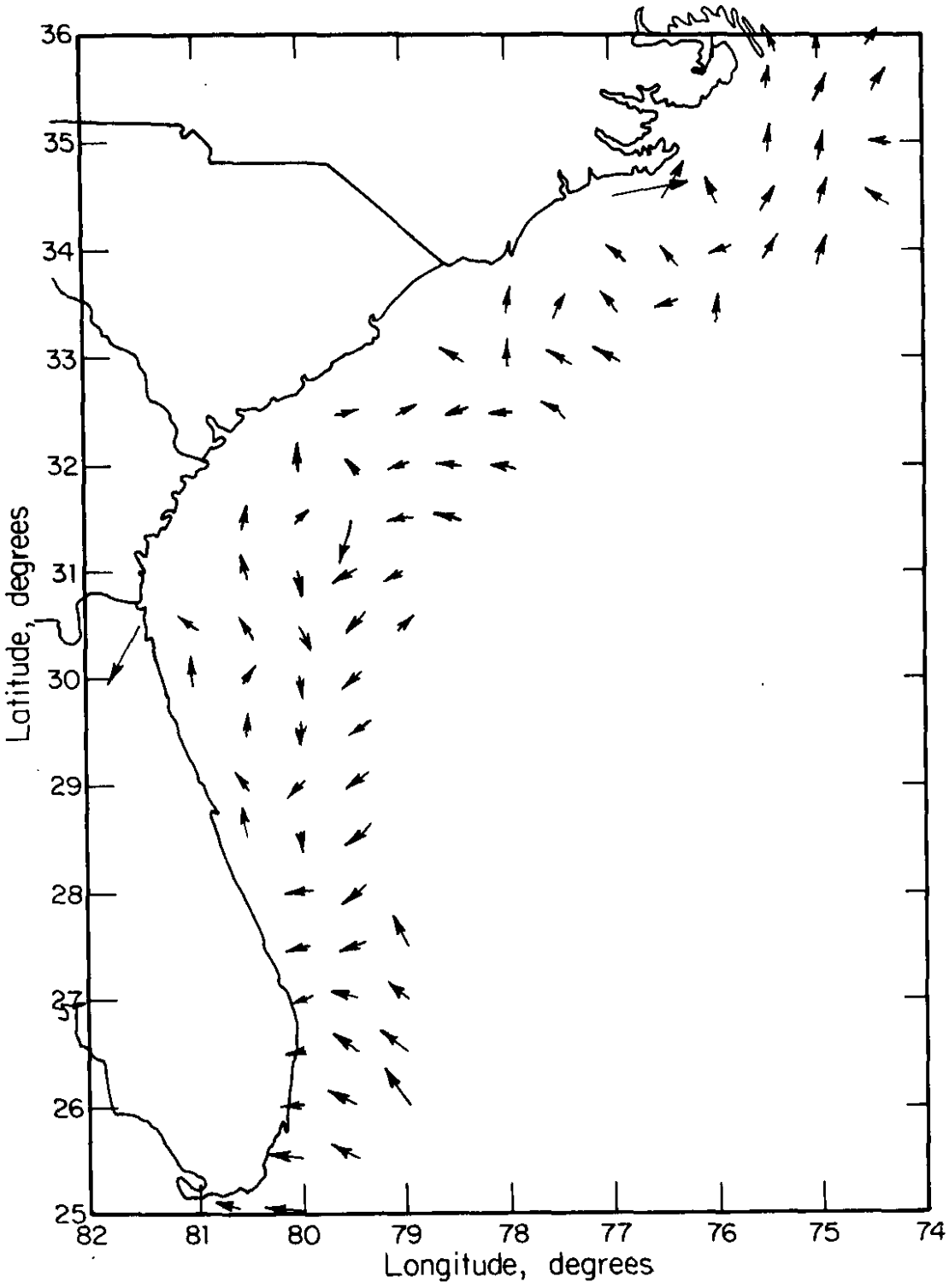

FIGURE 5. Mean Monthly Wind Vectors for August 1945-1963

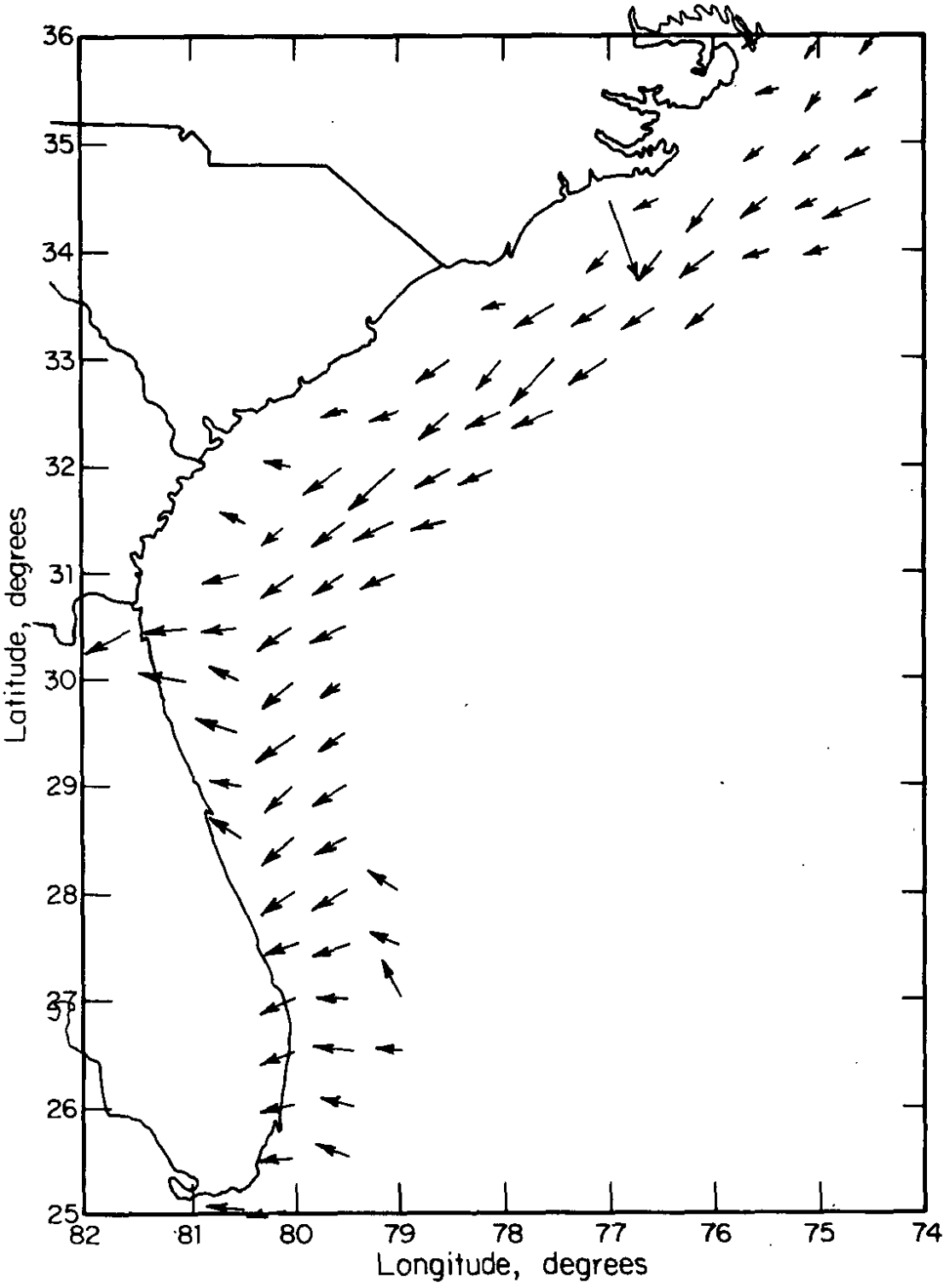

FIGURE 6. Mean Monthly Wind Vectors for September 1945-1963

ANALYSIS OF Z AND σ_z FOR NEAR GROUND RELEASES OF TRACERS IN THE ATMOSPHERE

A. H. Weber

Lagrangian similarity theory has been combined with statistical theory to make predictions about the rate of expansion of a plume release from ground level (Hunt, 1978). In neutral conditions the rate of growth of the plume's vertical dimension (σ_z or $\bar{Z}$) is found to be proportional to $\exp(-bz^{1.2})$. This result is quite different than the usually adopted Gaussian plume growth, i.e., $\exp(-bz^{2.0})$, but it is closer to the observational studies summarized by Pasquill (1974), which are close to $\exp(-bz^{1.5})$.

The value of the exponent on z above (which we shall define as s) is a slowly changing function of downwind distance, i.e.,

$$s \simeq 1 + 4\left[1 - \left(\frac{\sigma_z^{(p)}}{\bar{Z}/\sqrt{2}}\right)\right] \qquad (1)$$

where the concentration profile for a continuous ground level release is expressed in the form

$$\bar{C}^{(p)}(x,z) = \bar{C}^{(p)}(x,o)\ \exp\left[-\left(\frac{Az}{\sigma_z^{(p)}}\right)^s\right] \qquad (2)$$

Also, it is shown that vertical diffusion from a ground level source can be predicted in terms of measurable statistics of turbulence, i.e, the mean speed at some reference level $u(z_1)$, the standard deviation of the vertical wind direction angle (σ_E), and the roughness length.

PREDICTED DISPERSION COEFFICIENT σ_y AND σ_z

Several rather heuristic arguments are used to derive equations which predict the growth of the vertical and lateral extent of the plume; detailed theoretical discussions are given in Hunt and Weber (1978). Figures 1 and 2 show σ_z and $\bar{Z}$ as functions x for z_o = 0.03 m and z_o = 0.30 m.

To compare with existing data, the values of σ_z were plotted on the same axes with Briggs (1974) rural curves; Briggs' curves were extended from 10 to 100 m since originally the curves are defined over the more restricted region of 10^2 to 10^5 m. The values agree very well with one another at the short and medium ranges as shown in Figure 3.

Similar plots for the lateral dispersion coefficient, σ_y, and u_*T are shown in Figures 4 and 5 for z_o of 0.03 and 0.30 m, respectively. The Briggs' curve is again shown in Figure 6 for comparison. The agreement is not as good as for the vertical dispersion coefficient; Panofsky (1978) discussed the variation of σ_v/u_* with mesoscale terrain features. Since σ_v/u_* is not a universal constant, the lack of agreement of σ_y with site specific data is understandable.

The value of s from Equation (1) is shown as a function of downwind distance in Figure 7. The value decreases from near 1.25 to 1.10.

REFERENCES

J. C. R. Hunt and A. H. Weber. "A Lagrangian Statistical Analysis of Diffusion from a Ground Level Source in a Turbulent Boundary Layer." Accepted for publication in the **Quarterly Journal of the Royal Meteorological Society** (1978).

E. Pasquill. **Atmospheric Diffusion.** Ellis Hornwood Limited, John Wiley and Sons, 427 pp. (1974).

H. A. Panofsky, C. A. Egolf, and R. Lipschutz. "On Characteristics of Wind Direction Fluctuations in the Surface Layer." Accepted for publication in **Boundary Layer Meteorology** (1978).

G. A. Briggs. "Diffusion Estimation for Small Emissions." **Atmospheric Turbulence and Diffusion Laboratory Annual Report.** USAEC Report ATDL-106, National Oceanic and Atmospheric Administration (1974).

Mathematical Symbols

$\bar{u}$	Mean wind speed
u_1	Mean wind speed at the reference height z_1
z_1	Reference height for the measurement of u_1
$\bar{Z}$, σ_z	First and second moments of the vertical concentration distribution
σ_v	Second moment of the lateral velocity distribution
u_*	Friction velocity
σ_y	Second moment of the lateral concentration distribution
z_o	Roughness length
$\bar{C}^{(p)}_{(x,z)}$, $\bar{C}^{(p)}_{(x,o)}$	Concentration distribution for a continuous point source
$\sigma_z(p)$	Second moment of the concentration distribution for a continuous point source
b	Universal constant in the similarity relationship for $\bar{Z}$
x,y,z	Distance downwind, laterally, and vertically upward, respectively
s	Power of the vertical coordinate z in Equation (1)
T	Travel time of the diffusion cloud
σ_E	Vertical wind direction angle

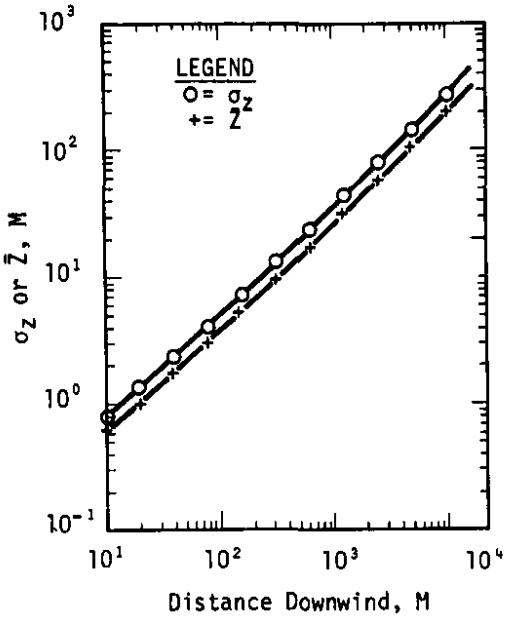

FIGURE 1. Lagrangian-Statistical Theory Predictions for σ_z and $\bar{Z}$ vs. Downwind Distance for z_o = 0.03 m

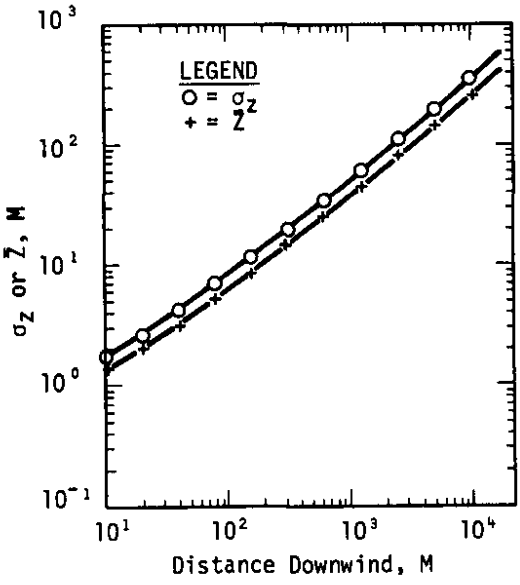

FIGURE 2. Lagrangian-Statistical Theory Predictions for σ_z and $\bar{Z}$ vs. Downwind Distance for z_o = 0.30 m

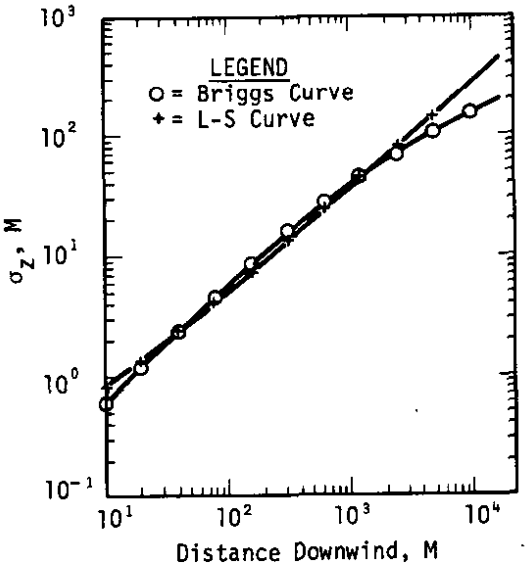

FIGURE 3. Briggs' Rural Curve (Extrapolated) for σ_z vs. Downwind Distance and Lagrangian-Statistical Theory Predictions for σ_z

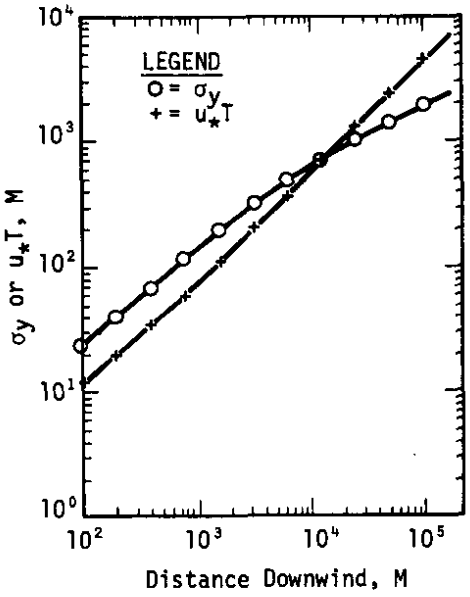

FIGURE 4. Lagrangian-Statistical Theory Predictions for σ_y and u_*T for z_o = 0.03 m ($\bar{u}t_L$ = 1000 m, z = 2 m)

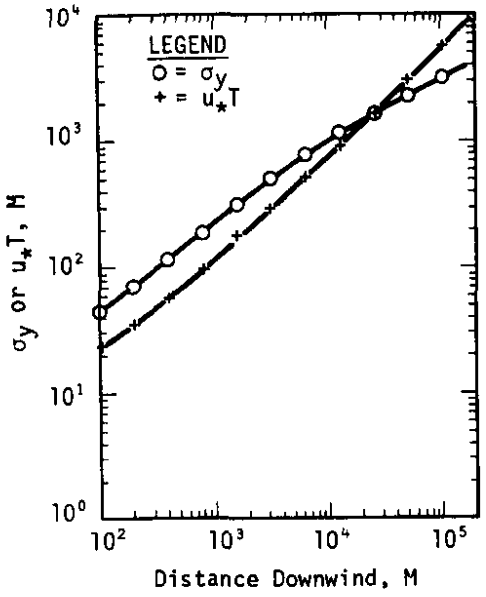

FIGURE 5. Lagrangian-Statistical Theory Predictions for σ_y and u_*T for z_o = 0.30 m ($\bar{u}t_L$ = 1000 m, z = 2 m)

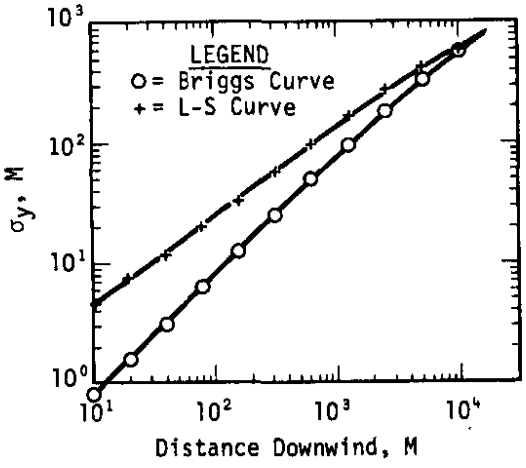

FIGURE 6. Brigg's Rural Curve for σ_y vs. Downwind Distance and Lagrangian-Statistical Theory Predications for σ_y ($\bar{u}t_L$ = 1000 m, z = 2m

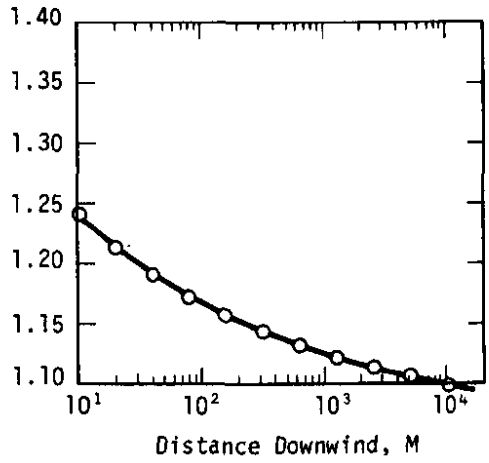

FIGURE 7. The Power s vs. Downwind Distance for z_o = 0.03 m

COMPARISON OF WIND DATA BETWEEN A COASTAL LAND BASE STATION AND THE SAVANNAH NAVIGATIONAL LIGHT TOWER

J. O. Blanton* and D. W. Hayes

The Savannah Navigational Light Tower located about 15 km off the coast of Savannah Beach, GA, is instrumented to measure meteorological data. Over-the-ocean wind velocities were compared with those that occur simultaneously over land coastal stations to determine if land-measured winds are representative of those that drive ocean coastal currents. On the average, over-the-ocean speeds exceed coastal land speeds by a factor of 2, and there are often differences in wind direction as great as 30 to 40 degrees between the two locations. These findings indicate that the extrapolation of winds measured at the coastal land station are not representative of those that drive ocean currents off the coast of Savannah, GA.

Further analysis of wind data taken during the winter at the base station show that 80 to 90% of the total variance is confined to periodicities in excess of 3 days. This reflects the variability associated with passing weather systems. Up to 10% of the total variance has a 24-hour periodicity. There is no significant difference in these percentages between land winds and ocean winds.

* Skidaway Institute of Oceanography.

DOSE CALCULATIONS FOR THE REGIONAL, CONTINENTAL, AND GLOBAL POPULATIONS FROM A HYPOTHETICAL NUCLEAR FUEL REPROCESSING PLANT LOCATED IN THE SOUTHEAST UNITED STATES

J. F. Schubert, R. E. Cooper, J. R. Watts, and C. E. Bailey

The population dose commitments that would result from operation of a hypothetical fuel reprocessing plant processing 3000 MTU/yr and located in the southeast U.S. were determined. The 50-yr (40-yr plant life plus 10 yr after shutdown) dose commitments are 42,030 man-rem to the regional population, 135,400 man-rem to the continental population, and 220,300 man-rem to the global population. The dose commitments are significantly less than the population doses from natural background radiation. The dose commitments from plant operations are 0.2% of regional, 0.01% of continental, and 0.001% of global doses from natural background radiation. Tritium, ^{14}C, and ^{85}Kr dominate the total population dose commitment, but their relative importance varies with pathways and the particular population being considered.

REFERENCE FACILITY

The reference facility is a nuclear fuel reprocessing plant located in the southeast U.S. at SRP. The hypothetical plant reprocesses fuel burned at 30 MW/MTU to a burnup of 33,000 MWD/MTU, and all fuel is cooled for at least 1 yr. The plant is assumed to have a 10 MTU/day capacity and an output of 3000 MTU/yr (85% online operation). The plant has an assumed lifetime of 40 yr with annual discharges of radionuclides to the atmosphere as shown in Table 1.

During the 40-yr period the dose rate from airborne material is constant because global recirculation is neglected; however, the dose rate from ground deposition increases because of buildup of deposited material on the ground. It is assumed that the material deposited is depleted only by radioactive decay. Shielding by buildings and terrain, and weathering are not taken into account.

TABLE 1

Annual Discharges of Radionuclides to the Atmosphere

Radionuclide	Curies/yr Released	Radionuclide	Curies/yr Released
^{3}H	2.2×10^{5}	^{106}Ru	5.0×10^{2}
^{14}C	3.5×10^{2}	^{129}I	5.0×10^{-1}
^{85}Kr	5.0×10^{6}	TRU*	5.0×10^{-2}

* TRU - Transuranic radionuclides treated as ^{239}Pu for transport and dosimetry effects.

ATMOSPHERIC TRANSPORT

The atmospheric transport, diffusion, and deposition calculations were made using the Pacific Northwest Laboratory U.S. Scale Assessment model (Wendell, 1976). In this code, emissions are simulated by discrete puff releases at one-hour intervals using gridded upper level winds over 12-hour intervals for 1975 and gridded hourly precipitation for 1975. For the continental U.S. a release of 1 Ci/sec and a release height of 62 m at 33.3°N latitude and 81.7°W Longitude were used as the source information for the models. Integrated surface level air concentrations with no deposition, with dry deposition, and with wet and dry deposition for each grid point (0.5° longitude) were calculated. These estimates were compared with results obtained using a code developed by Heffter (1975) and a regional code developed by Lange (1975). Air Resources Laboratory also performed the global-scale transport and diffusion calculations.

DOSE CALCULATIONS

The dose commitment calculations, the integrated air concentrations, and amounts deposited for each nuclide were used as input data. The external dose commitment to man is made up of two parts: 1) submersion of an individual in contaminated air, and 2) irradiation by exposure to contaminated ground surfaces (Killough, 1976).

The exposed individual is assumed to be an adult (20 yr old) who will live to an age of 70 yr. Thus, dose commitment in this discussion and Table 2 is to be interpreted as 50-yr dose commitment.

TABLE 2

50-Yr Dose Contributions by Isotope and Pathway Whole Body Dose, 1980 Startup.

Dose Category	Dose, man-rem	Percent of Total Dose					
		^{3}H	^{14}C	^{85}Kr	^{129}I	^{106}Ru	^{239}Pu
Atmospheric Submersion SE Regional	2,600	69.8	1.2	22.6	0.19	0.97	5.3
Atmospheric Submersion U.S. Total	104,100	87.2	10.5	2.08	*	0.03	.17
Atmospheric Submersion Global Recirculation	220,300	3.1	42.4	54.5	*	*	*
Ground Deposition SE Regional	23,160	*	*	*	0.7	99.3	*
Ground Deposition U.S. Total	31,300	*	*	*	0.7	99.3	*
Water Consumption SE Regional	6,050	100	*	*	*	*	*
Agricultural Production SE Regional	10,220	70.8	28.8	*	*	.36	*
Total Dose	397,730	28.3	26.9	30.8	.10	13.7	.08

* Indicates less than 0.01%.

The internal dose commitment (Killough, 1976) results from assimilation of radionuclides from air, food, and water. Even though the duration of the intake episode may be brief, the resulting deposition of radioactivity in a specified organ continues to deliver a dose to that organ at a rate which is proportional, at any given time, to the activity which remains in the organ at that time. This residual burden is diminished continuously by radioactive decay of the nuclide and by biological removal by the organ's metabolic processes.

The internal dose commitments to the regional population from agricultural products were determined by Lawrence Livermore Laboratory using the calculated deposition on each county in South Carolina and Georgia and detailed uptake models for each crop in each county. The internal dose commitment to the regional population for HTO and $^{14}CO_2$ was calculated by assuming that the water and carbon in agricultural products and water supplies were in equilibrium with the calculated air concentrations for HTO and $^{14}CO_2$, respectively, at each grid point.

The equilibrium concept was also used to calculate the U.S. whole body and organ dose commitments. The dose commitments calculated using the equilibrium assumption are recognized to be conservative, but are appropriate for calculating the maximum individual dose commitment. Most drinking water is obtained from wells and is lower in tritium content than surface water, which may be in equilibrium with tritium in atmospheric moisture. The equilibrium hypothesis assumes all food consumption is from locally grown food.

The population dose contributions are summarized in Table 2 for the whole body dose. The radionuclides ^{3}H, ^{14}C, ^{85}Kr, and ^{106}Ru are primary dose contributors to certain populations and dose pathways. Similar patterns exist for the major organ doses. The total impact from 50 yr of plant operation shows that the doses from ^{3}H, ^{14}C, and ^{85}Kr are very similar. For all population groups, the radiation doses from plant operations are less than 0.2% of the radiation doses from natural background radiation.

REFERENCES

J. L. Heffter, A. D. Taylor, and G. J. Ferber. **A Regional-Continental Scale Transport, Diffusion, and Deposition Model.** NOAA Tech. Memo. ERL ARL-50, Air Resources Laboratories, Silver Spring, MD (1975).

G. C. Killough and L. R. McKay. "A Methodology for Calculating Radiation Doses from Radioactivity Released to the Environment." ORNL-4992, **Health and Safety** (1976).

R. Lange. **ADPIC-A Three-Dimensional Transport-Diffusion Model for the Dispersal of Atmospheric Pollutants and Its Validation Against Regional Tracer Studies.** Report UCRL-76170, Rev. 2, Lawrence Livermore Laboratory (1975).

L. L. Wendell and C. E. Hane. "Preparation of Hourly Maps of Gridded Precipitation Scavenging Calculations." **Pacific Northwest Laboratory, Annual Report for 1975 to the USERDA Division of Biomedical and Environmental Research, Part 3, Atmospheric Sciences.** USERDA Report BNWL-2000 PT3, Battelle Pacific Northwest Laboratories, Richland, WA (1976).

DATA BASE FOR TERRESTRIAL FOOD PATHWAYS DOSE COMMITMENT CALCULATIONS

C. E. Bailey

A computer program is under development to allow calculation of the dose-to-man in Georgia and South Carolina from ingestion of radionuclides in terrestrial foods resulting from depositon of airborne radionuclides. This program is based on models described in Regulatory Guide 1.109 (USNRC, 1977). The data base describes the movement of radionuclides through the terrestrial food chain, growth and consumption factors for a variety of radionuclides.

DATA BASE

Radionuclides emitted to the atmosphere result in deposition directly on growing plants and the ground. Some of the material deposited on the plants subsequently appears in the edible portion of the plants by translocation. Uptake of radionuclides deposited on the ground by the root system of the plants into the edible portion also occurs. Radionuclides in animal products result from the presence of radionuclides in food ingested by the animals.

The data base consists of named data records to permit use of the facilities of the JOSHUA System and to provide direct-access read/write capability. The numerical data were generated by the Lawrence Livermore Laboratory (Ng, 1978), and new data can be easily added.

Two categories of data are required to calculate the dose-to-man via ingestion of terrestrial food: 1) data to allow calculation of the radionuclide concentration in foods; and 2) data to determine the dose-to-man from ingestion of food containing radionuclides.

The types and annual quantities of foods grown in Georgia and South Carolina are shown in Table 1 (Ng, 1978). Some of the crops, e.g., hay, corn silage, and sorghum silage, are consumed totally by animals. However, radionuclides present in these crops result in human uptake as a result of ingestion of animal products.

Calculations of dose-to-man are made for areas defined by county boundaries. Therefore, data in the data base are required for each county of each state that lies in the area of interest. The basic input required for the calculation is the deposition of each radioisotope on the ground surface in units of pCi/m^2-month.

DATA BASE RECORD DESCRIPTION

The information described in Tables 2 through 4 comprises the data base to support calculations of dose-to-man from ingestion of radioisotopes in terrestrial foods resulting from the release of radionuclides to the atmosphere. The records are structured so that additional information describing new regions, radionuclides, body organs, and foods can be easily added.

The records described in Table 2 are required to allow the data base to be defined on a county basis. These records provide identification of states and counties by numerical identification codes defined by the Federal Information Processing Standards.

The information provided in the data base to allow the calculation of the concentration of radionuclides in crops and animal products is described in Table 3. There is a record for each crop and animal product in each county.

The body organ description record, described in Table 4, gives the names of the organs for which doses will be calculated. Currently, these are whole body, bone, kidney, liver, thyroid, and the lower large intestine. The second record gives the dose commitment factor for the first year following ingestion of a radioisotope. There is one record of this type for each organ, and the dose commitment factor for all isotopes is given in the record for the organ.

REFERENCES

Y. C. Ng, W. A. Phillips, Y. E. Ricker, R. K. Tandy, and S. E. Thompson. **Methodology for Assessing Dose Commitment to Individuals and to the Population from Ingestion of Terrestrial Foods Contaminated by Emissions from a Nuclear Fuel Reprocessing Plant at the Savannah River Plant.** UCID Report 17743, Lawrence Livermore Laboratory, Livermore, CA (1978).

United States Nuclear Regulatory Commission. Regulatory Guide 1.109 (Rev. 1). **Calculation of Annual Doses to Man from Routine Releases of Reactor Effluents for the Purpose of Evaluating Compliance with 10 CFR Part 50, Appendix I.** USNRC, Office of Standards Development, Washington, DC (1977).

TABLE 1

Food Production in Georgia and South Carolina

	Raw Food Production, kg/yr	
	Georgia	South Carolina
Crop		
Apples	9.8×10^6	9.1×10^6
Barley	7.8×10^6	2.1×10^7
Cabbage	1.5×10^7	7.3×10^6
Cantaloupes	1.0×10^7	6.4×10^6
Corn	2.7×10^9	7.9×10^8
Cucumbers	-	3.1×10^7
Irish Potatoes	2.3×10^6	4.3×10^6
Oats	6.1×10^7	4.7×10^7
Peaches	3.7×10^7	9.8×10^7
Peanuts	7.6×10^8	1.4×10^7
Rye	5.3×10^7	2.0×10^7
Snap Beans	5.6×10^6	5.9×10^6
Sorghum	3.2×10^7	1.5×10^7
Soybeans	7.0×10^8	6.3×10^8
Sweet Corn	-	2.8×10^6
Sweet Potatoes	3.5×10^7	1.0×10^7
Tomatoes	8.3×10^6	2.5×10^7
Watermelon	1.2×10^8	8.7×10^7
Wheat	1.0×10^8	1.1×10^8
Corn Forage	-	4.7×10^7
Corn Silage	1.1×10^9	4.4×10^8
Hay	9.7×10^8	4.0×10^8
Sorghum Silage	1.8×10^8	1.1×10^8
Animal Product		
Beef	1.4×10^8	5.5×10^7
Chicken	7.2×10^8	4.9×10^7
Eggs	2.8×10^8	7.7×10^7
Milk	5.4×10^8	2.3×10^8
Pork	1.8×10^8	4.1×10^7

TABLE 2

Records for State and County Identification

1. State Description Record (One)
   - Number of states described
   - State name[a]
   - State code[a]
   - State population[a]
   - Number of counties in each state[a]
2. County Description Record (One for each state)
   - State name
   - County name[b]
   - County code[b]
   - Population of each county[b]
   - Area of each county[b]

---

a. Repeated for each state.
b. Repeated fore each county.

TABLE 3

Records for Calculation of Radionuclide Concentration in Foods

1. Crop Description Record (One for each crop in each state)
   - State name
   - Crop name
   - Month planted
   - Length of growing season
   - Total recoverable yield (kg/m^2)
   - Fraction of water contained
   - Fraction allocated for human utilization
   - Utilization ratio (amount utilized by humans/amount consumed by humans)
   - Ingestion rate, kg/person/yr

2. Animal Product Description Record (One for each animal product in each state)
   - State name
   - Animal product name
   - Fraction allocated for human utilization
   - Utilization ratio (amount utilized by humans/amount consumed by humans)
   - Ingestion rate, kg/person/yr

3. Crop Production Record (One for each county in each state)
   - State name
   - County name
   - Number of crops grown in county
   - Crop name[a]
   - Crop production in county, kg/yr[a]

4. Animal Product Production Record (One for each county in in each state)
   - State name
   - County name
   - Number of crops grown in county
   - Animal product name[b]
   - Animal product production in county, kg/yr[b]

TABLE 3, Contd

5. Isotope Description Record (One)

   Number of isotopes

   Isotope name[c]

   Isotope number

   Half-life, yr[c]

6. Isotope Behavior in Crops Record (One for each crop)

   Number of isotopes

   Iostope number[c]

   Translocation factor for isotope from aerial parts of crop to edible parts[c]

   Soil to plant concentration factor[c]

   Fraction of activity remaining after preparation and processing for human consumption[c]

7. Isotope Behavior in Animal Products Record (One for each animal)

   Number of isotopes

   Isotope number[a]

   Transfer coefficient for isotope from animal feed to food derived from animal[c]

   Fraction of activity remaining after preparation and processing for human consumption[c]

8. Animal Feeding Schedule Record (One for each animal product)

   Number of crops used as food

   Crop name[a]

   Feeding schedule of crop, kg/animal/day[a]

---

a. Repeated for each crop.
b. Repeated for each animal product.
c. Repeated for each isotope.

TABLE 4

Records for Calculation of Dose-to-Man

1. Body Organ Description Record (One)

   Number of organs

   Organ name[a]

   Organ number[a]

2. Dose Commitment Factor Record (One for each organ)

   Organ name

   Number of isotopes

   Isotope number[a]

   Dose commitment factor for organ for first year of exposure[a]

a. Repeated for each isotope.

COMPUTER METHODS DEVELOPMENT FOR ENVIRONMENTAL STUDIES

COMPUTATIONAL SYSTEMS IN SUPPORT OF ENVIRONMENTAL SCIENCES

J. E. Suich

The JOSHUA (Honeck, 1975) scientific data management facilities are being extended to incorporate features of general utility in the environmental sciences (Suich, 1978; Crawford, 1977). At present, several new capabilities are in limited use on environmental data sets:

- Interchange of data sets with other DOE sites in a machine independent format (Brooks, 1978) including JOSHUA data sets (Johnson, 1979) (Figure 1).
- Retrieval of data (from JOSHUA data sets) meeting stated criteria on "record names" and "data values" (Figure 2).
- Interactive graphical display of retrieved data as "time series," either for scalar data or "profiles" of scalar data (Figure 3).
- "Mapping" of selected data on a background of SRP cartographic features (Figure 4).
- Making JOSHUA data sets available to other analysis packages, currently SAS (Barr, 1976) and MARK IV (Informatics, 1975) and vice versa (Figure 5).

At present, SRL is in the process of obtaining new hardware and software packages, and developing new systematic geographical capabilities. The above computing features may therefore be implemented under newer, less-parochial systems. Functional capabilities, however, are firmly established.

REFERENCES

A. J. Barr, et al., "A User's Guide to SAS 76," **SAS Institute, Inc.** (1976).

A. A. Brooks, **Draft Proposal: American National Standard Specifications for an Information Interchange Data Descriptive File,** X3L5/589F (corrected), Oak Ridge National Laboratory, Oak Ridge, TN (to be issued).

T. V. Crawford, et al. "Computational Systems in Support of Environmental Samples, **Environmental Transport Division Annual Report - 1977** Report DP-1489, E. I. du Pont de Nemours & Co., Savannah River Laboratory, Aiken, SC (1978).

Geographic Exchange Standard and Primer, IWGDE, October 1978, PNL-2748 (1978).

H. C. Honeck, **The JOSHUA System,** USERDA Report DP-1380, E. I. du Pont de Nemours & Company, Savannah River Laboratory, Aiken, SC (1975).

A. J. Johnson, "User's Guide for Standard Interchange Data Files," DPSTM-IWADE, 1979).

"Mark IV Systems Reference Manual," **Informatics, Inc.** (1975).

J. E. Suich and H. C. Honeck. "Extensions to the JOSHUA GDMS to Support Environmental Science and Analysis Data Handling Requirements," in **Generalized Data Management Systems and Scientific Information,** OECD report, 1978.

a.

```
    4758.TEMPLATE.WXOBS.?DATE.WINDS.?TIME
LIST-> 5 NESTS  12 LOOPS  20 VARIABLES
NSTA,NLVL,(LEVEL(J),(ID(I,J),WDIR(I,J),WSPD(I,J),I=1,NSTA),J=1,NLVL)

  TYPE-> 1(NTEGER)*2  I(NTEGER)*4  R(EAL)*4  R(EAL)*8
C(HARACTER)*N  WHERE 0<N<64
C* 4 ID
```

b.

```
    4758.DDF.WXOBS.?DATE.WINDS.?TIME
   TAG                  DATA
:<000000>   :SIMPLE  ALPHA     &WXOBS.?DATE.WINDS.?TIME.@

:<000001>   :VECTOR  ALPHA     &RECORD ID&DATE!TIME&(2A(8))@

:<100001>   :SIMPLE  IMPLCIT   &NSTA@

:<100002>   :SIMPLE  IMPLCIT   &NLVL@

:<100003>   :VECTOR  IMPLCIT   &LEVEL(I)I=1,NLVL&&(I(7))@

:<100004>   :ARRAY   ALPHA     &ID(I,J)I=1,NSTA;J=1,NLVL&&(A(4))@

:<100005>   :ARRAY   SCALED    &WDIR(I,J)I=1,NSTA;J=1,NLVL&&(S(10))@

:<100006>   :ARRAY   SCALED    &WSPD(I,J)I=1,NSTA;J=1,NLVL&&(S(10))@
```

a'. JOSHUA record description (TEMPLATE).

b'. IWGDE Data Description File (DDF).

FIGURE 1. Data Base Exchange. The upper display (a.,b.) is the SRL internal (JOSHUA) record description of some meteorological data. The lower display (a'., b'.) is the corresponding machine-independent DOE interchange format. The exchange process can be essentially an automatic procedure despite inter-site computer differences.

```
SYSTEM=JUDGES.QUERY;SOURCE=LAKE3277.TEMPLATE;
RECORD=LAKES.DAILY.PARPOND.?STATON.QUALITY.PROFILE.SALL;
STATON(LIST)=2,5,7;
ELEMENTS=JULDAY,OBS,DEP;
RETRIEVE=DEP.LE.3.AND.JULDAY.GE.8766.AND.JULDAY.LE.9862;
```

FIGURE 2. JOSHUA Information Retrieval. The requested records are for all (SALL) water QUALITY PROFILES in the LAKES data set, for selected STATIONs in PARPOND. The LIST of STATIONs is numbers 2, 5, and 7. Data ELEMENTS desired from the records are JULian DAY number, OBServed value, and DEPth of observation. Only those observations are to be RETRIEVEd which satisfy the conditions that DEPth is Less than Equal to 3 meters, and JULian DAY between 8766 and 9862.

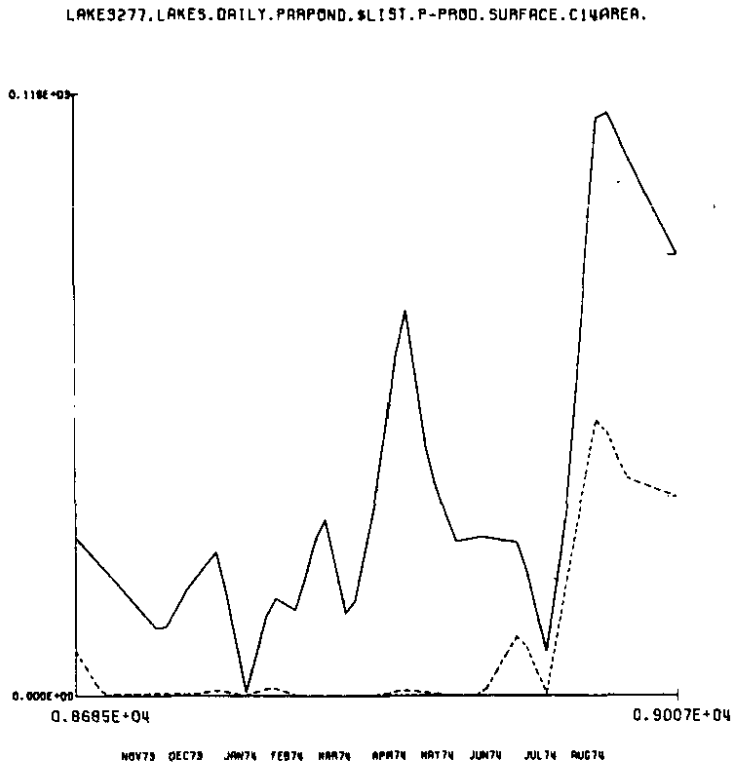

FIGURE 3. Time Series Graphical Display. A comparative (at two stations given $LIST) display of DAILY measurements of primary productivity (P-PROD) at the SURFACE of Carbon-14 fixation (C14AREA). In this case, (X,Y) pairs of (time, observation) are elements of the data records. In other cases, the JUDGES.QUERY system can be utilized to retrieve appropriate (X,Y) values.

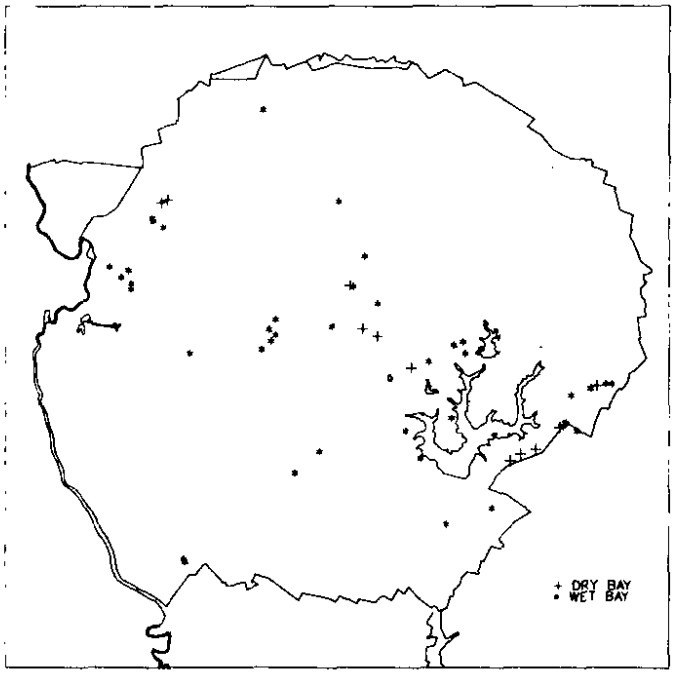

FIGURE 4. SRP Mapping. The user has requested a display of the location Carolina Bays and of ponds that fall within a specified "window" on the SRP site. Cartographic features selected in this case are water bodies and the site boundary. Other available map features include area fences, roads, surveyor's grid lines, streams, secondary roads, etc.

```
JOSHUA INPUT--

SYSTEM=JUDGES.QUERY;
TARGET=DBI;
etc...


SAS INPUT--

PROC GREAD;
etc...
```

FIGURE 5. The upper frame shows an extension to Fig. 2 in which the facilities of the JUDGES.QUERY system are available to extract JOSHUA data for export to the Data Base Interface. The lower frame shows the simplicity of importing this data into a SAS data set, following which all facilities of that system are immediately available.

EXTENSIONS TO THE JEREMIAH ATMOSPHERIC COMPUTATIONAL SYSTEM

M. R. Buckner, F. Beranek, and M. M. Pendergast

A modular environmental transport and dose system, known as JEREMIAH (Buckner, 1977), has been under development to provide a computational framework for transport model evaluation and parametric studies. The objective is to provide a fast-running, reliable system which will provide reasonable estimates of the dose resulting from a chronic or acute radioactive release. More sophisticated models are also being provided in the system to perform generic and scoping studies for use in tuning the simpler model. The overall structure of the JEREMIAH system is shown in Figure 1. New modules in the system include ATSTAB, which determines the atmospheric stability category, and AD2MOM, which solves the three-dimensional advective-diffusion equation.

ATSTAB

Meteorological observations, available from the WIND system as either archived data for chronic releases or current data for accidental releases, are analyzed by ATSTAB to determine the stability category based on Turner's method (Turner, 1964), for airport weather observations. The stability category is then passed to GRIDW for use in adjusting the wind speeds according to the following relation:

$$W_r = W_m \left(\frac{h_r}{h_m} \right)^s$$

where W = the wind speed, at release height, r, and the measurement height, m,

h = height above ground (m),

s = adjustment exponent based on stability category (Crawford, 1976).

Advective wind fields are developed from the meteorological data by the GRIDW module using an objective analysis scheme (Fleming, 1969; Crawford, 1975). Wind fields for three grid networks (grid spacing of 2.5 km, 10 km, and 40 km) centered on the SRP site are developed.

The wind fields and stability category are then passed to either ADPLUM or AD2MOM for calculation of the transport of release material. ADPLUM uses the Gaussian segmented plume model to simulate the atmospheric diffusion process. Plume centerline trajectories are determined by a bilinear interpolation of the wind fields in space and time. The grid point concentrations are determined by applying the Gaussian plume equation based on a time-dependent source at each point in the grid network. The horizontal and vertical Gaussian dispersion coefficients are determined by either the BNL or Briggs (Gifford, 1976) correlations which are presented in Table 1. The spread of the plume between trajectory points is based on the current stability category and the distance traveled during the transport time step.

AD2MOM

The AD2MOM module provides a second option for performing the transport calculation. AD2MOM first performs a mass-consistent wind analysis and then solves the three-dimensional advective-diffusion equation. The GRIDW wind fields are used as first guess fields in a three-dimensional variational procedure to develop mass consistent winds. The two-dimensional wind fields are extrapolated in the vertical, based on a user-specified clockwise twist of the winds as a function of height. The variational procedure based on a Sasake variational treatment of the equation of continuity is then applied to develop three-dimensional wind fields for the transport calculation. The three-dimensional advective-diffusion equation is solved by the method of second moments originally developed by Egan and Mahoney (Egan, 1973) and implemented at SRL (Crawford, 1977). A transformation from the physical domain to a calculational domain (Crawford, 1974) is applied to account for the spacial variation of the mixed-layer height and ground-level elevation (topography).

Using either of the transport options, the pollutant concentrations are accumulated as integrated concentrations by grid point. The calculation then proceeds to the next observation set, and the sequence of calculations is repeated. This procedure is continued for a specified number of observations or until the pollutant is transported beyond the extent of the grid network. The integrated concentrations are then combined with population data by the POPDOS module (Figure 1) to determine the total dose received at any point in the grid network. The overall execution of the modules is the executive module JEM.

FUTURE DEVELOPMENT OF THE JEREMIAH SYSTEM

Evaluation and verification of the models and options provided in the JEREMIAH system have been performed using the SRP

Kr-85 sampler network data. This effort has demonstrated the utility of the JEREMIAH system for model comparison and evaluation. Future plans include the modification of ADPLUM to model dry deposition and to allow specification of a time-dependent mixing-layer height, the incorporation of other numerical algorithms in the three-dimensional transport module for comparison of solution efficiency and accuracy, and increased detail in the modeling of pathways for human exposure and consumption.

REFERENCES

M. R. Buckner. "The JEREMIAH Atmospheric Transport and Dose Computational System,"**Savannah River Laboratory Environmental Transport and Effects Research, Annual Report FY-1977**, DP-1489, E. I. du Pont de Nemours and Co., Savannah River Laboratory, Aiken, SC (1977).

T. V. Crawford. "A Computer Program for Objective Analysis and Display of Meteorological Fields," **Savannah River Laboratory Environmental Transport and Effects Research, Annual Report - 1974**, Report DP-1374, E. I. du Pont de Nemours and Co., Savannah River Laboratory, Aiken, SC (1975).

T. V. Crawford. "Modeling Transport and Dispersion of Pollutants Over Irregular Terrain with Second Moments and Cubic Splines." **Savannah River Laboratory Environmental Transport and Effects Research, Annual Report - 1974**, Report DP-1374, E. I. du Pont de Nemours & Co., Savannah River Laboratory, Aiken, SC (1974).

T. V. Crawford et al. "Power Law Profiles of Mean Winds and Horizontal and Vertical Standard Deviations of Wind Direction at the Savannah River Plant." **Savannah River Laboratory Environmental Transport and Effects Research, Annual Report - 1976**, DP-1455, E. I. du Pont de Nemours and Co., Savannah River Laboratory, Aiken, SC (1976).

T. V. Crawford. "Three-Dimensional Modeling of Pollutant Releases Using Second-Order Moments," **Savannah River Laboratory Environmental Transport and Effects, Annual Report, FY-1977** DP-1489, E. I. du Pont de Nemours and Co., Savannah River Laboratory, Aiken, SC (1977).

B. A. Egan and J. R. Mahoney. "Numerical Modeling of Advection and Diffusion of Urban Area Source Pollutants," **J. Appl. Meteorology**, II, 312-322 (1973).

R. J. Fleming. "AFGWC Fine-Mesh Upper Air Analysis Model," AFGWC Report TM 69-2 (December 1969).

F. A. Gifford. "Turbulent Diffusion - Typing Schemes: A Review," **Nuclear Safety**, Vol. 17, No. 1, pp. 68-86 (1976).

D. B. Turner. "A Diffusion Model for an Urban Area, **J. Appl. Meteorology**, 3 (1): 83-91 (1964).

TABLE 1

Gaussian Dispersion Coefficient Correlations

Stability	Reference	σ_y	σ_z
Stable	Battelle Northwest Laboratories	$0.15\sigma_\theta \cdot \chi^{0.71}$	$0.15\sigma_e \cdot \chi^{0.71}$
Unstable		$0.45\sigma_\theta \cdot \chi^{0.86}$	$0.45\sigma_e \cdot \chi^{0.86}$
1	Briggs	$(0.22X)(1 + 0.0001X)^{-0.5}$	$0.20X$
2		$(0.16X)(1 + 0.0001X)^{-0.5}$	$0.12X$
3		$(0.11X)(1 + 0.0001X)^{-0.5}$	$(0.08X)(1 + 0.0002X)^{-0.5}$
4		$(0.08X)(1 + 0.0001X)^{-0.5}$	$(0.06X)(1 + 0.0015X)^{-0.5}$
5		$(0.06X)(1 + 0.0001X)^{-0.5}$	$(0.03X)(1 + 0.0003X)^{-1}$
6, 7		$(0.04X)(1 + 0.0001X)^{-0.5}$	$(0.016X)(1 + 0.0003X)^{-1}$

Where X - downwind distance (m)

σ_θ - standard deviation of the horizontal wind direction (deg)

σ_e - standard deviation of vertical wind direction (deg)

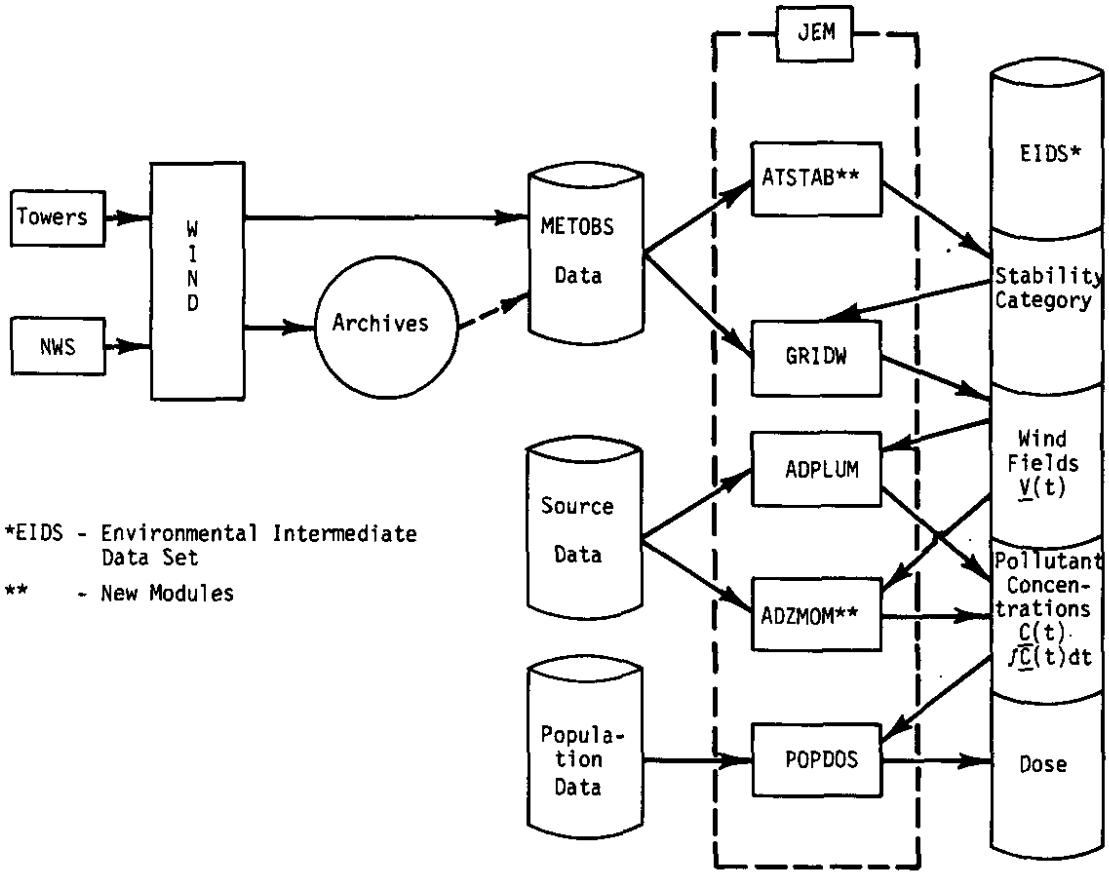

FIGURE 1. JEREMIAH Atmospheric Transport System

MODELING POLLUTANT DISPERSION OVER IRREGULAR TERRAIN WITH SECOND MOMENTS AND CUBIC SPLINES

D. W. Pepper and A. J. Baker*

A general three-dimensional numerical code has been developed to predict pollutant releases when the terrain is irregular and mixing depth varies with time. Advection is calculated with the quasi-Lagrangian scheme of moment distribution within a cell volume. Three-dimensional diffusion is solved with cubic spline interpolation functions. Coordinate transformations and the time-splitting procedure of fractional steps are used to solve the three-dimensional equation set. To ensure that the wind field is mass-consistent, a variational analysis is made with Lagrangian multipliers to adjust the interpolated velocity components throughout the solution domain.

MATHEMATICAL MODEL

For mesoscale analysis, the solution domain is the three-dimensional space bounded by the topography, the mixed height, and a suitable box surrounding the release location. The equations used to account for the terrain-lid variability and surface deposition have been given previously (Reynolds, 1973; Calder, 1968).

In order to specify the wind field throughout the three-dimensional region, a subjective analysis and interpolation scheme is used to calculate a first-guess wind field based on data from instrumented towers and NWS data. A mass-consistent wind field model is then used to calculate corrections to the interpolated wind vectors at each node point such that continuity is satisfied. A Sasaki variational statement is minimized to determine the mass-consistent correction to the initial velocity field. Lagrangian multipliers obtained from the Euler-Lagrangian equations are used to readjust the velocity components.

An O'Brien K-theory model and surface similarity theory are used to determine the diffusion coefficient distribution (O'Brien, 1970; Yu, 1977).

Surface similarity theory is used to calculate K_Z from the Monin-Obukhov universal relations with measured wind velocities and temperatures in the surface layer region ($Z \simeq 60$ m). The

* University of Tennessee

O'Brien cubic profile is then used to calculate the vertical diffusivity above the surface layer region to the top of the mixed layer.

NUMERICAL MODEL

The governing equation of concentration transport is split into two equations such that

$$\frac{\partial(\overline{Z}C)}{\partial t} + \frac{\partial}{\partial x}(U\overline{Z}C) + \frac{\partial}{\partial y}(V\overline{Z}C) + \frac{\partial}{\partial z}(WC) - S\overline{Z} = 0 \qquad (1A)$$

$$\frac{\partial(\overline{Z}C)}{\partial t} = \frac{\partial}{\partial x}\left[K_x \overline{Z} \frac{\partial C}{\partial x}\right] + \frac{\partial}{\partial y}\left[K_y \overline{Z} \frac{\partial C}{\partial y}\right] + \frac{\partial}{\partial z}\left[\frac{K_z}{\overline{Z}} \frac{\partial C}{\partial z}\right] \qquad (1B)$$

where C = concentration

W = f (topography, x, y, z)

S = source/sink term

$\overline{Z}$ = lid height - topography

K = eddy diffusivity

Successive solutions to Equation 1 give the final solution at one time step. A more detailed derivation of Equation 1 is given by Reynolds (1973).

The method of second moments is used to solve Equation 1. The method calculates the zeroth, first, and second moments of the concentration within a mesh and then advects and diffuses the concentration by maintaining conservation of the moments. The moments correspond to the mean concentration, center of mass, and scaled distribution variance (moment of inertia), respectively (Egan, 1972).

Equation 1B is recast as an algebraic equation system using cubic spline interpolation to establish derivatives. The cubic spline method is based on continuous-curvature cubic spline relations used as interpolation functions for the second derivative diffusion terms. Equation 1B can either be solved by time-splitting the equation into three one-dimensional relations (Yanenko, 1970), or solved with a tri-tridiagonal algorithm in an alternating direction sequence.

RESULTS

To assess model accuracy, the advection of a continuous area source was analyzed using a six cell source, each with a unit release advected in a two-dimensional constant wind field. Figure 1 compares numerical predictions to the analytical solution (Pederson, 1974). The results are nearly identical, with computed peak centerline values as well as the width of the plume accurately maintained.

A test or two-dimensional advection-diffusion in the x-y plane is shown in Figure 2 for a continuous area source emission consisting of four cells each containing 250 units. Analytical results were obtained by Christensen and Prahm (1976). Peak centerline values are predicted by the numerical model within 3% (average) of the analytical values. The lateral spread of concentration is nearly identical, deviating by only a few percent within each cell.

The effect of a series of surface irregularities on a continuous elevated emission is shown in Figures 3 and 4. Figure 3 shows the distribution of the ground plane concentration isopleths. The continuous release occurs at a height of 200 m at the left-center cell denoted with a dot (Figure 3a). A 200 m peak surface elevation occurs 11 km downwind from the source. The source rate is equal to 1 g/sec, and the atmospheric stability condition is assumed neutral. The transport coefficients were obtained from Pasquill stability curves at 1000 m distances (Pasquill, 1974). Essentially steady-state concentration isopleths are shown in Figure 3c. For reference, Figure 3d illustrates centerline topography; maximum ground level concentration occurs at the peak elevation.

The effect of this topography is more evident in Figure 4 where ground level centerline C/Q values are plotted as a function of longitudinal distance. The computed solutions in both cases agree reasonably well with the Gaussian plume analytical solution adjusted for topography by Kao (1976).

REFERENCES

K. L. Calder. "The Numerical Solution of Atmospheric Diffusion Equation by Finite Difference Methods." **Dept. of Army Tech. Memo.** 130 (1968).

O. Christensen and L. P. Prahm. "A Pseudospectral Model for Dispersion of Atmospheric Pollutants." **J. Appl. Meteor.** 15, 284 (1976).

B. Egan and I. B. Mahoney. "Numerical Modeling of Advection and Diffusion of Urban Area Source Pollutants." **J. Appl. Meteor. 11,** 312 (1972).

S. K. Kao. "A Model for Turbulent Diffusion Over Terrain." **J. Atmos. Sci. 33,** 157 (1976).

J. J. O'Brien. "A Note on the Vertical Structure of the Eddy Exchange Coefficient in the Planetary Boundary Layer." **J. Atmos. Sci. 27,** 1213-1215 (1970).

F. Pasquill. **Atmospheric Diffusion: The Dispersion of Wind-borne Material from Industrial and Other Sources.** 2nd Edition. John Wiley and Sons, New York (1974).

L. B. Pederson and L. P. Prahm. "A Method for Numerical Solution of the Advestion Equation." **Tellus 26,** 594 (1974).

S. D. Reynolds, P. M. Roth, and J. H. Seinfeld. "Mathematical Modeling of Photochemical Air Pollution-I: Formulation of the Model." **Atmos. Environ. 7,** 1033 (1973).

N. N. Yanenko. **The Method of Fractional Steps. Solution of Problems of Mathematical Physics in Several Variables.** Springer-Verlag, Heidelberg, Germany (1970).

T. Yu. "A Comparative Study of Parameterization of Vertical Turbulent Exchange Processes." **Monthly Weather Rev. 104,** 57 (1977).

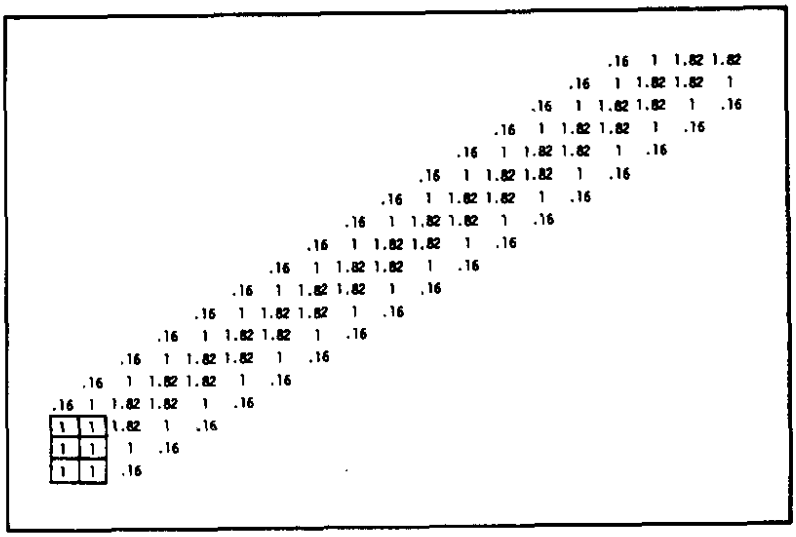

Analytical Solution (Pedersen & Prahm, 1974)

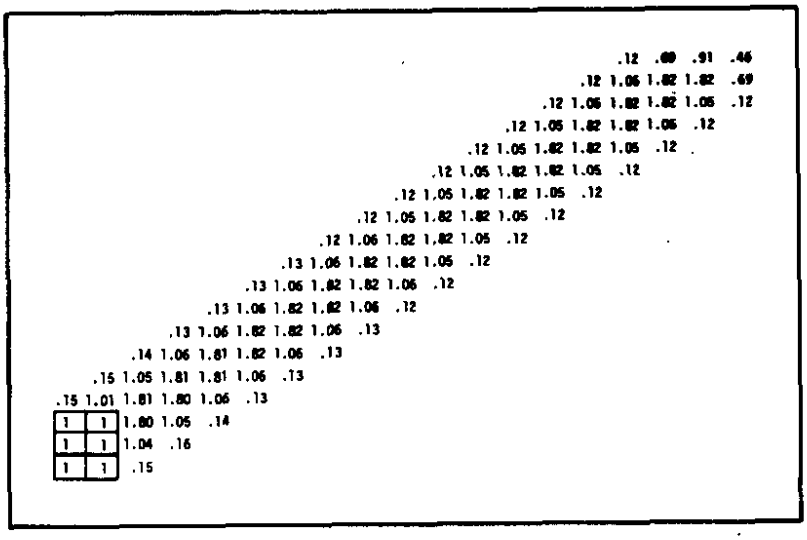

Numerical Solution

FIGURE 1. Advection of an Area Source. Q = 1/cell; U = (1,1,0); $\Delta X = \Delta Y$; $\Delta t = 0.5$.

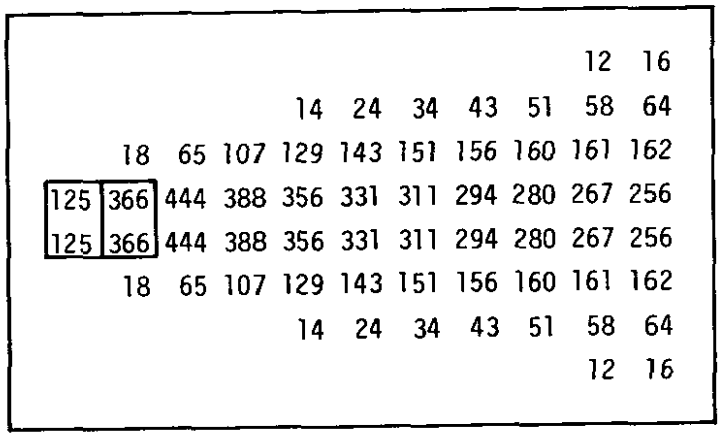

									12	16
				14	24	34	43	51	58	64
	18	65	107	129	143	151	156	160	161	162
125	366	444	388	356	331	311	294	280	267	256
125	366	444	388	356	331	311	294	280	267	256
	18	65	107	129	143	151	156	160	161	162
				14	24	34	43	51	58	64
									12	16

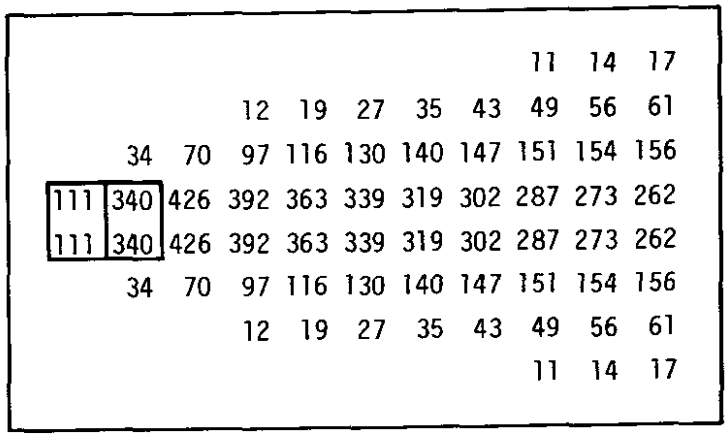

									11	14	17
				12	19	27	35	43	49	56	61
	34	70	97	116	130	140	147	151	154	156
111	340	426	392	363	339	319	302	287	273	262
111	340	426	392	363	339	319	302	287	273	262
	34	70	97	116	130	140	147	151	154	156
				12	19	27	35	43	49	56	61
									11	14	17

(values less than 10 suppressed)

$$c(x,y) = \frac{Q}{1.121x^{\frac{1}{2}}} e^{-\frac{2.5y^2}{x}}$$

Analytical Solution (Christensen & Prahm, 1976)

Numerical Solution

FIGURE 2. Advection-Diffusion from Four Sources. Q = 250/cell; U = (1,0,0); k_y = 0.1; $\Delta X = \Delta Y = 1$; $\Delta t = 0.5$.

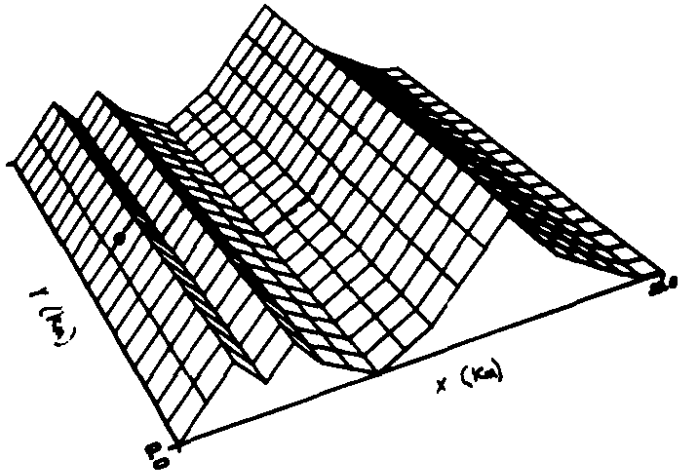

a) Topographic Surface

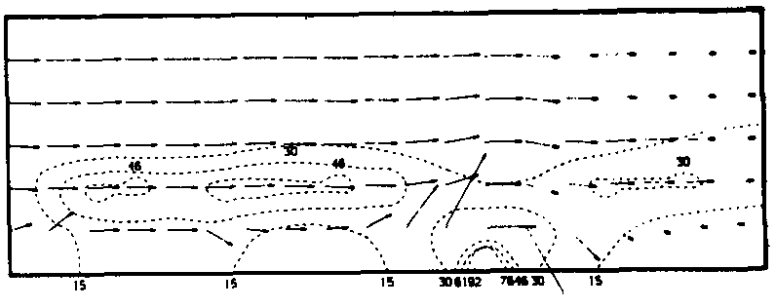

b) Concentration Isopleths at t = 1 hour; Wind Vectors Drawn for Steady State Velocities (Vertical Velocity Component Increased to Enhance Visualization)

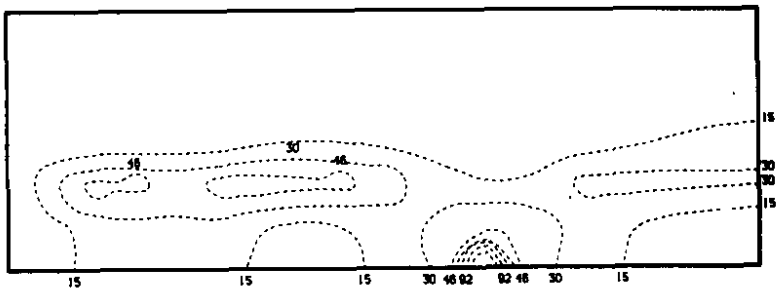

c) Concentration Isopleths at t = 4 hours (~ Steady State)

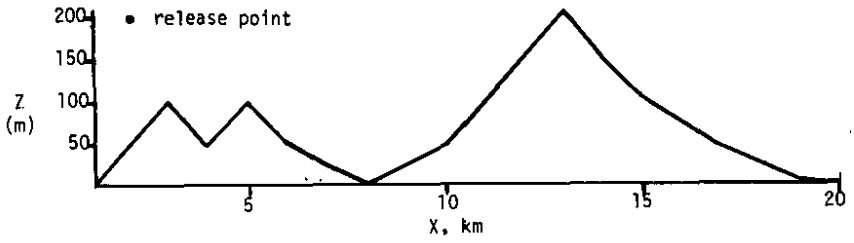

d) Topography in the x-z Plane at y = ½

FIGURE 3. Concentration Isopleths in the §-ρ Plane at n = 1/2 (Dotted Lines Denote C/Q Values in m^{-3})

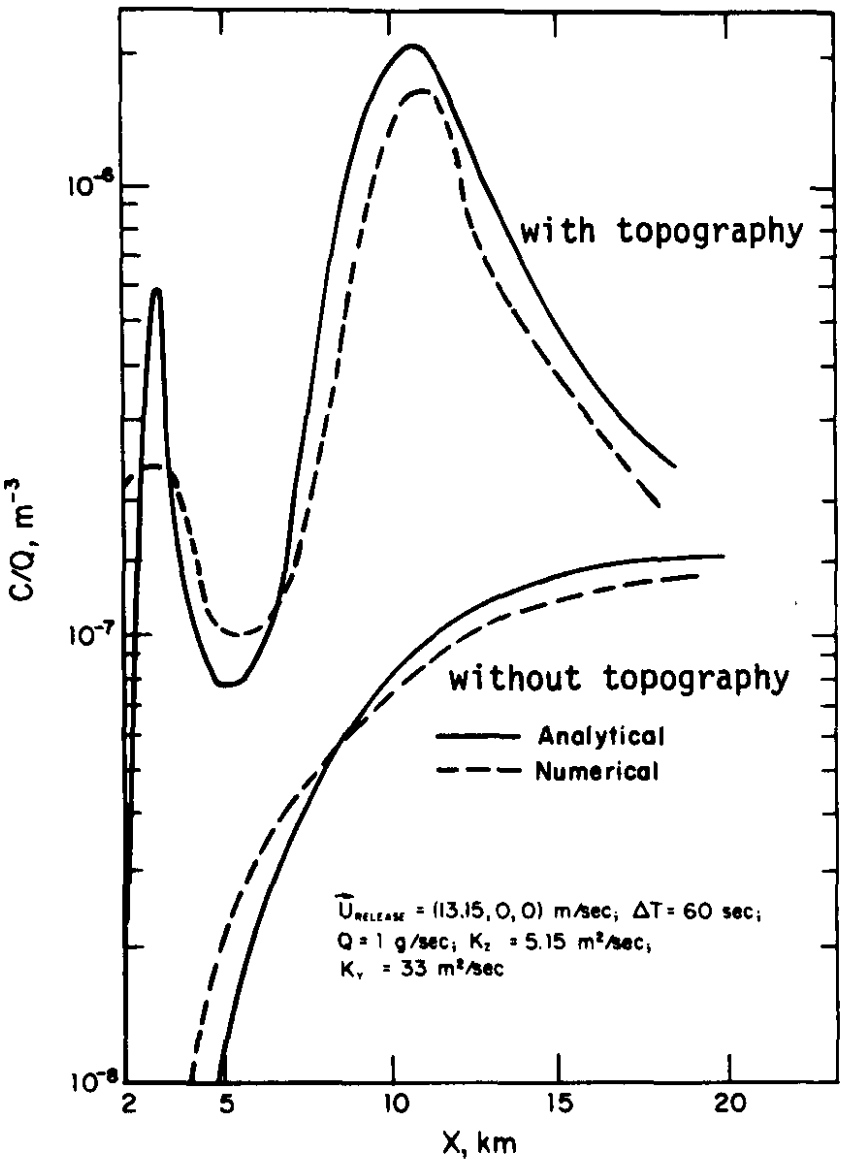

FIGURE 4. Ground Level Centerline C/Q Values With and Without Topography

A SIMPLE FINITE ELEMENT RECURSION RELATION FOR CALCULATING RECIRCULATING FLOW

D. W. Pepper and R. E. Cooper

A time-split finite element recursion relation based on linear interpolation functionals (chapeau functions) has been developed for solving the nonlinear equation of motion for recirculating flow. The relation has the advantages of finite element accuracy and finite difference speed and simplicity. One particular type of recirculating flow problem which has received considerable attention is cavity flow. Experimental, analytical, and numerical results are well known for a wide range of conditions; this problem lends itself to testing and verifying new and improved numerical schemes. This problem is used to test the accuracy and applicability of the time-split finite element recursion algorithm to describe fluid motion. Results from the test problems show good agreement with other methods reported in the literature. The speed and ease of application of this method makes its use in three-dimensional environmental calculations promising.

PROBLEM

We shall consider the laminar motion in an incompressible, constant-property, Newtonian fluid in a square cavity. The flow in the square cavity is induced by the top wall moving in its own plane. Figure 1 shows the physical geometry of the problem.

The governing equations are expressed as follows:

$$\nabla^2\psi = -\omega \tag{1}$$

$$\frac{\partial\omega}{\partial t} + \frac{\partial u\omega}{\partial x} + \frac{\partial v\omega}{\partial y} = \frac{1}{Re}\nabla^2\omega \tag{2}$$

$$u = \frac{\partial\psi}{\partial y},\quad v = -\frac{\partial\psi}{\partial x} \tag{3}$$

where ψ, u, v, and ω are dimensionless streamfunction, horizontal and vertical velocity components, and vorticity, respectively; Re

denotes the Reynolds number. The boundary conditions to be satisfied are:

$$u(o,y) = u(1,y) = v(x,o) = x(x,1) = 0$$

$$u(x,1) = 1$$

Equation 1 is solved by the cyclic reduction technique as used by Pepper and Harris (1977). Equation 2 is solved by the method of fractional steps and the finite element recursion relation. The recursion relation is based on the linear basis functional algorithm derived by Pepper and Baker (1979) for the one-dimensional advection-diffusion equation. For equal element length and constant velocity, the relation is fourth-order accurate in space.

The basic recursion relation for one-dimensional horizontal transport is written in the form

$$[\dot{\phi}_{i-1} + 4\dot{\phi}_i + \dot{\phi}_{i+1}] + \frac{1}{\Delta x}[\dot{\phi}_{i-1}(-u_{i-1}-2u_i) + \dot{\phi}_i(u_{i-1}-u_{i+1}) +$$

$$\dot{\phi}_{i+1}(2U_i + u_{i+1})] + \frac{6k}{\Delta x^2}[-\phi_{i-1} + 2\phi_i - \phi_{i+1}] + F = 0 \qquad (4)$$

where F is a body force term, u_i is the velocity at node point i, ϕ is vorticity, $\dot{\phi}$ denotes a time derivative, i-1, i, and i+1 are node point locations, and k is 1/Re.

In order to reduce numerical dispersion errors associated with solution of Equation 4, the inertia terms are modified to

$$\left[\left(\frac{\Delta x}{6} + \frac{\rho}{2}\right)\dot{\phi}_{i-1} + \frac{2\Delta x}{3}\dot{\phi}_i + \left(\frac{\Delta x}{6} - \frac{\rho}{2}\right)\dot{\phi}_{i+1}\right] +$$

$$\frac{2}{\Delta x}\left[\phi_{i-1}\left\{-u_{i-1} - 2u_i + \frac{\rho}{2}\left(\frac{u_i+u_{i-1}}{\Delta x}\right)\right\} + \phi_i\left\{u_{i-1} - u_{i+1} + \right.\right.$$

$$\left.\left.\frac{\rho}{2}\left(\frac{u_{i+1}+2u_i+u_{i-1}}{\Delta x}\right)\right\} + \phi_{i+1}\left\{2u_i+u_{i+1} - \frac{\rho}{2}\left(\frac{u_i+u_{i+1}}{\Delta x}\right)\right\}\right] +$$

remaining terms (5)

where ρ is a dissipation parameter with $\rho = \rho(\Delta x)$. This particular filtering scheme was employed by Raymond and Garder (1976) to reduce troublesome dispersive waves in telescoping meshes; ρ acts as

an artificial diffusion coefficient $O(\Delta x^3)$ which damps short waves while minimally affecting the desired long wave distribution.

Equation 5 is solved with the Thomas algorithm.

RESULTS

Solutions to the equation set for laminar recirculating flow in a square cavity were obtained for Reynolds numbers of 100, 400, and 1000. In all three test cases, a grid (element) spacing of 1/20 was used with $t = .001$, $\rho = .001$, and a 21 x 21 mesh. Figures 2(a,b,c) show contours of streamfunction and velocity vectors. Streamfunction and vorticity values at the primary vortex centers for $100 \leq Re \leq 1000$ are in good agreement with results obtained by others (Bozeman, 1973; Tuann, 1978; Burggraf, 1966; Nallasamy, 1977). Specific values are compared in Table 1.

REFERENCES

J. D. Bozeman and C. Dalton. "Numerical Study of Viscous Flow in a Cavity." **J. Comp. Phys. 12**, 348 (1973).

O. R. Burggraf. "The Structure of Steady Separated Flows." **J. Fluid Mech. 24**, 113,151 (1966).

M. Nallasamy and K. Krishna Prasad. "On Cavity Flow at High Reynolds Numbers." **J. Fluid Mech. 79, Part 2**, 391-414 (1977).

D. W. Pepper and A. J. Baker. "A Simple One-Dimensional Finite Element Algorithm with Multi-Dimensional Capabilities," **Num. Heat Transfer 1**, 1-10 (1979).

D. W. Pepper and S. D. Harris. "Numerical Simulation of Natural Convection in Closed Containers by a Fully Implicit Method." **J. Fluids Engr. 99 (1) 4**, 649 (1977).

W. H. Raymond and A. Garder. "Selective Damping in a Galerkin Method for Solving Wave Problems with Variable Grids." **Monthly Weather Rev. 104**, 1583-1590 (1976).

Shih-Yu Tuann and M. D. Olson. "Review of Computing Methods for Recirculating Flows." **J. Comp. Phys. 29, 1-19** (1978).

TABLE 1

Square Cavity Flow Comparisons

Re	Reference	Grid	Primary Vortex ψ	Primary Vortex ω
100	Tuann (1978)	8 x 8	0.1035	3.098
	Bozeman (1973)	51 x 51	0.1032	---
	Present	21 x 21	0.1051	2.957
	Burggraf (1966)	41 x 41	0.1015	3.14
400	Tuann (1978)	8 x 8	0.1168	2.415
	Present	21 x 21	0.1008	2.070
	Burggraf (1966)	41 x 41	0.1017	2.142
1000	Tuann (1978)	8 x 8	0.1299	2.653
	Bozeman (1973)	51 x 51	0.081	---
	Nallasamy (1977)	51 x 51	0.0977	0.0
	Present	21 x 21	0.0804	1.5

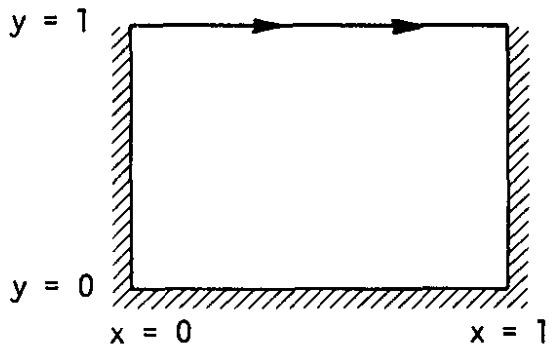

Rectangular cavity

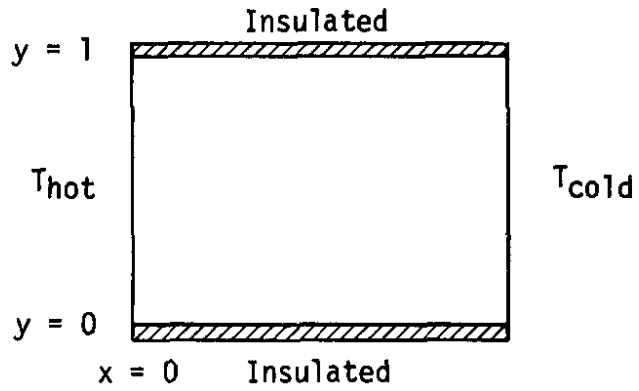

Enclosed container

FIGURE 1. Physical Geometries

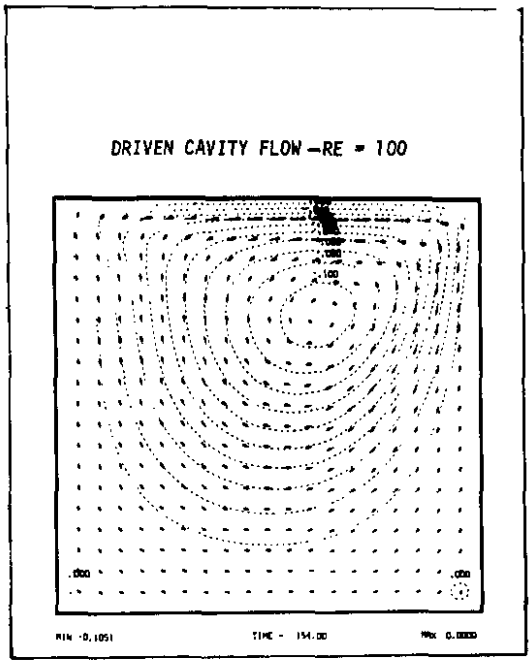

FIGURE 2a. Driven Cavity Flow
Re = 100

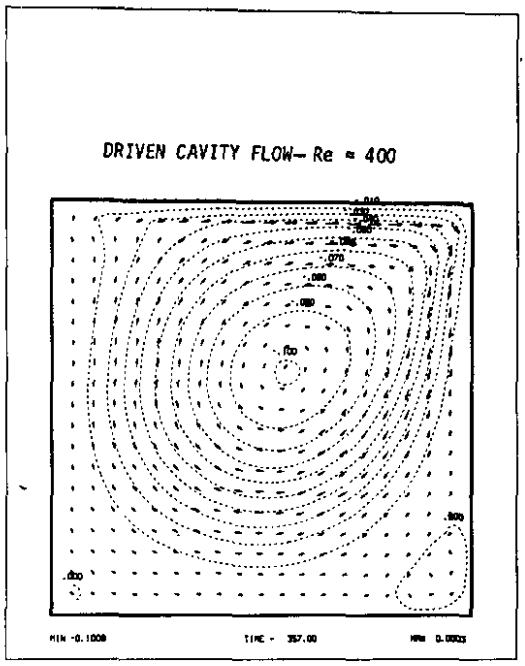

FIGURE 2b. Driven Cavity Flow
Re = 400

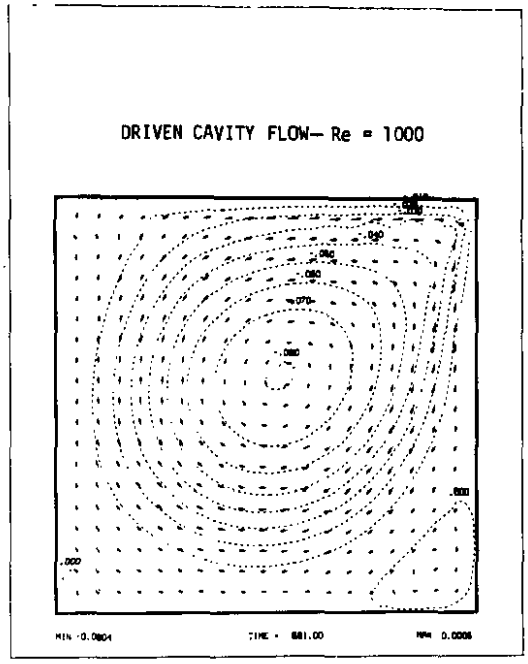

FIGURE 2c. Driven Cavity Flow
Re = 1000

THE SOLUTION OF COUPLED PARTIAL DIFFERENTIAL EQUATIONS USING A TRI-TRIDIAGONAL SOLUTION ALGORITHM

R. E. Cooper

A computer method has been developed to solve systems of equations where there are three unknowns at each node point. The three unknowns are expressed as a coupled system of three equations, and in finite difference form each equation is tridiagonal. The result is a tri-tridiagonal system of equations which are solved by an algorithm obtained from von Rosenberg (1971). Test problem results have been obtained which agree well with results in the literature.

DISCUSSION

In the study of two- and three-dimensional flow fields associated with the advective transport and diffusion of fluids, one may often encounter systems of coupled partial differential equations. In environmental applications, this situation may arise when describing flow fields to determine wake effects and particle trajectories induced by obstacles in a flow path. It may also arise because of numerical methods used to solve partial differential equations. In some instances, there are three unknowns to be solved for at each node of a numerical scheme. In this case it becomes advantageous to use the tri-tridiagonal solution algorithm (von Rosenberg, 1971) to facilitate a solution of the problem.

The tri-tridiagonal system of equations may be expressed in matrix form as:

$$A_i \phi_{i-1}^{n+1} + B_i \phi_i^{n+1} + C_i \phi_{i+1}^{n+1} = D_i^n \qquad (1)$$

where A, B, and C represent 3 x 3 matrices of coefficients, the ϕ's are column vectors in the unknown variable, and D is a known column vector. The subscripts designate node points, and the equation represents a single row or column in the unknown variable ϕ.

Classical problems of fluid flow are often used to evaluate numerical solution techniques. Two problems for which there

exists a large amount of data in the literature are the driven cavity and free convection flow problems. These are used to test the technique presented here and demonstrate two different applications of the tri-tridiagonal algorithm. The first requires the solution of three unknowns due to the choice of the solution method. The second application solves for three different physical parameters.

DRIVEN CAVITY PROBLEM

The first problem studied was the advection and transport of vorticity within a cavity driven by a constant velocity at the upper boundary. This method, after Rubin and Graves (1976), uses cubic splines to determine node point first and second derivatives in the unknown variable. The finite difference form of the system of equations solved for a given row i in this case is

$$\omega_i^{n+1} = \omega_i^n + \frac{\Delta t}{2}\left[u_i m_i^{n+1} + v_i \ell_i^n + \frac{1}{Re}\left(M_i^{n+1} + L_i^n\right)\right]$$

$$m_{i-1}^{n+1} + 2m_i^{n+1} + m_{i+1}^{n+1} = \frac{3}{h}\omega_{i+1}^{nH} - \frac{3}{h}\omega_{i-1}^{n+1} \qquad (2)$$

$$M_{i-1}^{n+1} + 2M_i^{n+1} + M_{i+1}^{n+1} = \frac{6}{h^2}\omega_{i+1}^{n+1} - \frac{12}{h^2}\omega_i^{n+1} + \frac{6}{h^2}\omega_{i-1}^{n+1}$$

where ω is the vorticity, m and M are first and second derivatives, u and v are horizontal and vertical velocities, and h is the mesh width. First and second derivatives in the vertical are denoted by ℓ and L and are assumed known when sweeping horizontally. The entire mesh is alternately swept horizontally and then vertically. It is to be noted that Equation 2 may be cast in the same form as Equation 1. The solution of Equation 2 is an iterative process in which steady state is reached.

The advantage of the cubic spline approach as solved by the tri-tridiagonal method is improved accuracy over standard finite difference methods. A disadvantage is the fact that the tri-tridiagonal solution algorithm requires the same amount of time whether the system to be solved is loosely or tightly coupled. In this case the matrices A, B, C, and D are about 50% full.

FREE CONVECTION FLOW PROBLEM

The other problem studied by this method is similar to the first, but in this case the flow is totally enclosed within a

cavity. The flow is driven by buoyancy resulting from heating one side of the enclosure. Required solutions in this case are for vorticity, temperature, and streamfunction. The equations solved are:

$$\frac{\partial w}{\partial t} + u\frac{\partial w}{\partial x} + v\frac{\partial w}{\partial y} - Pr\left(\frac{\partial^2 w}{\partial x^2} + \frac{\partial^2 w}{\partial y^2}\right) - RaPr\frac{\partial T}{\partial x} = 0 \qquad (3a)$$

$$\frac{\partial T}{\partial t} + u\frac{\partial T}{\partial x} + v\frac{\partial T}{\partial y} - \frac{\partial^2 T}{\partial x^2} - \frac{\partial^2 T}{\partial y^2} = 0 \qquad (3b)$$

$$\frac{\partial \psi}{\partial t} + \frac{\partial^2 \psi}{\partial x^2} + \frac{\partial^2 \psi}{\partial y^2} + w = 0 \qquad (3c)$$

where Ra is the Raleigh number, Pr is the Prandtl number, T is the temperature, and ψ is the streamfunction. The time derivative for ψ is an artifact to obtain the transient solution as a system of parabolic equations; this is a very loosely coupled system since there is no coupling between Equations 3b and 3c. However, the solution does converge quite rapidly using the tri-tridiagonal method.

Results from these test problems show good agreement with solutions obtained in the literature. This solution method will be used and tested against environmental data for further evaluation.

REFERENCES

D. V. von Rosenberg. **Methods for the Numerical Solution of Partial Differential Equations.** American Elsevien Publishing Company, Inc., New York (1971).

S. G. Rubin and R. A. Graves, Jr. **A Cubic Spline Approximation for Problems in Fluid Mechanics.** NASA TR R-436, (October 1976).

ENVIRONMENTAL CHEMISTRY STUDIES

DISTRIBUTION OF IODINE-129 RELEASED FROM SRP IN SOIL AS A FUNCTION OF DISTANCE

T. J. Anderson

The impact of SRP airborne ^{129}I emissions is distinguishable from background at distances of 160 km from the source with a high sensitivity neutron activation analysis. An existing probability distribution model based on 2 years of meteorological data provides a reasonable estimate of ^{129}I deposition as a function of direction and distance. The vertical distribution of ^{129}I in the sandy clay soils indicates slow vertical transport, implying a long residence time in regions of the soil which are subject to agricultural activity.

ANALYSIS AND SAMPLING METHODS

A high sensitivity neutron activation analysis (detection level = 3.8 fCi) (Currie, 1968) was used to determine the long-lived fission product ^{129}I in vegetation-litter and soil along two azimuths from SRP. Natural iodine (^{127}I) was also determined by the method. Based on predictions of the CHIDIS wind dispersion model, the azimuths were selected for minimum and maximum transport of ^{129}I.

Samples were taken at four distances along each azimuth with particular attention to the following: whenever possible, the number of each type of sample collected at a site was large enough (maximum of 10) to form a good representative composite. The sampling techniques defined the area of each sample allowing easy comparison with the dispersion model. Finally, soil core processing techniques were developed which eliminated the problem of vertical cross-contamination resulting from driving the core tubes into the ground.

RESULTS

Data from analysis of the samples appears in Tables 1 and 2. Table 1 represents the maximum transport direction, and Table 2, the minimum. The log of the ^{129}I area concentration (amount of ^{129}I in a soil layer, 1 m^2 in area and 2.5 cm thick) was empirically related to depth by a least squares fit (Figure 1). Integration of each resultant equation to an infinite soil depth gives a

finite value representing the total amount of ^{129}I deposited on a unit area of soil. Adding the vegetation-litter area concentration results in an estimate of the total unit area deposition of ^{129}I. The total ^{129}I area deposition for each site is plotted as a function of distance from the source in Figure 2. Also included are the corresponding CHIDIS predictions based on an assumed average release rate of 6×10^{-9} Ci/sec of ^{129}I for 21 years and a nominal deposition velocity of 0.01 m/sec.

Both the maximum and minimum transport data describe curves of the same general shape that the model predicts. The maximum transport data describe a smooth curve with little scatter. On the other hand, considerable scatter is seen in the minimum transport data. The 19- and 79-km sites of the minimum transport azimuth were unlike the remaining sites because they lacked forestation; the 19-km site was a forest clearing, and the 79-km site was a pasture. All other sites were well forested. The low ^{129}I area concentrations of the two unique sites may be largely due to the lower efficiencies of nonforested sites for collection of airborne pollutants (Rickard, 1974). The remaining six sites could be described reasonably well by a single curve. The agreement with the model is quite acceptable when the uncertainties in assumed deposition velocities and historical emission rates are considered.

The rapid decrease of ^{129}I concentration with increasing soil depths -- half-depths on the order of 8 cm were found -- indicates slow vertical transport on the time scale of emission. This in turn implies continued accumulation of ^{129}I in layers of soil which are subject to agricultural activity. However, $^{129}I/^{127}I$ atom ratios in all soil samples in this study were orders of magnitude below the limiting specific activity calculated for the maximum permissible thyroid burden (Palms, 1974).

REFERENCES

L. A. Currie. "Limits for Qualitative Detection and Quantitative Determination: Application to Radiochemistry." **Anal. Chem. 40,** 586 (1968).

J. M. Palms and V. R. Veluri. **Summary of the Analysis Associated with the Environmental Impact of ^{129}I Released by the Barnwell Nuclear Plant.** EMP-122, Emory University, Atlanta, GA (1974)

W. H. Rickard, D. G. Watson, Betty Klepper, J. F. Cline, J. F. Brauer, and J. E. Fager. **Iodine-129 in Soil and Vegetation in the Environs of Nuclear Fuel Reprocessing Plants.** USAEC Report BNWL-1850, PT2, Battelle Pacific Northwest Laboratories, Richland, WA (1974).

TABLE 1

^{129}I and ^{127}I in Vegetation-Litter and Soil Samples
103°C Azimuth - Direction of Maximum Predicted Transport

Distance From Source (km)	*Layer Depth (cm)*	^{129}I *(pCi/m²)*	^{127}I *(mg/m²)*	$^{129}I/^{127}I$ *Atom Ratio*
19	Veg-Litter	3.8 ±0.2	2.0 ±0.1	(11 ±0.8) × 10^{-6}
19	0 - 2.7	20.4 ±0.6	18 ±1	(6.7 ±0.4) × 10^{-6}
19	15.2 - 17.9	4.4 ±0.2	32 ±1	(0.81 ±0.04) × 10^{-6}
19	30.5 - 33.2	1.5 ±0.2	47 ±2	(0.19 ±0.03) × 10^{-6}
19	61.0 - 63.7	-0.06 ±0.3	55 ±4	-
48	Veg-Litter	0.80 ±0.06	1.4 ±0.1	(3.4 ±0.3) × 10^{-6}
48	0 - 2.7	6.8 ±0.4	18 ±1	(2.2 ±0.2) × 10^{-6}
48	15.2 - 17.9	1.7 ±0.2	39 ±2	(0.26 ±0.03) × 10^{-6}
48	30.5 - 33.2	0.8 ±0.1	37 ±2	(0.12 ±0.02) × 10^{-6}
48	61.0 - 63.7	0.3 ±0.3	51 ±3	-
84	Veg-Litter	0.21 ±0.02	0.76 ±0.03	(1.6 ±0.2) × 10^{-6}
84	0 - 2.7	5.7 ±0.2	35 ±2	(0.96 ±0.06) × 10^{-6}
84	15.2 - 17.9	0.68 ±0.07	57 ±3	(0.070 ±0.008) × 10^{-6}
84	30.5 - 33.2	0.19 ±0.07	63 ±3	(0.018 ±0.007) × 10^{-6}
84	61.0 - 63.7	0.2 ±0.3	52 ±3	-
159	Veg-Litter	0.11 ±0.04	1.0 ±0.1	(0.6 ±0.2) × 10^{-6}
159	0 - 2.7	1.2 ±0.2	40 ±2	(0.18 ±0.03) × 10^{-6}
159	15.2 - 17.9	0.17 ±0.06	56 ±3	(0.018 ±0.003) × 10^{-6}
159	30.5 - 33.2	0.2 ±0.2	80 ±3	-
159	61.0 - 63.7	0.7 ±0.4	49 ±3	(0.008 ±0.005) × 10^{-6}

TABLE 2

^{129}I and ^{127}I in Vegetation-Litter and Soil Samples
170° Azimuth - Direction of Minimum Predicted Transport

Distance From Source (km)	*Layer Depth (cm)*	^{129}I *(pCi/m²)*	^{127}I *(mg/m²)*	$^{129}I/^{127}I$ *Atom Ratio*
19	Veg-Litter	0.29 ±0.02	0.52 ±0.03	(3.3 ±0.3) × 10^{-6}
19	0 - 2.5	6.6 ±0.3	17 ±0.5	(2.3 ±0.04) × 10^{-6}
19	16.8 - 19.6	1.2 ±0.2	41 ±1	(0.17 ±0.03) × 10^{-6}
19	33.3 - 36.1	0.24 ±0.08	47 ±1	(0.03 ±0.01) × 10^{-6}
19	66.5 - 69.3	0.1 ±0.1	29 ±0.5	-
40	Veg-Litter	0.56 ±0.05	1.6 ±0.02	(2.1 ±0.2) × 10^{-6}
40	0 - 2.6	9.1 ±0.4	14 ±0.2	(3.8 ±0.2) × 10^{-6}
40	15.7 - 18.4	1.8 ±0.1	40 ±1	(0.27 ±0.02) × 10^{-6}
40	31.5 - 34.1	0.38 ±0.05	40 ±1	(0.056 ±0.008) × 10^{-6}
40	63.0 - 65.6	0.40 ±0.09	173 ±2	(0.014 ±0.003) × 10^{-6}
79	Veg-Litter	0.006 ±0.004	0.1 ±0.001	-
79	0 - 2.9	0.66 ±0.08	24 ±0.3	(0.16 ±0.02) × 10^{-6}
79	17.1 - 20.0	0.13 ±0.08	46 ±1	(0.016 ±0.010) × 10^{-6}
79	34.3 - 37.1	0.15 ±0.08	64 ±1	(0.014 ±0.007) × 10^{-6}
79	68.6 - 71.4	0.16 ±0.08	68 ±2	(0.014 ±0.007) × 10^{-6}
150	Veg-Litter	0.04 ±0.02	1.1 ±0.01	(0.21 ±0.11) × 10^{-6}
150	0 - 2.8	0.7 ±0.1	NA[a]	-
150	16.9 - 19.7	0.21 ±0.06	50 ±1	(0.025 ±0.007) × 10^{-6}
150	33.8 - 36.6	0.05 ±0.04	40 ±1	-
150	67.5 - 70.3	0.05 ±0.03	27 ±1	(0.011 ±0.007) × 10^{-6}

a. NA = not analyzed

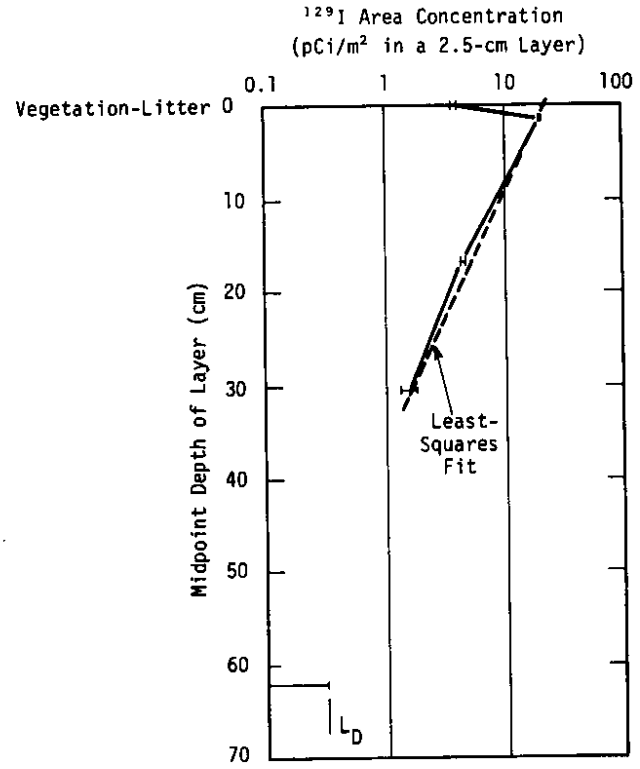

FIGURE 1. ^{129}I Area Concentration Versus Depth for 19-km Site - 103°C Azimuth

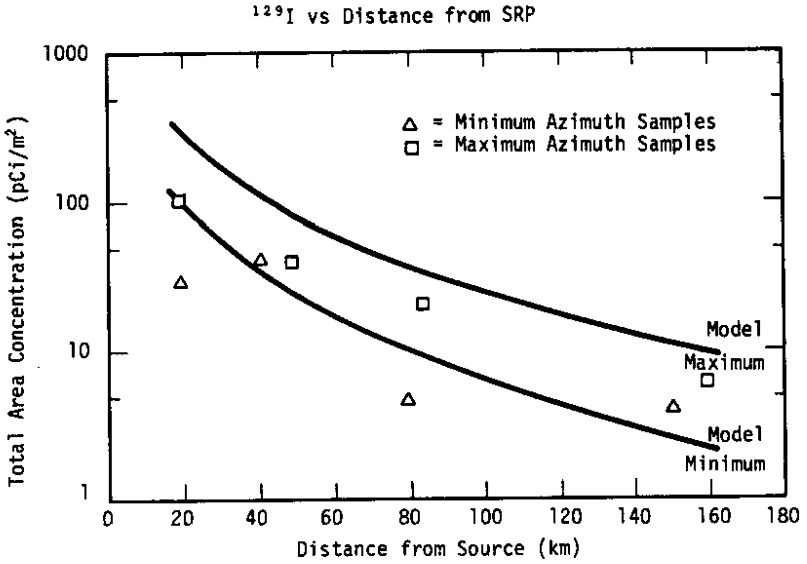

FIGURE 2. ^{129}I Area Concentration Versus Distance from SRP Reprocessing Areas

METHODOLOGY FOR THE DETERMINATION OF ENVIRONMENTAL TECHNECIUM-99

T. J. Anderson

A mass spectrometric isotope dilution technique has been developed with ^{97}Tc as a yield tracer to measure as little as 0.1 pg of environmental ^{99}Tc. A unique aspect of the method is loading the sample into the mass spectrometer in the form of a single ion-exchange resin bead, thereby improving the signal-to-noise ratio over conventional solution loading. Application of a modified method has detected ^{99}Tc in samples from around SRP's seepage basins and has confirmed its high mobility in the local wafer saturated soil.

INTRODUCTION

Technecium-99, a long-lived ($t_{1/2}$ = 2.1 x 10^5 years) fission product produced in high yield (6.3% from ^{235}U), is environmentally important because of its potential to accumulate and move through soil under certain circumstances (Brown, 1967; Routson, 1977). Pathways to man are not well defined, and certain quantitative aspects are controversial (Till, 1978). While the behavior of Tc in the human body has been studied with regard to acute doses of ^{99m}Tc used for medical diagnostic purposes (Beasley, 1966; Shukla, 1977; Baumann, 1956), very little is known about long-term uptake of environmental forms (Sodd, 1968).

Direct counting of environmental levels of ^{99}Tc is difficult because of its low specific activity and emission of only low-energy beta particles. Surface ionization mass spectrometry provides a sensitive and specific alternative measurement technique. A chemical procedure is required to rid ^{99}Tc of potential interferences and to convert it to a form suitable for mass spectrometry. In addition, ^{97}Tc must be added to allow correction for losses in the isolation and measurement steps.

METHOD

The procedure involves adding ^{97}Tc, ion-exchange purification, ambient temperature evaporative concentration under vacuum, two stages of ion-association solvent extraction, and uptake by a pair of single ion-exchange beads. For solid samples, fusion and solvent extraction steps precede the ion-exchange purification. Evaluation trials with ^{99}Tc standards produced recoveries of 32 to 64% from ion exchange through resin bead uptake. Decontamination

from naturally occurring ^{97}Mo and ^{99}Ru, potential interferences in the measurement of ^{97}Tc and ^{99}Tc, has been good enough to allow detection of 0.1 pg of ^{99}Tc. (A nonfundamental instrument limitation prevents detection of smaller amounts.) Single resin bead loading has increased the mass spectrometric ^{99}Tc ionization efficiency an average of 50-fold compared to conventional solution loading, promising a proportional increase in the method's sensitivity.

Concurrently with development of the method's chemistry, 460 ng of commercially unavailable ^{97}Tc was isolated from neutron-irradiated ^{96}Ru. This amount is sufficient for about 500 analyses.

RESULTS

Application of the isolation scheme coupled with liquid scintillation counting to high concentration aqueous environmental samples taken from SRP's seepage basin system has confirmed the high mobility of ^{99}Tc in water-saturated soil. Samples from seepage basins F-3 and H-4 contained 0.7 and 0.1 nCi/L of ^{99}Tc, while samples from a spring fed by F-3 that was 1700 ft away contained 0.2-0.3 nCi/L.

REFERENCES

D. J. Baumann, N. Z. Searle, A. A. Yalow, E. Siegel, and S. M. Seidlin. "Behavior of the Thyroid Toward Elements of the Seventh Periodic Group." **Am. J. of Physiology 185**, 71 (1956).

T. M. Beasley, H. E. Palmer, and W. B. Nelp. "Distribution and Excretion of Technetium in Humans." **Health Physics 12**, 1425 (1966).

D. J. Brown. "Migration Characteristics of Radionuclides Through Sediments Underlying the Hanford Reservation." **Disposal of Radioactive Wastes into the Ground**, 215, Vienna, IAEA (1967).

R. C. Routson, G. Jansen, and A. V. Robinson. "^{241}Am, ^{237}Np, and ^{99}Tc Sorption on Two United States Subsoils from Differing Weathering Intensity Areas." **Health Physics 33**, 311 (1977).

S. K. Shukla, G. B. Manni, and C. Cipriani. "Behaviour of Pertechnetate Ion in Humans." **J. of Chromatography 143**, 522 (1977).

V. J. Sodd and B. J. Jacobs. "Analysis of Human Thyroids for ^{99}Tc." **Health Physics 14**, 593 (1968).

J. E. Till, F. O. Hoffman, and D. E. Dunning, Jr. "Assessment of ^{99}Tc Releases to the Atmosphere - A Plea for Applied Research." ORNL/TM-6260, Oak Ridge National Laboratory, Oak Ridge, Tennessee (1978).

THE PHYSICAL AND CHEMICAL CHARACTERISTICS OF PLUTONIUM-BEARING PARTICLES RELEASED TO THE ATMOSPHERE FROM THE SAVANNAH RIVER NUCLEAR FUEL REPROCESSING PLANT

S. M. Sanders

In this study, particulate plutonium released to the atmosphere from the 291-F stack was found to be carried on aggregates composed mainly of crustal materials which have a geometric mean diameter of 5.4 μm. About 10^6 of these particles containing an average of less than 1 fCi of ^{239}Pu per particle are released to the atmosphere per minute. This gives an average concentration in the off-gas of about 5 plutonium-bearing particles/ft^3.

METHOD

A method developed at SRL was used to identify and study individual plutonium-bearing airborne particles by using their fission-fragment and alpha-particle tracks made in a polycarbonate film with a nuclear-track emulsion coating. Membrane filters, used to collect the particles from atmospheric effluents, were cast into films composed of a polycarbonate matrix containing the particles. When a particle was located, the amount of ^{239}Pu was determined by counting the tracks, isolating a small portion of the film containing the particle, removing the emulsion, dissolving the polycarbonate, oxidizing the track replicas, and analyzing the elemental composition of the ^{239}Pu-bearing particle by an electron microprobe.

RESULTS

Most of the collected particles were composed of aggregates of crustal materials. Of the particles, 3.6% were organic and 1.7% were metallic (iron, chromium, and nickel). High enrichment factors for titanium, manganese, chromium, nickel, zinc, and copper were evidence of the anthropogenic nature of some of the particles. The amount of plutonium in most particles was very small (<1 fCi). Thus plutonium concentrations had to be determined by the fission track counting method. Only one particle contained sufficient plutonium for detection by electron microprobe analysis. This was a 1-μm-diameter particle containing 73% PuO_2 by weight (estimated to be 170 fCi of ^{239}Pu) in combination with Fe_2O_3 and mica. The plutonium-bearing particles were generally

larger than natural aerosols. The geometric mean diameter of those collected from the mechanical line exhaust was larger than that of particles collected from the wet cabinet exhaust (12.3 μm vs. 4.6 μm). Particles from the mechanical line also contained more plutonium per particle than those from the wet cabinets. The amount of plutonium per particle decreased with the distance of each sampling point from the mechanical line.

The size and ^{239}Pu content distribution among particles collected from the sand filter effluent and at the 50-ft level of 291-F stack were almost the same. The geometric mean and standard deviation of the diameter of ^{239}Pu-bearing particles at the 50-ft level was 5.43 ÷ 2.69 μm. The relatively large size of these particles is believed due to coagulation of submicrometer particles by thermal and turbulent mechanisms to form larger agglomerates. The elemental composition of these particles, which contain very small amounts of plutonium in combination with crustal elements not used in the recovery process, supports this assumption. Scanning electron micrographs also show these particles to be agglomerates of smaller dissimilar particles.

Fleischer and Raabe (1977) have observed alpha-decay-induced fragmentation of $^{239}PuO_2$ particles probably caused by the heavy, recoiling nuclei. When suspended in water, these particles produced fragments, or subparticles, which contained from 50 to 10,000 ^{239}Pu atoms, the abundance of which follows a lower-law relation with the largest particles being the least abundant. The possibility exists that PuO_2 particles, large enough to be trapped on HEPA filters, fragmented due to alpha decay. The small fragments then passed through the filters where they coagulated with dust composed of crustal elements. The larger dust particles did not pass through the HEPA filters, but entered the exhaust system through leaks in the ducts illustrated in Figure 1. Such leaks would be undetected as long as the exhaust system remained under negative pressure with respect to the atmosphere.

The geometric mean and standard deviation of the number of fission fragment tracks per ^{239}Pu-bearing particle collected from the 50-ft level during July, August, and September 1977 were 17.01 ÷ 1.65 tracks. When irradiated with thermal neutrons, 1.0 fCi of ^{239}Pu in a mixture of low irradiation plutonium will produce 52.6 fission fragments. Only about half, or 26.3, of the fragments will produce tracks in the polycarbonate film. Thus, the calculated geometric mean radioactivity on the ^{239}Pu-bearing particles leaving the stack was 0.65 fCi/particle. During these three months, a total of 82 μCi of ^{239}Pu was discharged to the environment. This amounts to an average of 0.62 nCi/min. Thus, during this period about 10^6 ^{239}Pu-bearing particles per minute were discharged from the 291-F stack to the environment. With a flow rate in the stack of 2×10^5 ft^3/min, the average ^{239}Pu-bearing particle concentration in stack air was 5 particles/ft^3.

REFERENCE

R. L. Fleischer and O. G. Raabe. "Fragmentation of Respirable PuO_2 Particles in Water by Alpha Decay - A Mode of Dissolution." **Health Physics** 32, 253-257 (1977).

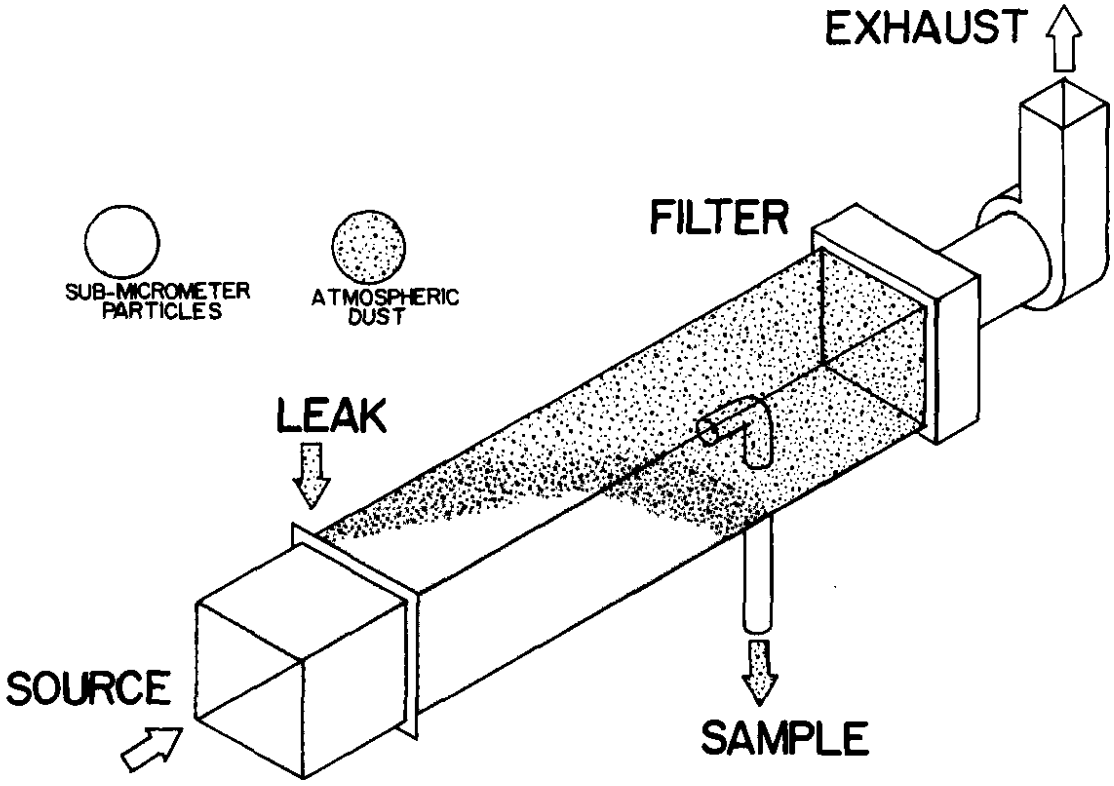

FIGURE 1. Formation of Plutonium-Bearing Particles in Exhaust Systems by the Coagulation of Sub-Micrometer Plutonium Particles with Atmospheric Dust

DEVELOPMENT OF A BOREHOLE PROBE DETECTOR FOR MEASUREMENT OF RADIONUCLIDE TRANSPORT IN GROUND WATER

W. W. Bowman

Auxiliary equipment and procedures have been developed for operation of a borehole probe to measure gamma activities in soil surrounding ground water monitoring wells at a detection limit of about 0.02 pCi/g. By measuring these activities as a function of depth in burial ground monitoring wells, the rate and extent of migration of activities from the burial trenches toward the water table can be quantified.

DESCRIPTION

The borehole probe detector is a high resolution (1.8 in. at 1332 keV) intrinsic germanium device with 14% efficiency relative to a 3 in. NaI detector at 1332 keV. The probe assembly is 3 inches in diameter by 76 in. long and consists of a detector in a liquid nitrogen-cooled vacuum cryostat, a liquid nitrogen reservoir, a preamplifier, and a high voltage bias supply. The assembly is leak tight with a 75 ft section of garden hose containing electronic signal and power cables also serving as a nitrogen vent. The liquid nitrogen reservoir has sufficient capacity for 32 hours of operations. The borehole probe is lowered into a monitoring well by a steel cable wound on a spool driven by a time-controlled, variable-speed motor. The rate of lowering can be set from 1/16 in. to 9 ft per minute.

Gamma ray spectra are acquired by a 4096 channel pulse height analyzer and automatically recorded on magnetic tape. The pulse height analyzer and associated electronics are housed in a small travel trailer and are powered by a motor generator (115 VAC). Programs have been written for the IBM 360-195 to transfer the spectra from magnetic tape to disk and to reduce the spectra to lists of photopeak energies, areas, and statistical errors.

METHODS

The procedures and equipment were tested by profiling natural activities (Th, U, and ^{40}K) in a background well near the burial ground. Each spectrum was acquired for 1000 sec during which the probe was automatically lowered 6 in. The system acquired 96

spectra traveling 48 ft in about 27 hr of unattended operation. Figure 1 shows photopeak area (counts/1000 sec) versus depth (ft) profiles in monitoring well S1 for three naturally occurring gamma rays: 911 keV from the thorium daughter ^{228}Ac, 609 keV from the uranium daughter ^{214}Bi, and 1460 keV from ^{40}K. The relatively low counting statistics account for the majority of the microstructure of these profiles. Interesting features include rather constant ^{40}K concentration below about 25 ft and the expected close tracking of U and Th concentrations over most of the profile except for the relatively high uranium concentrations in strata at about 20 to 25 ft and below about 45 ft. Only naturally occurring activities were observed; however, preliminary analyses of these data show that gamma activities are low as 0.02 pCi/g are detectable.

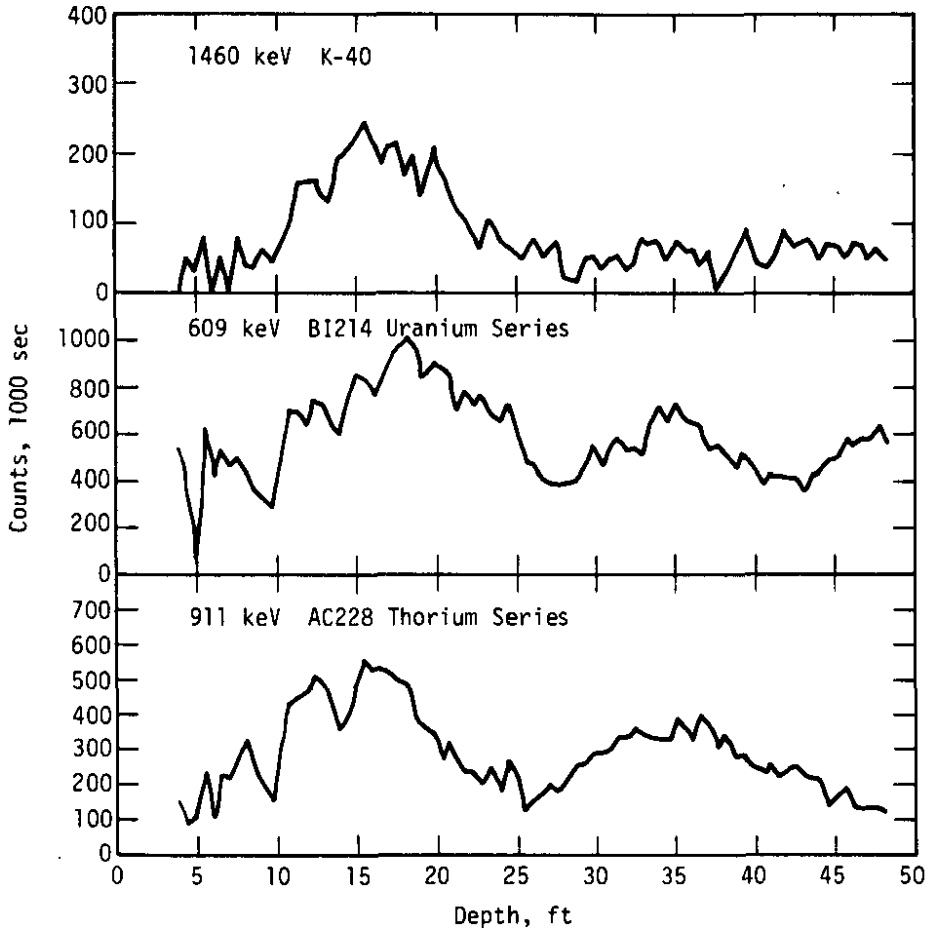

FIGURE 1. Natural Activities - Well S1

AQUATIC STUDIES

TRANSPORT PROCESSES IN THE NEARSHORE ZONE

J. O. Blanton* and D. W. Hayes

The Savannah Navigational Light Tower (SNLT) Oceanic and Meteorological Data System measures ocean currents and meteorological data in the nearshore zone about 15 km off the mouth of the Savannah River. The data collected for the winter-spring period in 1977 have been analyzed (Blanton, 1978). The principal variance in the SNLT currents was associated with tidal currents. The alternating storage and ejection of water out of the Savannah River estuary affects tidal currents out as far as SNLT. The tidal current ellipses at SNLT orient their major axes directly toward the river mouth. The ebb and flood velocities can reach $\pm$40 cm/sec (1.4 km/hr). The currents flowing along the coast vary slowly with the changing weather patterns.

REFERENCE

J. O. Blanton, L. L. Bailey, and W. S. Chandler, Skidaway Institute of Oceanography, Savannah, GA; and D. W. Hayes, A. S. Dicks, and P. D. Shugart. **Data Report Number 1, Oceanographic and Meteorological Data 15 km Off the Coast of Georgia.** Report 78-6, Marine Science Center, University of Georgia, Savannah, GA (1978).

* Skidaway Institute of Oceanography

HYDROGEN SULFIDE CONCENTRATION IN BEAVER DAM CREEK

D. L. Kiser

Concentration-time profiles calculated with LODIPS for various hypothetical releases of hydrogen sulfide from the heavy water extraction facility predict lethal conditions for swamp fish from releases as small as 568 kg discharged over a period of 30 minutes or from releases of 1818 kg discharged over a period of 6 hours or less. The necessary volatilization and oxidation coefficients for LODIPS were derived from field measurements following planned releases of H_2S.

Upsets in the operation of the wastewater strippers in the Girdler-Sulfide (GS) heavy water extraction facility in D Area have released significant amounts of dissolved H_2S to Beaver Dam Creek. Because H_2S is toxic to fish in concentrations as low as 1 mg/liter, the downstream environmental impact of H_2S releases from D Area (Figure 1) was evaluated.

CALCULATION OF TIME-CONCENTRATION PROFILES FOR H_2S IN CREEK

LODIPS models the transport of a tracer or pollutant in a stream to predict downstream concentration-time profiles (Crawford, 1975). The code computes transport of a tracer or pollutant in a stream by solving the one-dimensional equation which takes into account both turbulent diffusion and differential mass transfer:

$$\underbrace{\frac{C(x,t)}{t}}_{\text{Term I}} = \underbrace{\frac{\partial}{x} D(x) \frac{\partial}{x} C(x,t)}_{\text{Term II}} - \underbrace{\frac{\partial}{x} [U(x)\ C(x,t)]}_{\text{Term III}} + \underbrace{\sum_{j-i}^{j} S_J}_{\text{Term IV}} \quad (1)$$

where

$C(x,t)$ = concentration of pollutant in stream or river at a point x and time t

$D(x)$ = dispersion coefficient at a point x

$U(x)$ = longitudinal transport velocity at a point x

S_j = uptake or release of particles by a dead zone (j=1) or interactive phase (j>1) within the stream

J = total number of source/sink effects.

In Equation 1,

Term I = temporal change in concentration

Term II = turbulent diffusion

Term III = longitudinal convective mass transfer

Term IV = source/sink effects within the stream.

Equation 1 can be simplified to:

$$\partial \frac{C(x,t)}{\partial t} = D_r \cdot \frac{\partial^2 C(x,t)}{\partial x^2} - \bar{U}_r \cdot \frac{\partial C(x,t)}{\partial t} + \sum_{j=1}^{J} S_j \qquad (2)$$

Equation 2 requires site-specific characterization of the dispersion (D_r), the mean velocity ($\bar{U}_r$), and an empirical dilution factor to adjust the concentration for sidestream(s) entering the main stream. Equation 2 models only a single stream and does not take into account further dilution by tributary streams. Table 1 lists values for D_r, $\bar{U}_r$, and the dilution factors calculated from an experiment with Rhodamine WT dye in the effluent channel from D Area (Figure 1). Because Rhodamine WT does not interact significantly with the stream or the stream environment and the dead zone effect was not significant within the reaches listed in Table 1, Term IV is zero.

To model hydrogen sulfide transport, volatilization and oxidation of H_2S in the stream were measured during planned releases of 18 and 118 kg of H_2S; without these sink effects, LODIPS had grossly overpredicted downstream concentrations of H_2S (Crawford, 1978). With values established for all necessary parameters, LODIPS was used to predict downstream H_2S concentrations for postulated releases.

H_2S RELEASES LETHAL FOR SWAMP FISH

Sufficient information has been published (Bonn, 1967; Vanhorn, 1949; Shelford, 1917) to develop a relationship between aqueous concentration and time-integrated concentrations lethal to fish. Fish are known to inhabit the creek as far up as the creek delta. Time-integrated concentrations were therefore calculated at this point (Location 4 in Figure 1) to develop a relationship between the release duration from D Area and the amount of H_2S released that would result in potentially lethal conditions for swamp fish.

Figure 2 shows that a release of 568 kg of H_2S over a period of 30 minutes, or of 1818 kg over a period of 6 hours or less, would be lethal to swamp fish.

REFERENCES

E. W. Bonn and B. J. Follis. "Effects of Hydrogen Sulfide on Channel Catfish (Ictalurus punctatus)." **Trans. Amer. Fish. Soc. 96**, (1), 31 (1967).

T. V. Crawford, et al. "Computer Modeling of Stream and River Systems," **Savannah River Laboratory Environmental Transport and Effects Research Annual Report-1974.** Report DP-1374, E. I. du Pont de Nemours & Co., Savannah River Laboratory, Aiken, SC (1975).

T. V. Crawford, et al. "Water Level Fluctuations in Coastal Plain Sediments at SRP," **Savannah River Laboratory Environmental Transport and Effects Research Annual Report - 1977.** Report DP-1489, E. I. du Pont de Nemours & Co., Savannah River Laboratory, Aiken, SC (1978).

V. E. Shelford. "An Experimental Study of the Effects of Gas Waste on Fishes, With Special Reference to Stream Pollution." **Bull. Illinois State Lab. Nat. Hist. 11**, 381 (1917).

W. M. Vanhorn, J. B. Anderson, and M. Katz. "The Effect of Kraft Pulp Mill Wastes on Some Aquatic Organisms." **Trans. Amer. Fish. Soc. 79**, 55 (1949).

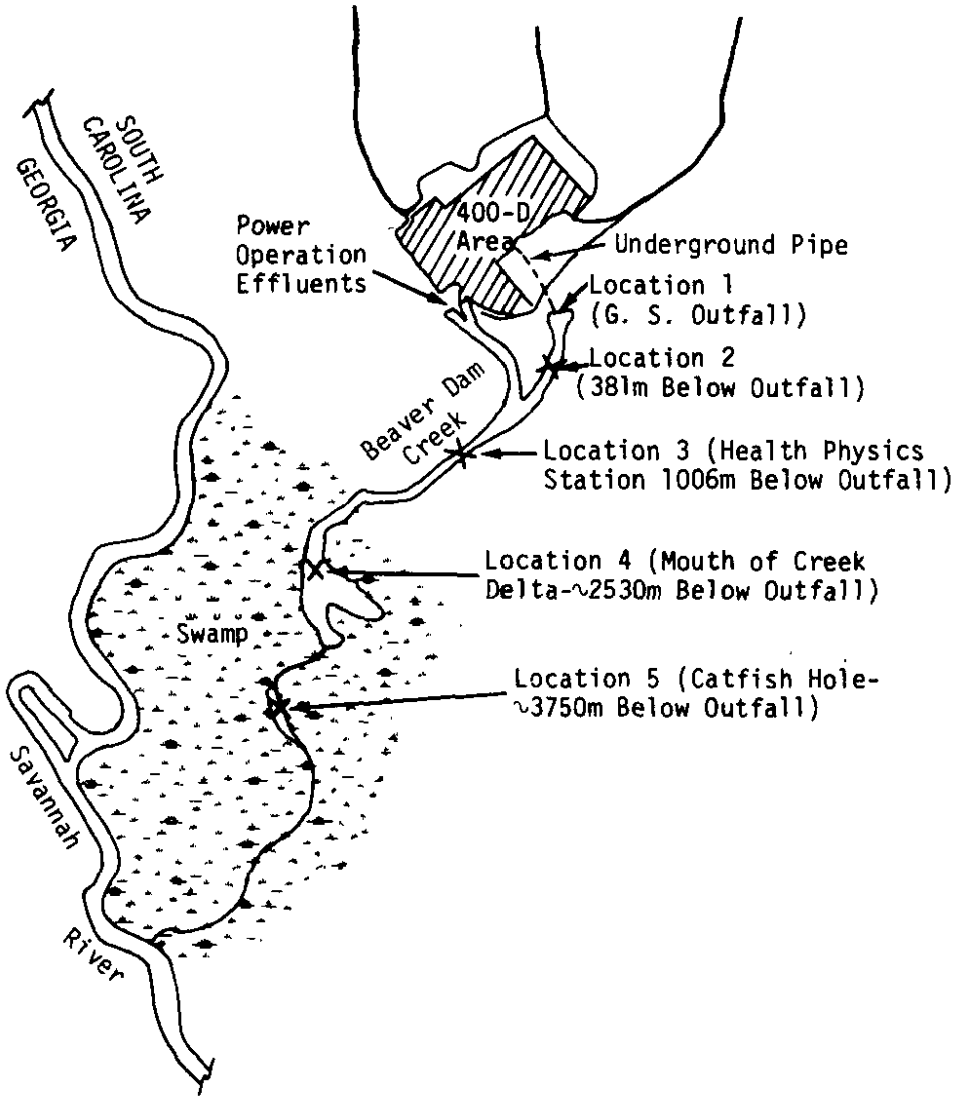

FIGURE 1. The Beaver Dam Creek Region Below the 400 Area at SRP

TABLE 1

Parameters for Calculation of H_2S Time-Concentration Profiles in Beaver Dam Creek by LODIPS

Reach[a]	Mean Velocity $\bar{U}_r$, m/min	Dispersion D_r, m^2/min	Stream Dilution Factor	Coefficient for Oxidation,[b] min^{-1}	Coefficient for Volatilization, min^{-1}
L-1 to L-2	14.87	9.07	1.00	0.0034	0.0364
L-2 to L-3	23.16	55.28	0.23	0.0034	0.0206
L-3 to L-4	25.79	55.28	1.00	0.0034	0.0206
L-4 to L-5	7.74	306.58	1.00	0.0034	0.0206

a. Shown in Figure 1.
b. The oxidation coefficient depends on the amount released. The value 0.0034 is appropriate only for a release of 454 kg of H_2S.

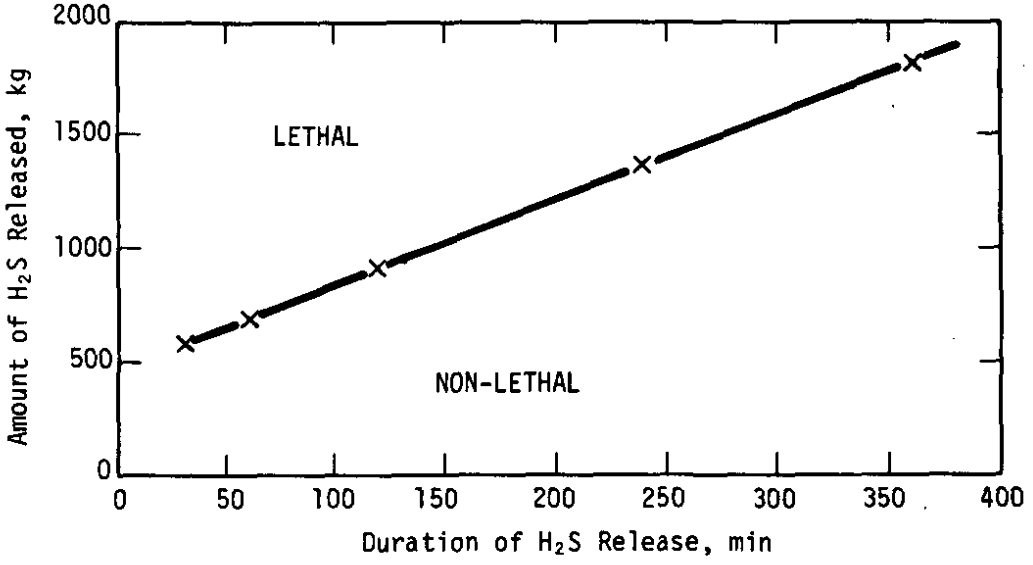

FIGURE 2. H_2S Release from D Area that Would Kill Fish in Beaver Dam Creek, as Predicted by LODIPS

STABLE CESIUM TRANSPORT IN AN AQUATIC SYSTEM

D. L. Kiser

A field experiment in Four Mile Creek at the SRP site was conducted to determine how cesium transport differed from conservative transport. Measurements following the release of stable cesium chloride to Four Mile Creek showed that most of the cesium released was transported downstream; however, the sorption-desorption behavior decreased the maximum concentration and increased the travel time and duration in comparison to a conservative dye tracer at sampling stations downstream.

PROCEDURE

The region selected for the study was representative of the types of streambeds encountered in SRP creeks (Figure 1). Flow measurements at Road E, Road 4, and Road C at the time of the release were 31, 144, and 238 L/sec, respectively. The release consisted of a Rhodamine WT dye discharge (1 liter) to provide conservative flow values followed one hour later by the cesium chloride release (100 gm of ^{133}Cs). Downstream dye and cesium concentrations are shown in Figures 2, 3, 4, and 5.

ANALYSIS

Examination of the concentration-time curves indicates cesium sorption decreased the ratio of the peak concentration at the last station to the peak concentration at the first station significantly in comparison with the dye. The dye ratio (Road C-4/Road E) is 3.57×10^{-3} whereas the cesium ratio (Road C-4/near Road E) is 7.84×10^{-4}. However, the cesium desorption, illustrated by the large tailing effect at Road C (Figure 4) and Road C-4 (Figure 5), maintained most of the cesium in transport as shown by a comparison of the dye and the cesium time-integrated concentration ratios for the first and second reaches. For the first reach, the time-integrated concentration ratio (Road 4/near Road E) for the cesium is 88% of that for the dye. For the second reach, the time-integrated concentration ratio (Road C/Road 4) for the cesium is 89% of that for the dye. Inadequate sampling of the tailing effect of the cesium in the third reach results in an invalid comparison in that reach. The sorption-desorption increased the peak-to-peak travel time between the dye and the cesium from 1 hour at the stations near Road 4 and near Road E to 1.5 hours at Road C station and 2.5 hours at Road C-4 station.

The results suggest that most of the cesium released to Four Mile Creek was transported downstream and the use of a stream model to calculate downstream arrival times and concentrations based on dye measurements will overpredict actual concentrations.

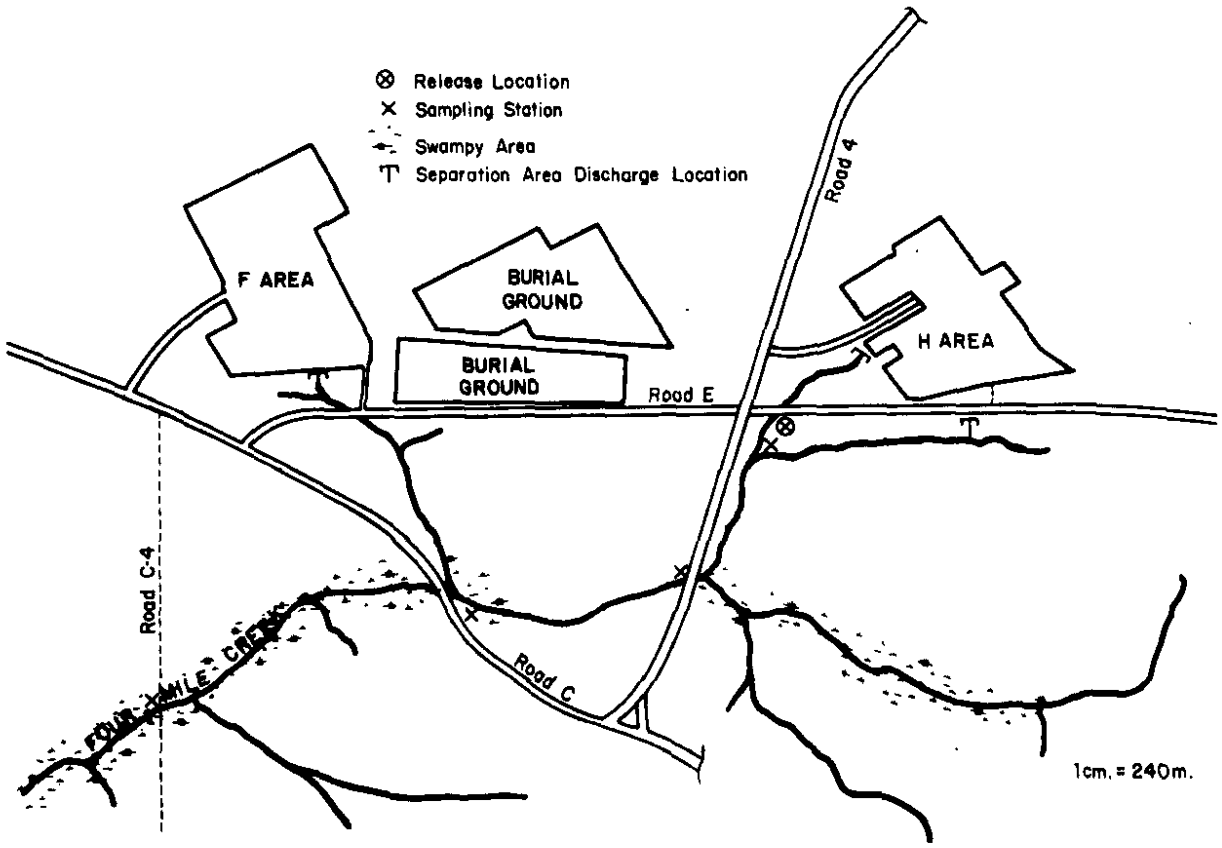

FIGURE 1. Four Mile Creek Region Below the Separation Areas of SRP

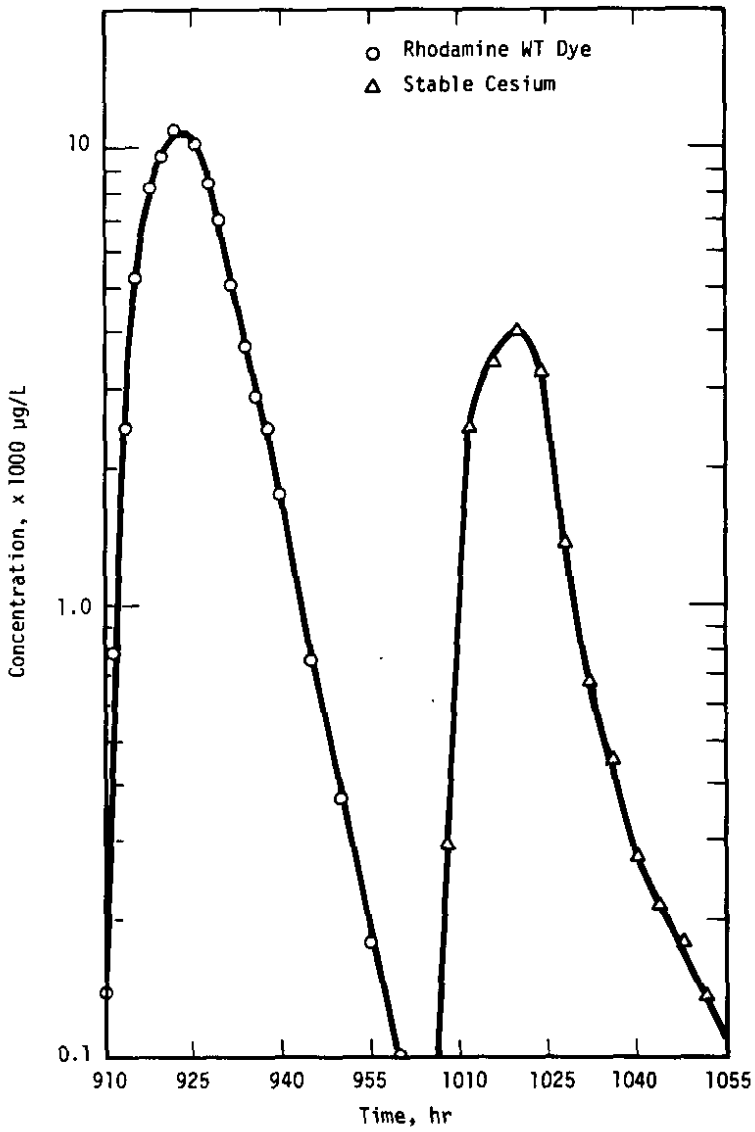

FIGURE 2. Profiles of the Dye - Cesium Passage Near Road E on Four Mile Creek

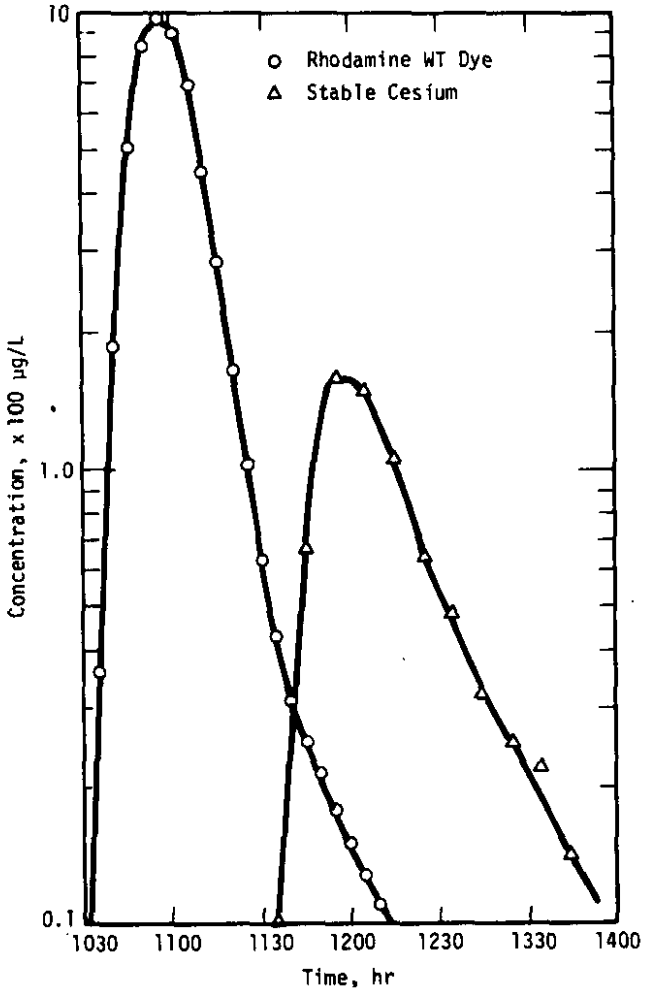

FIGURE 3. Profiles of the Dye - Cesium Passage at Road 4 on Four Mile Creek

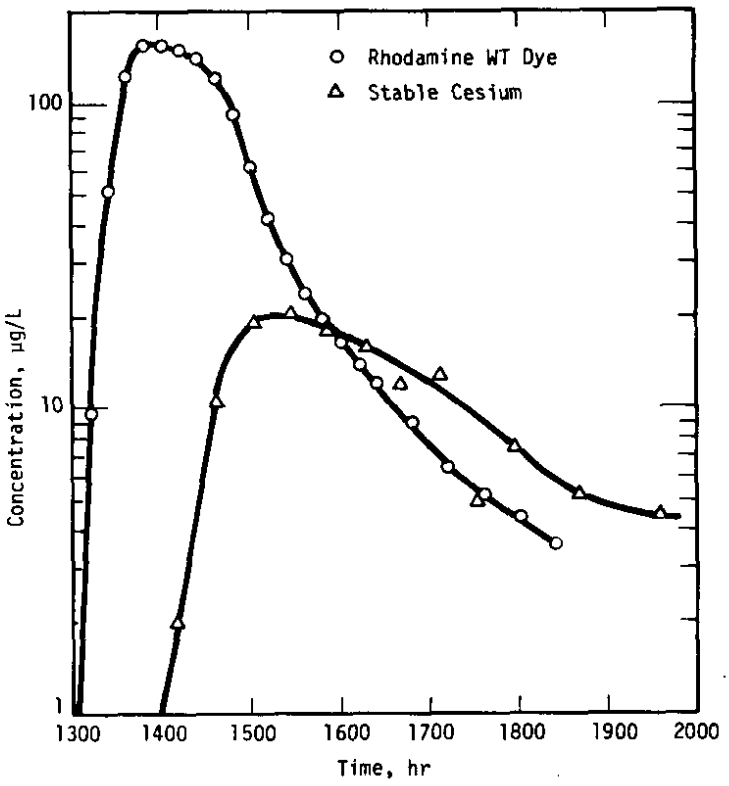

FIGURE 4. Profiles of the Dye - Cesium Passage at Road C on Four Mile Creek

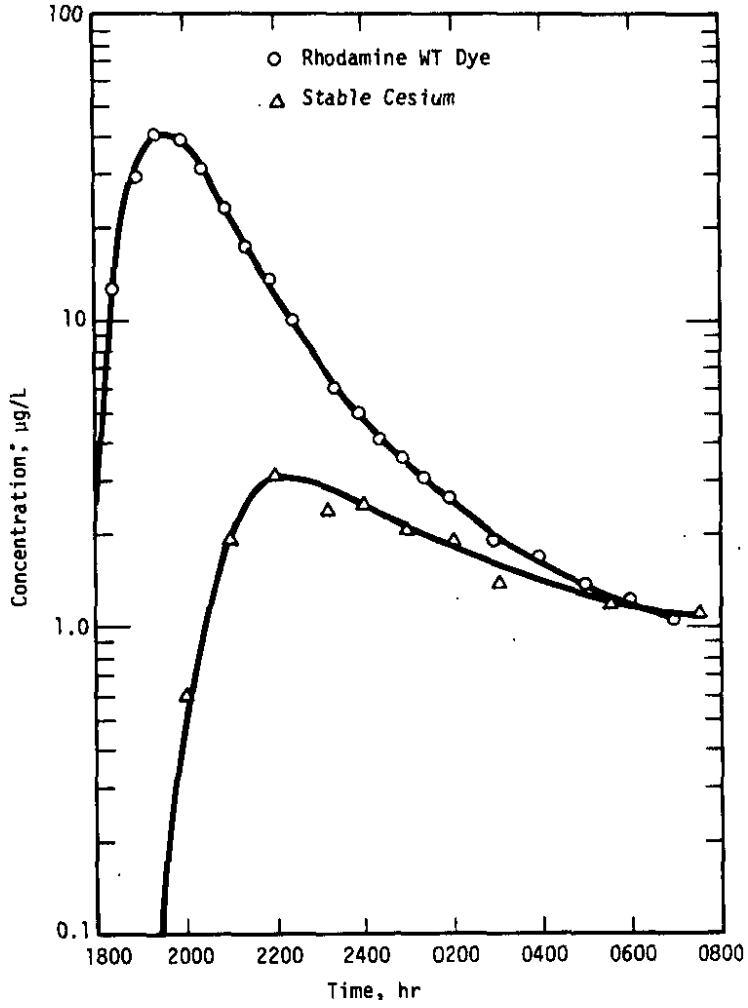

FIGURE 5. Profiles of the Dye - Cesium Passage at Road C-4 on Four Mile Creek

PLUTONIUM AND AMERICIUM IN THE SEDIMENT OF THE SAVANNAH RIVER ESTUARY

D. W. Hayes

Sediment samples from various locations in the Savannah River estuary were examined for their plutonium, americium, and natural alpha-radiation levels. The americium and plutonium levels represent less than 1% of the gross alpha activity from the naturally occurring radionuclides and do not differ greatly from values reported elsewhere.

PLUTONIUM IN SEDIMENTS

The sediment that accumulated at the mouth of the Savannah River provides an opportunity to evaluate the influence of upstream nuclear facilities on the resulting concentrations of plutonium and americium. Sediment samples were collected from the upstream (tidal fresh water) and downstream (mouth) portions of the estuary. The plutonium concentrations in the sediment from the tidal fresh water region and near the mouth of the estuary were comparable (Table 1). The values are not greatly different from other locations that only receive transuranic input from nuclear weapons fallout. (Plutonium concentrations have been reported for Great Lake sediments [up to 200 fCi/g], Atlantic coastal waters like Buzzard's Bay [about 60 to 70 fCi/g], and previous values in the Savannah River system [about 10 to 30 fCi/g].) Fallout ^{238}Pu to $^{239,240}Pu$ ratios are generally less than 0.1. If ratios are greater than this, it is usually indicative of other sources of plutonium in the system. The ratios for the Savannah River estuary cores are reported in Table 1. Only in the fresh water core in the upper 0 to 15 cm were ratios found to be different from fallout, and these ratios were greater by a factor of two and presumably resulted from SRP releases to the river system.

AMERICIUM IN SEDIMENTS

If americium dynamics are different in estuaries than in fresh or sea water systems, this difference would be evidenced from the ^{241}Am to $^{239,240}Pu$ ratios. The average value for such ratios in shallow near-shore sediments and in Lake Michigan sediments varies from 0.14 to 0.34, with an average of 0.22. No fractionation between americium and plutonium has been found in

these sediments, even when the radionuclides are being lost from the sediment following upward migration. With the exception of one value of 0.62, the ^{241}Am to $^{239,240}Pu$ ratios for the two sediment cores reported in Table 1 are not significantly different from those quoted in the literature. The indication is that the chemistries of americium and plutonium are similar in this estuarine system and that the ^{241}Am has grown in from ^{241}Pu. The transuranic alpha activity in these cores represents less than 1% of the gross alpha activity from the natural radionuclides that are present.

TABLE 1

Plutonium, Americium, and Gross Alpha Activities in the Savannah River Estuary (all are dry weights)

Location	Core Depth Interval, cm	^{238}Pu, fCi/g	$^{239,240}Pu$, fCi/g	$\frac{^{238}Pu}{^{238,239}Pu}$ Ratio	^{241}Am, fCi/g	$\frac{^{241}Am}{^{239,240}Pu}$ Ratio	Gross Alpha, fCi/g
Tidal Fresh Water	0 to 5	4.3 ±3.3	27.2 ±3.3	0.16 ±0.05	11.5 ±4.1	0.42 ±0.16	24,000
	5 to 15	6.1 ±1.2	35.5 ±2.8	0.17 ±0.04	4.0 ±1.9	0.11 ±0.05	20,000
	15 to 30	2.8 ±1.3	30.9 ±2.8	0.09 ±0.04	5.4 ±1.9	0.17 ±0.06	20,000
	30 to 50	0.4 ±0.4	10.6 ±1.0	0.04 ±0.04	2.0 ±0.8	0.19 ±0.08	18,000
	50 to 70	0.05 ±0.10	0.05 ±0.05	- -	0.23 ±0.23	- -	18,000
Mouth of Estuary	0 to 5	3.2 ±1.1	50.6 ±4.1	0.06 ±0.02	11.1 ±1.7	0.22 ±0.04	10,000
	5 to 15	1.7 ±1.0	21.6 ±2.2	0.08 ±0.05	3.0 ±2.3	0.14 ±0.11	13,000
	15 to 25	0.2 ±0.2	2.9 ±0.5	0.07 ±0.07	1.8 ±0.6	0.62 ±0.23	12,000
	45 to 65	-	0.5 ±0.5	-	-	-	13,000

RADON-222 IN BIOLOGICALLY PRODUCED GAS FROM A REACTOR COOLING POND

C. B. Fliermans, D. W. Hayes, and N. D. Johnson

Radon-222 emanation rates were obtained from 4 sampling sites with sediment temperatures of 25, 30, 35, and 43°C. The highest discharge rates observed were equivalent to the minimum estimate for the terrestrial flux rate of radon-222.

INTRODUCTION

Radon-222 is a naturally occurring radioisotope (Adams, 1972; Boltwood, 1905) and is a member of the uranium-238 decay series having a 3.82-day half-life. Radon-222, a radioactive gas, may be formed in aquatic systems through an enrichment of radium-226, which is dissolved naturally in waters. Radium is probably precipitated as an iron and/or manganous salt and is then trapped in the sedimentary muds. As radium decays, it produces gaseous radon-222 that may escape into the atmosphere. The average radon-222 concentration in the atmosphere is estimated at 0.21 pCi/L (Gemesi,1972), and the global flux ranges from 0.01 to 2.5 atoms/cm^2 sec with a mean of 0.75 atom/cm^2 sec (3.5 mCi/day) (Wildening, 1972). A steady state inventory of radon-222 in the atmosphere is approximately 19 mCi. The flux of radon-222 generally depends on the following physical transport properties: the porosity of the substrate in which the gas is trapped, initial radium-226 concentration, vegetative cover, depth of water and/or ice covering, and changes in atmospheric conditions. The transport of radon-222 from aqueous sediments via biologically produced gases released from the sediments differs from the physical transport processes and may depend primarily on the production rate of biological gases such as CO_2, O_2, and CH_4.

MATERIAL AND METHODS

Sampling techniques, procedures, and methodology have been described previously (Fliermans, 1978).

RESULTS AND DISCUSSION

Previous sampling data from various sites at SRP demonstrated that sediment gases were composed primarily of methane, a biologically produced gas, which at times accounted for 80% of the gases present.

Vibrating reed electrometry measurements demonstrated that the radioactivity of the gas from the various locations decayed with a half-life of 3.8 days, consistent with radon-222 (Figure 10). The data further demonstrated that the highest levels of radon-222 were generally observed in the sediments of Pond 2 near the incoming ambient stream as compared to the region of the reactor cooling water. Gas samples from these sediments contained 571 pCi of radon-222 per liter of gas. Samples from the site closest to the input of the reactor cooling water had the lowest level of radon-222, 82 pCi/L.

Sediment cores were taken along a sediment thermal gradient from 43 to 17°C, and the levels of the parent nuclide, radium-226, were measured for 10-cm-depth intervals. In all core samples, the level of radium-226 decreased with increasing sediment depth so that the highest levels of radium-226 were associated with the surface sediments. The distribution pattern of radium-226 in the sediment cores is not understood, although the data may reflect deposition by surface runoff or sediment transport via input waters.

The maximum level of sediment gases discharged from Pond 2 without agitation has been measured as high as one liter/m^2 day. Thus, if the observed concentration of 571 pCi/L for radon-222 can be used as an upper level for radon-222 in this habitat, then the emanation rate for radon-222 is approximately 571 pCi/m^2 day. Assuming that a secular equilibrium exists between radon-222 and radium-226 and that the average concentration of radium-226 is 3 pCi/g dry weight of sediment, then <1% of the radon-222 produced by radium-226 is removed from the system by the biologically produced sediment gases. Discharge rate from this sediment system, based on the highest sediment gas discharge rates observed, is equivalent to 0.01 atom/cm sec, which is the minimum estimate for terrestrial flux rate of radon-222. Thus, the terrestrial average of radon-222 released by physical transport appears to be more important than sediment flux mediated by biological gassing.

REFERENCES

J. A. S. Adams, W. M. Lowder, and T. F. Gesell. **The Natural Radiation Environment II.** Proceedings of the Second International Symposium on the Natural Radiation Environment. USAEC Report CONF-720805, (1972).

B. B. Boltwood. "The Origin of Radium." **Lond. Edinb. Dubl. Phil. Mag. 9,** 603 (1905).

C. B. Fliermans, D. W. Hayes, and N. D. Johnson. "Radon-222 in Biologically Produced Gas from a Reactor Cooling Pond." **Health Physics** 34, 701-704 (1978).

J. Gemesi, D. Szy, and A. Toth. **Radon-222 Content in the Internal Atmosphere of Hungarian Residential Buildings.** USAEC Report CONF-720805-P2, 751 (1972).

M. H. Wildening, W. E. Clements, and D. Stanley. **Radon-222 Flux Measurements in Widely Separated Regions.** USAEC Report CONF-720805-P2, 717 (1972).

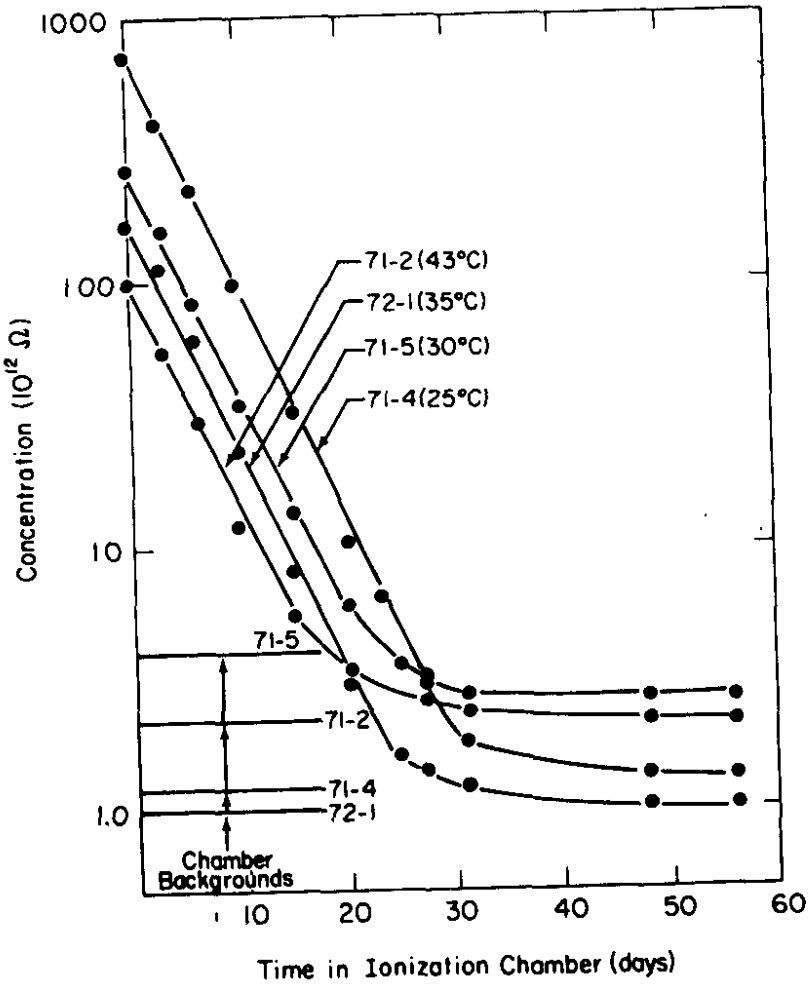

FIGURE 1. Measured Radon-222 Decay Curves by Vibrating Reed Electrometry for Gas Samples Collected from a Thermally Altered Pond. Solid Lines are the decay curves for the samples. Background levels for each ionization chamber are depicted by horizontal symbol lines.

EFFECT OF REACTOR OPERATIONS ON THE PRODUCTIVITY OF THE ALGAL-BACTERIAL MAT COMMUNITY IN THE P-CANAL COOLING SYSTEM

D. L. Tison,* D. H. Pope,** E. W. Wilde, and C. B. Fliermans

Algal community structure and activity were studied from 55° to 40°C along a thermal gradient, and at ambient temperatures during a reactor down period. The community structure and percent-dissolved organic matter data suggest that algal populations may respond to thermal stress by increasing the amount of photosynthetically fixed CO_2 released as dissolved organic matter.

INTRODUCTION

The algal-bacterial mat community which developed in a lotic microcosm was used to determine community structure and activity. The microcosm consisted of a wooden trough (1m x 15m) which received heated water directly from the hot water discharge canal of a nuclear reactor at SRP. Sample sites at 55°, 50°, 45°, and 40°C on the trough were chosen in order to monitor the development and effect of ambient temperatures on different thermally adapted communities.

RESULTS AND DISCUSSION

Data for primary productivity measurements before, during, and after a short-term (8 days) period of the reactor not operating are shown in Figure 1. On March 19, a mature algal-bacterial mat exposed to the thermal effluent was present. Reactor operations ceased the night of March 19. The results on March 21 and 24 are after 2 and 5 days, respectively, of exposure of the mat communities to ambient temperatures. On March 28 reactor operations were resumed, but were not yet at full capacity.

The results of primary productivity measurements shown in Figure 1 indicate that the algae at 55°, 50°, and 45°C were themophilic. When these algae were exposed to ambient temperatures during the reactor down period (March 21 and 24), the amount of $^{14}CO_2$ fixed into particulate biomass (plates on left in Figure 1) decreased, while the percentage of fixed $^{14}CO_2$ released as dissolved organic matter (% DOM) increased. After reactor operation resumed on May 28, fixation of $^{14}CO_2$ into particulate biomass

* SRL Graduate Participant from Rensselaer Polytechnic Institute
** Rensselaer Polytechnic Institute

increased and % DOM decreased at the 55°, 50°, and 45°C sites as the temperature returned to near the optimum for the thermophilic microorganisms. The productivity data for the 40°C site suggest that a mixed thermophilic and mesophilic algal population was present. This is indicated by the data showing an increase in particulate productivity after 5 days exposure to ambient temperatures suggesting an increase in mesophilic productivity not seen at the other sites. The decrease in % DOM at the 40°C site after reactor operations ceased on March 19 may indicate that a predominantly mesophilic algal population was present. These conclusions are supported by direct algal counts and bio-volume data which showed that the algal populations at 55° and 50°C sites consisted solely of the thermophilic blue-green algae Phormidium sp. and Mastigocladis laminosus. At 45°C, the thermophilic blue-green alga Oscillatoria sp. was also present. The 40°C algal population consisted of not only the thermophilic blue-green algae found at the other sites, but also a large number of mesophilic eucaryotic algae.

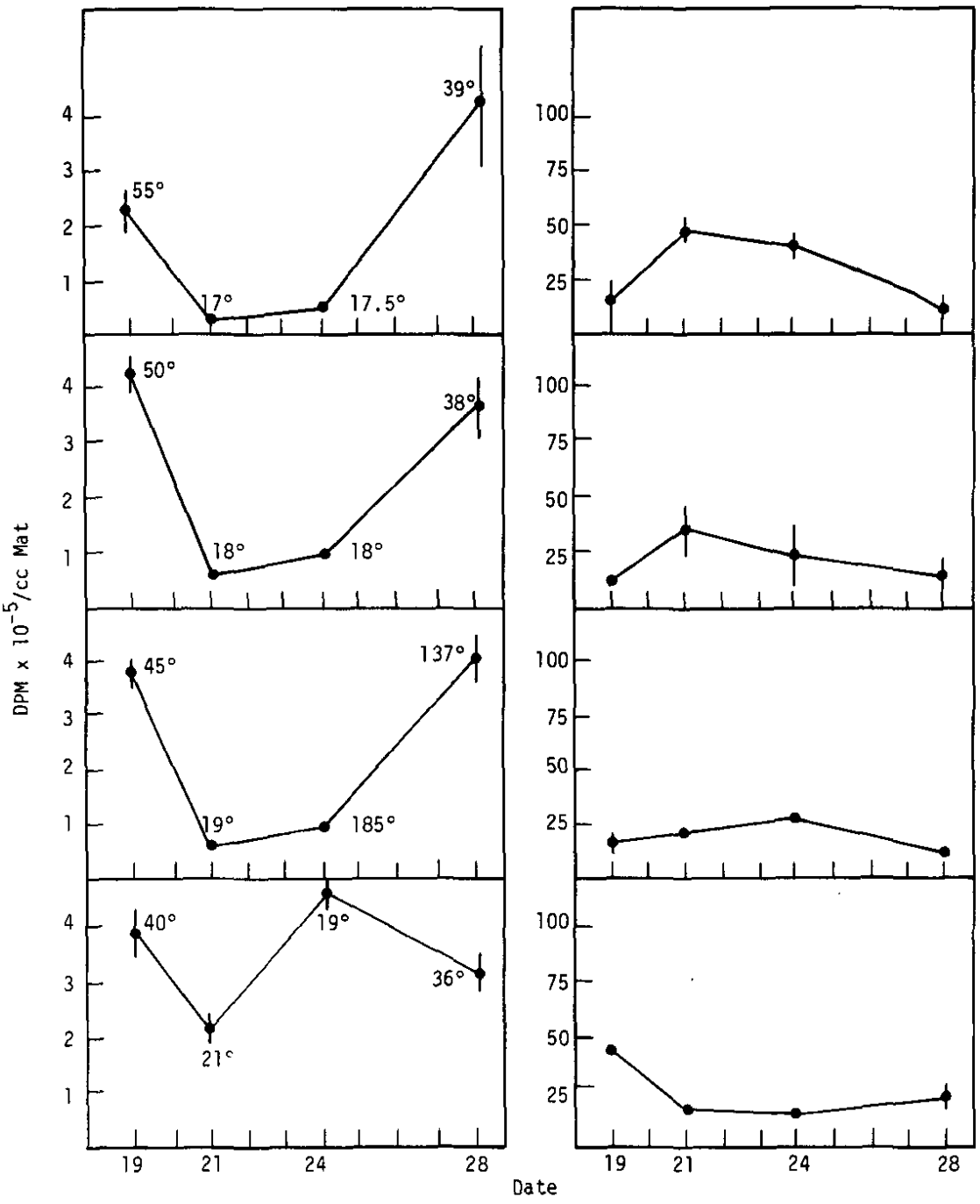

FIGURE 1. Results of a Short-Term Reactor Down Period on Algal Primary Production. The plates on the left show incorporation of $^{14}CO_2$ into particulate biomass. In situ temperatures are shown for each site at the date of sampling. The plates on the right show the percentage of photosynthetically fixed $^{14}CO_2$ released as dissolved organic matter (% DOM). Bars represent ± 1 standard deviation.

MINERALIZATION OF DEGRADED SUBSTRATE AS AN INDICATOR OF THERMAL STRESS IN HETEROTROPHIC BACTERIA

D. L. Tison,* D. H. Pope,** and C. B. Fliermans

Organisms growing in the thermally altered cooling water of an SRP nuclear production reactor are exposed to large temperature fluctuations due to reactor operations. Data from experiments on algal-bacterial mat communities, indicate that the percentage of substrate mineralized increases when the heterotrophs are at temperatures other than their adapted temperatures.

RESULTS

Results of a temperature shift experiment in the P-canal microcosm are shown in Figure 1. The percentage of substrate mineralized (the plates on the right of Figure 1) appeared to increase as the heterotrophic population was shifted away from the temperature at which the sample was taken. The heterotrophic populations at 55° and 50°C increased the percentage of substrate mineralized when incubated at 45° and 40°C. This 45°C population appeared to increase the percentage of mineralized ^{14}C-glucose when shifted above and below the *in situ* temperature. The percentage of mineralized substrate by the 40°C heterotrophic population was high at all temperatures.

Plate count data from the mats at these sites showed that the heterotrophic populations at 55°, 50°, and 45°C consisted of eurythermophiles (broad temperature range thermophiles) whereas the 40°C site had a predominantly mesophilic population. We postulated that an increase in the percentage of mineralized substrate might be a physiological indication of thermal stress on heterotrophic microbial populations.

ANALYSIS

This hypothesis was tested in the laboratory using pure bacterial cultures adapted to different temperatures. The results for *E. coli* adapted to 15° and 37°C, and a thermophilic SRL 261

* SRL Graduate Participant from Rensselaer Polytechnic Institute.
** Rensselaer Polytechnic Institute.

adapted to 25° and 55°C are shown in Figures 2 and 3, respectively. These results, along with those from the psychrotroph Pseudomonas fluorescens adapted to 5° and 25°C (data not presented), show that when these organisms were shifted either above or below their adapted temperature, the percentage of mineralized substrate increased. However, once these organisms had adapted to a temperature the percentage of mineralized substrate decreased. These results indicate that the percentage of mineralized substrate may be used as an indicator of short-term thermal stress in heterotrophic microbial communities.

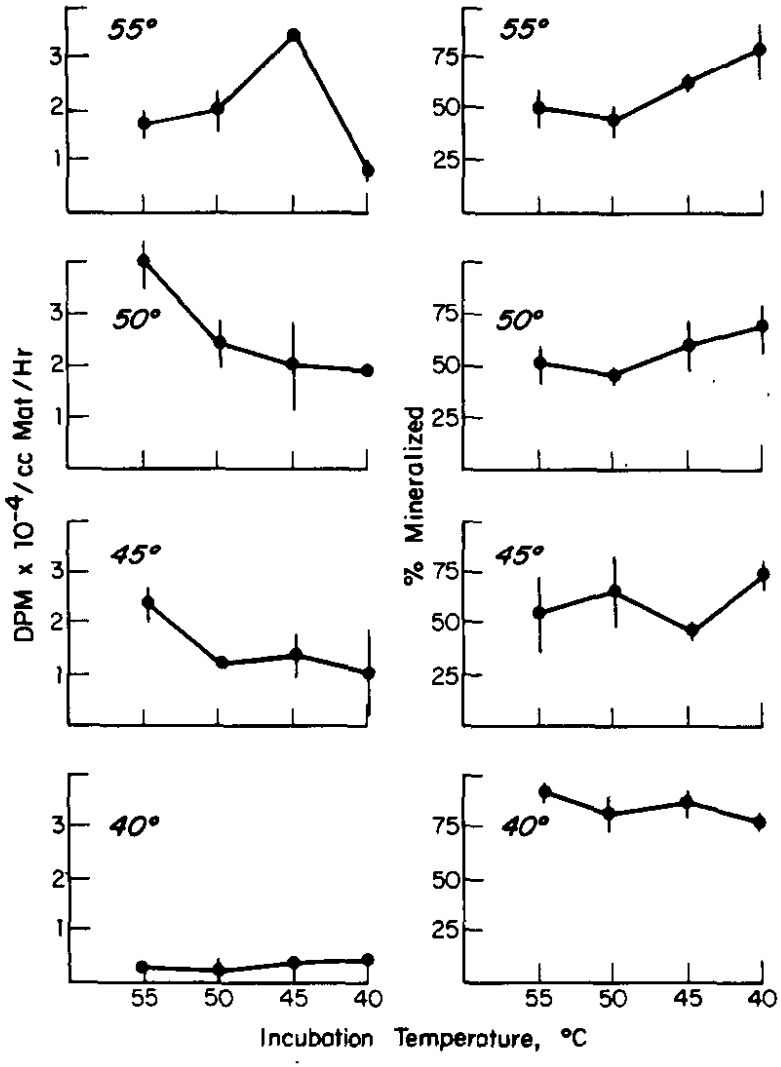

FIGURE 1. Results of Temperature Shift Experiments Conducted with the P-Canal Microcosm Communities. The plates on the left show the amount of UL-^{14}C- glucose incorporated into particulate biomass. The temperature of the sample site is indicated at the upper left corner. The plates on the right show the percentage of UL-^{14}C-glucose mineralized. Bars represent ±1 standard deviation.

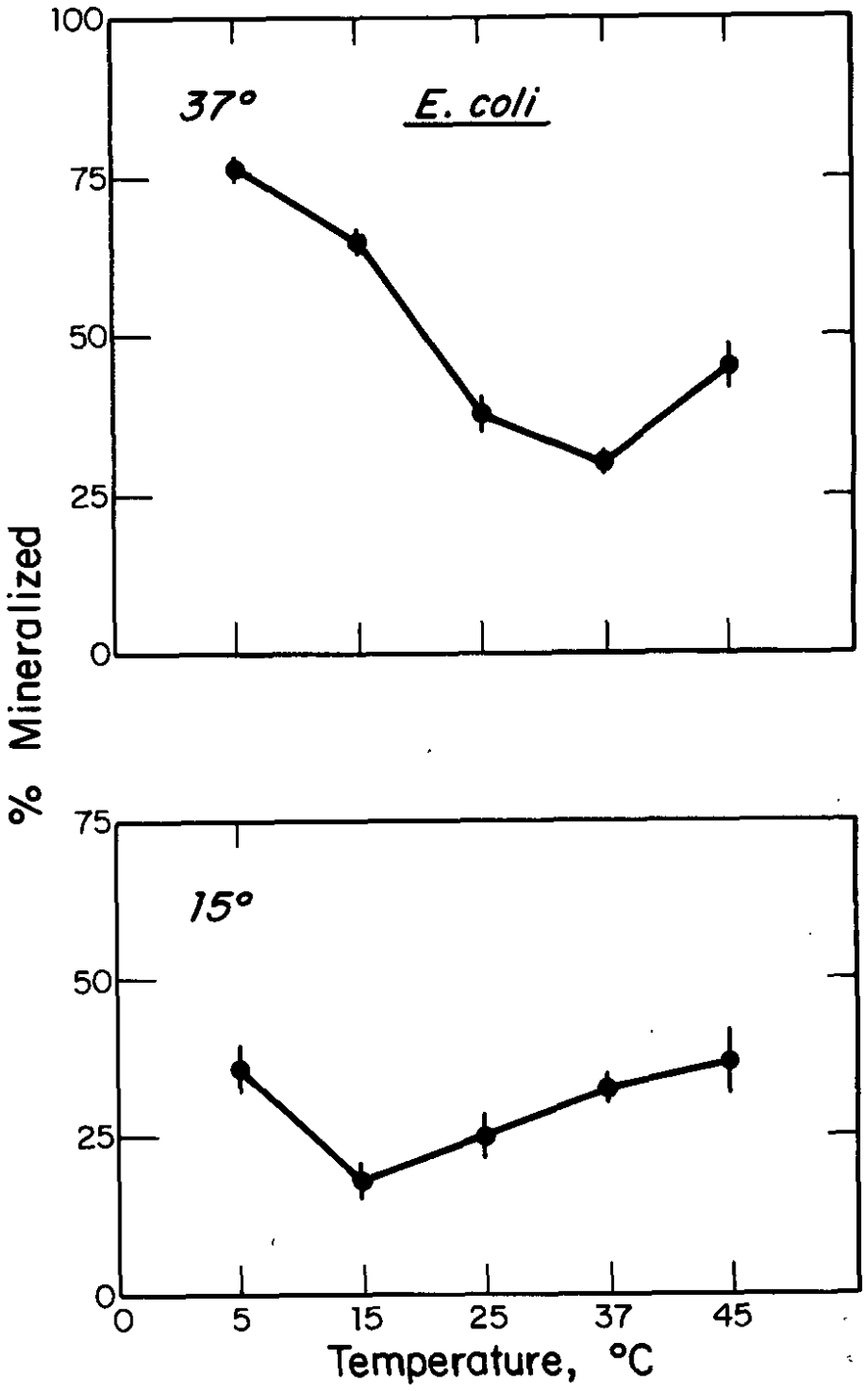

FIGURE 2. Results of Laboratory Temperature Shift Experiments With Escherichia coli K-12 Adapted to 37°C (top) and 15°C (bottom). Bars represent ±1 standard deviation.

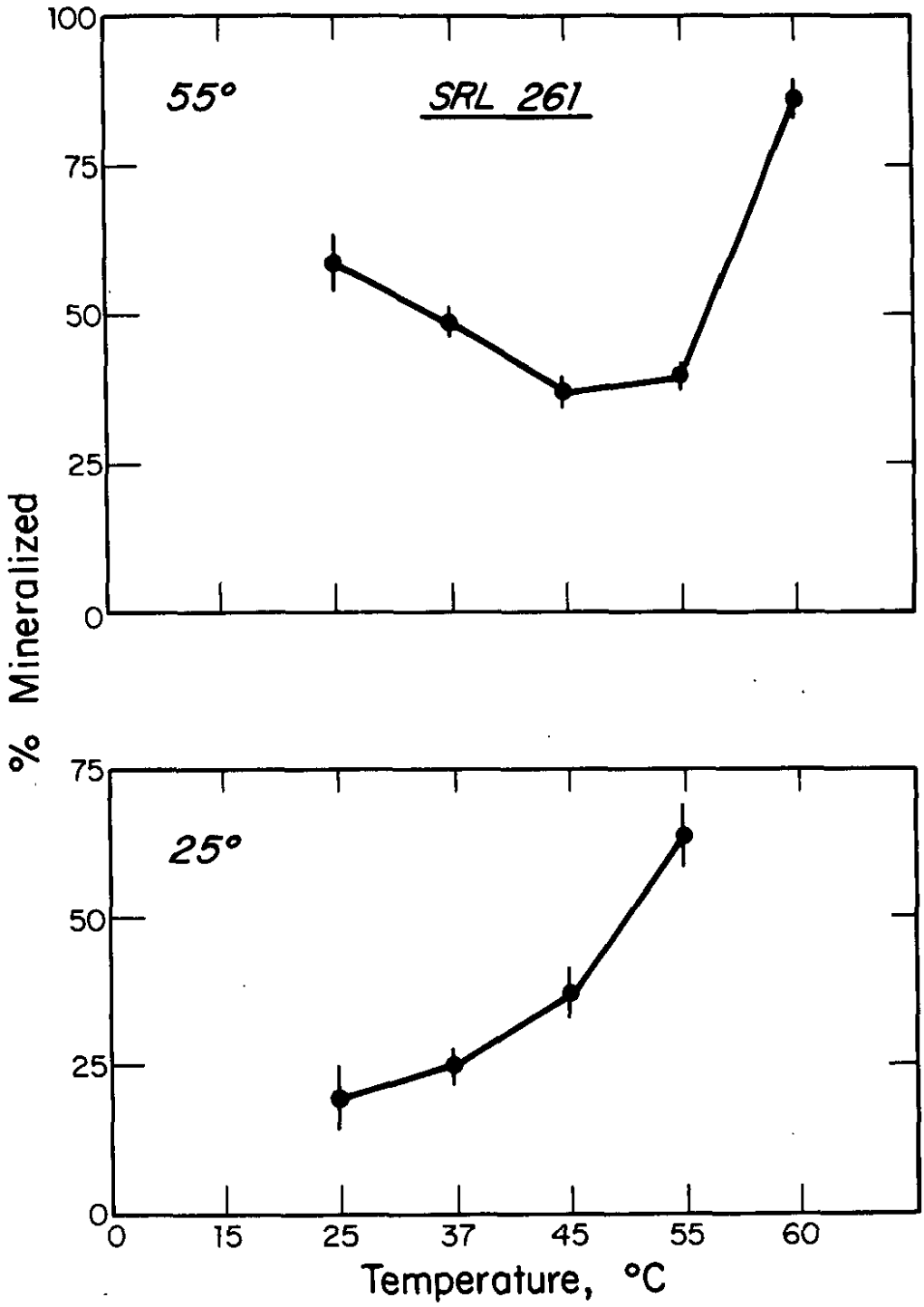

FIGURE 3. Results of Laboratory Temperature Shift Experiments with a Thermophilic Isolate, SRL 261 Adapted to 55°C (top) and 25°C (bottom). Bars represent ±1 standard deviations.

COMMUNITY DEVELOPMENT IN A THERMAL GRADIENT MICROCOSM

D. L. Tison,* D. H. Pope, and C. B. Fliermans**

The thermal gradients created by the thermally altered cooling water from SRP nuclear production reactors provide a unique situation for studying de novo development of thermophilic microbial communities. A lotic microcosm as described previously (See Tison, p.135) allowed for development of microbial communities affected only by thermal conditions. Autotropic and heterotrophic structure and function during development of microbial communities at 60°, 55°, 50°, and 45°C are described in this paper. No photoautotrophic uptake of $^{14}CO_2$ occurred at 60°C. Maximum primary productivity occurred at 55°C. Bacterial populations and primary productivity values were closely related at the temperatures of this study.

MATERIAL AND METHODS

A microcosm receiving heated water from the hot water discharge canal of a nuclear reactor was used to follow de novo community development in the algal-bacterial mat at 60°, 55°, 50°, and 45°C. The trough was scraped to bare board and allowed to dry for several days until P-reactor began operation at which time flow was restored to the trough.

Primary productivity was measured by a modification of the ^{14}C - technique and heterotrophic activity was monitored by utilization of ^{14}C-glucose as described previously (See Tison, p.135). Bacterial numbers were determined by spread plate counts on 0.1% peptone, 0.1% yeast extract, 1.5% agar incubated at 55°, 37°, and 25°C.

RESULTS AND DISCUSSION

The data in Figure 1 demonstrate that no photoautotrophic uptake of ^{14}C occurred at 60°C. This is consistent with the observations of Castenholz (1976) that Mastigocladus laminosus, a predominant member of the thermophilic algal bacterial mat on the

* SRL Graduate Participant from Rensselaer Polytechnic Institute
** Rensselaer Polytechnic Institute

trough, is limited to temperatures below 58°C. The small amount of productivity at 60°C is attributed to chemoautotrophic methanogenic bacteria (Tison, unpublished data). Maximum primary productivity was found at 55°C and may have been inhibited by either cyanophage or grazing protozoa causing "plaque" areas in the mat. The observed trend in % DOM is consistent with our earlier observation.

Secondary heterotrophic (^{14}C-glucose) production rates (Figure 2) at 60°C reached a maximum and stabilized after 2 weeks of development. The 60°C heterotrophic population was dominated by a sheathed bacterium resembling Sphaerotilus natans. The bacterial populations found at 55° and 50°C appeared to increase along with the primary productivity at these sites. Plate counts from 45°C revealed that the bacterial population was mainly mesophilic. The low rates of glucose utilization at 45°C are probably a result of the inability of the mesophiles to function well at this temperature. The low rates of primary production at 45°C may also have limited bacterial numbers there. These results suggest that bacterial activity is closely coupled with primary productivity. This may be due to the dependence of the heterotropic populations on the organic substrates excreted by the algae.

REFERENCES

R. W. Castenholz. "The Effect of Sulfide on the Blue-Green Algae of Hot Springs." In New Zealand and Iceland. J. **Phycol.** 12, 56-68 (1976).

D. L. Tison, D. H. Pope, and C. B. Fliermans. "Mineralization of Degraded Substrate as an Indicator of Thermal Stress in Heterotrophic Bacteria." (This volume).

D. L. Tison, D. H. Pope, E. W. Wilde, and C. B. Fliermans. "Effect of Reactor Operations on the Productivity of the Algal-Bacterial Mat Community in the P-Canal Cooling System." (This volume).

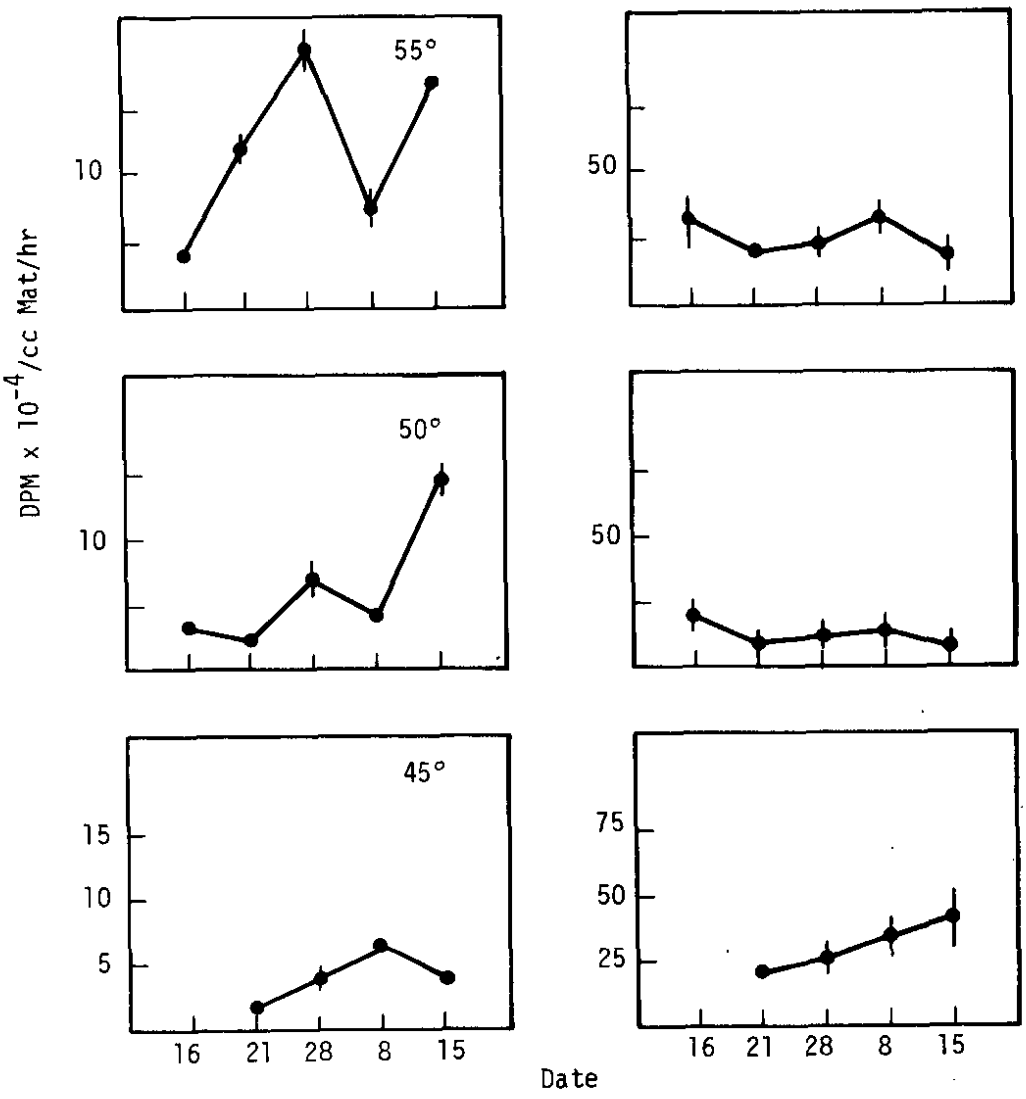

FIGURE 1. Primary Productivity of Developing Algal-Bacterial Mat Communities. The plates on the left show incorporation of $^{14}CO_2$ into particulate biomass. Site temperatures are shown in the upper right of the particulate plates. On the right the percentage of fixed CO_2 released as extracellular products is shown. Bars represent ± 1 standard deviation.

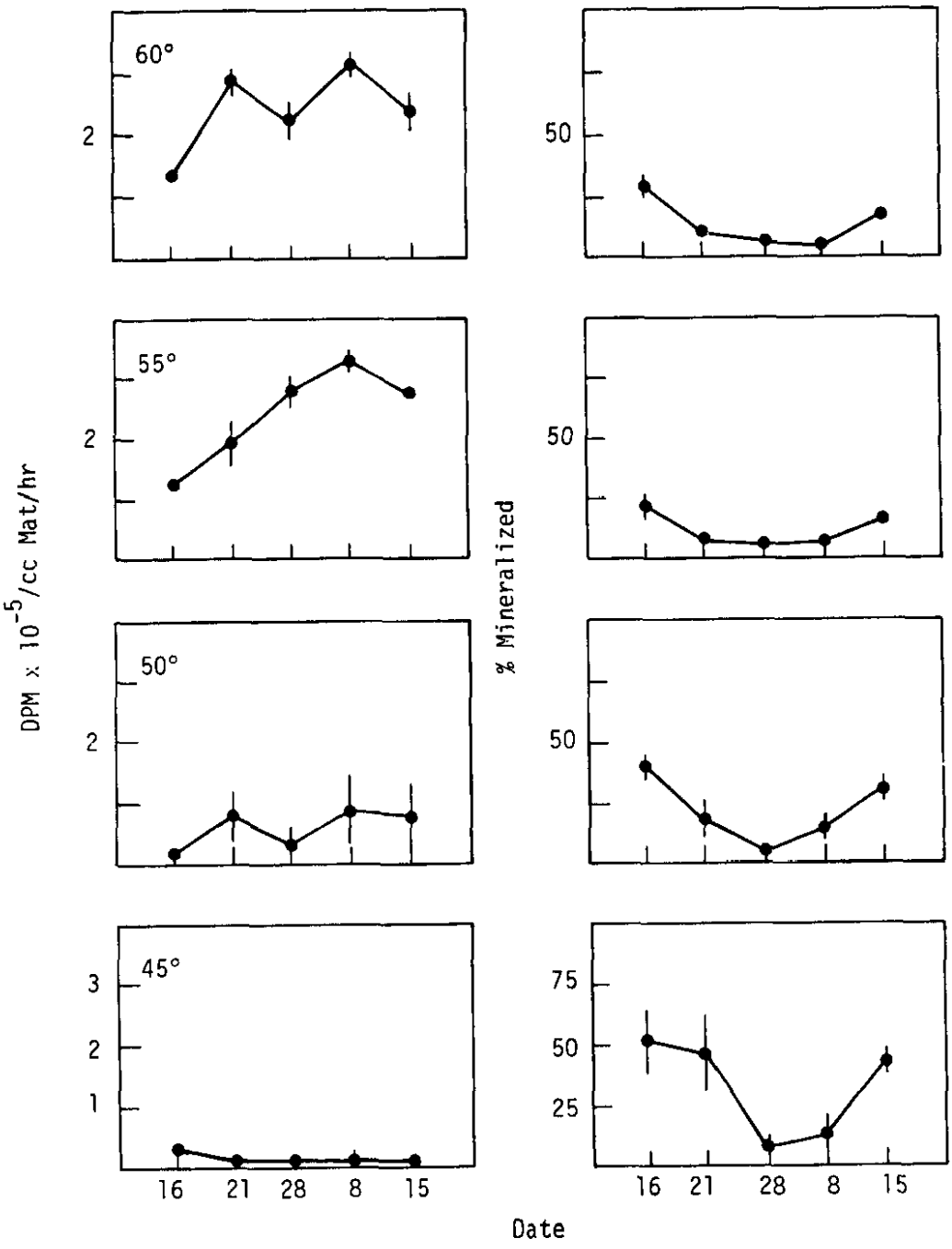

FIGURE 2. ^{14}C-Glucose Heterotrophy of Developing Algal-Bacterial Mat Communities. The plates on the left show incorporation of ^{14}C into particulate biomass. The temperatures at each site are given in the upper left. The percentage of ^{14}C-glucose respired as $^{14}CO_2$ is shown in the plates on the right. Bars represent ± 1 standard deviation.

ULTRASTRUCTURE OF RED-SORE LESIONS ON LARGEMOUTH BASS (Micropterus salmoides): ASSOCIATION OF THE CILIATE Epistylis sp. AND THE BACTERIUM Aeromonas hydrophila

T. C. Hazen,* M. L. Raker,* G. W. Esch,* and C. B. Fliermans

Investigations of red-sore lesions on largemouth bass found that Aeromonas hydrophila was the most likely primary cause. An alternative possibility, Epistylis, is probably just associated with the lesions.

INTRODUCTION

In the southeastern U.S., the gram-negative bacterium Aeromonas hydrophila (Chester) appears to be intimately associated with the peritrich ciliate Epistylis sp. in causing red-sore disease. Common among centrarchid and other game fishes, the disease may reach epizootic proportions, resulting in massive fish kills (Rogers, 1977), i.e. Dean (1974) reported that more than 34,000 fish died of the disease in Badin Lake, North Carolina in 1973.

The external pathologic changes include scale erosion and hemorrhea of the pit-like lesions. These lesions may cover 75% of the body surface of a largemouth bass and ultimately result in hemorrhagic septicemia and death. It has been demonstrated that a correlation between thermal loading and a seasonal periodicity exists in infected fish in Par Pond, a cooling reservoir for a nuclear production reactor near Aiken, SC. A significant relationship has also been shown between the body condition of the fish and the probability of being infected with red-sore disease.

The primary invader in red-sore disease is the stalked, colonial ciliate Epistylis sp. (Rogers, 1977), with secondary involvement by the gram-negative bacterium A. hydrophila. Rogers has suggested that the stalk of Epistylis sp. produces an enzyme that causes scale erosion, allowing secondary invasion of waterborne A. hydrophila. Other researchers (Lom, 1973) maintain that the stalk does not produce lytic enzymes; Epistylis sp. would thus be incapable of producing the lesion which is considered typical of the disease. Though A. hydrophila and Epistylis sp. appear to be intimately associated in the 'red-sore' phenomenon,

* Wake Forest University

the exact nature of their relationship to each other and to the host, Micropterus salmoides Lacépède, is unresolved. In this study, transmission and scanning electron microscopy have been used to examine the nature of these relationships.

MATERIALS AND METHODS

Sampling sites, techniques, procedures, and methodology have been described previously (Hazen, 1978).

RESULTS

Cultures and stained scrapings of bass lesions from 114 fish revealed that 96% contained cultivable A. hydrophila, while Epistylis sp. was observed in only 35% of the same lesions. The quantities of A. hydrophila cultivated from the lesions also indicated that large numbers of viable bacteria were present. Impression slides of the lesions, stained with anti-A. hydrophila conjugate were positive and further substantiated that this bacterium was present in large numbers and was not a spurious contaminant. Swabs from the same areas of both infected and uninfected fish yielded less than 1% positive cultures and, when positive cultures were found, they indicated low densities of A. hydrophila.

Scanning electron-micrographs revealed large numbers of rod-shaped bacteria closely adhering to the stalk of Epistylis sp. (Figure 1). Transmission electron-micrographs of longitudinal (Figure 2) and transverse sections (Figure 3) of the stalk revealed a close association of the bacteria and the ciliates.

DISCUSSION

The basis for the intimate association between A. hydrophila and the stalk of Epistylis sp. is not readily explainable. The stalk has been reported to exude a mucilaginous material (Lom, 1973) which may act as either a nutrient source for the bacteria or may have "adherence" qualities which are lacking on other nearby surfaces. Both transverse and longitudinal sections of Epistylis sp. stalks, covered with bacteria, contain a fuzzy material which may represent the mucilaginous coat.

A. hydrophila was found associated with 96% of the red-sore lesions examined, while Epistylis sp. was observed in only 35% of these lesions. It was shown in other studies that high densities of A. hydrophila can induce lesions in bass held in laboratory aquaria while Epistylis sp. alone will not produce lesions (Lom, 1973). A. hydrophila is known to produce a number of lytic enzymes

(Bernheimer, 1974) while Epistylis sp. is said to be incapable of producing such enzymes (Lom, 1973). Sections of the stalk did not reveal any organelles capable of producing enzymes, and the scarcity of mitochondria further suggested an inactive role for the stalk. It is reasonable to assume that if Epistylis sp. could induce lesions, the point of attachment of the protozoon to the fish surface would be the site of the pathologic changes. Our evidence and that of Lom, however, suggest a benign relationship.

Contrary to Rogers, our results indicate that the etiologic agent of red-sore disease is not Epistylis sp. but the gram-negative bacterium, A. hydrophila. Thus, as the primary invade, A. hydrophila appears to induce the lesion and Epistylis sp. seems to be a secondary, but benign, ectocommensal; or, alternatively, a teletroch of Epistylis sp. attaches to the surface of a fish, develops into a colony, and then is subsequently colonized by A. hydrophila. Once the density of A. hydrophila reaches a threshold level on Epistylis stalks, the bacteria produce lytic enzymes in sufficient quantity to cause a lesion.

The frequency of occurrence of A. hydrophila in lesions free of Epistylis sp. and our observations that A. hydrophila alone can induce lesions in fish held in aquaria indicate that A. hydrophila is most likely the primary cause of red-sore disease in largemouth bass.

REFERENCES

A. W. Bernheimer and L. S. Avigad. "Partial Characterization of Aerolysin, a Lytic Exotoxin from Aeromonas hydrophila." **Infect. Immun. 9**, 1016-12 (1974).

J. Dean. "Fish Disease Outbreak." **Wildlife in North Carolina 38**, 18-19 (1974).

T. C. Hazen, M. L. Raker, G. W. Esch, and C. B. Fliermans. "Ultrastructure of Red-Sore Lesions on Largemouth Base." **J. Protozool 25**, 351-355 (1978).

J. Lom. "The Mode of Attachment and Relation to the Host in Apiosoma piscicola and Epistylis lwoffi, Ectocommensals of Freshwater Fish." **Folia Parasitol 20**, 105-112 (1973).

W. A. Rogers. "Disease in Fish Due to the Protozoan Epistylis in the Southeastern U.S." **Proc. Southeast. Assn. Game Fish Commissioners, 25th Ann. Conf.**, 193-6 (1971).

FIGURE 1. Scanning Electronmicrograph of Stalk from Largemouth Bass Lesion Covered with Rod-Shaped Bacteria (X 10,000)

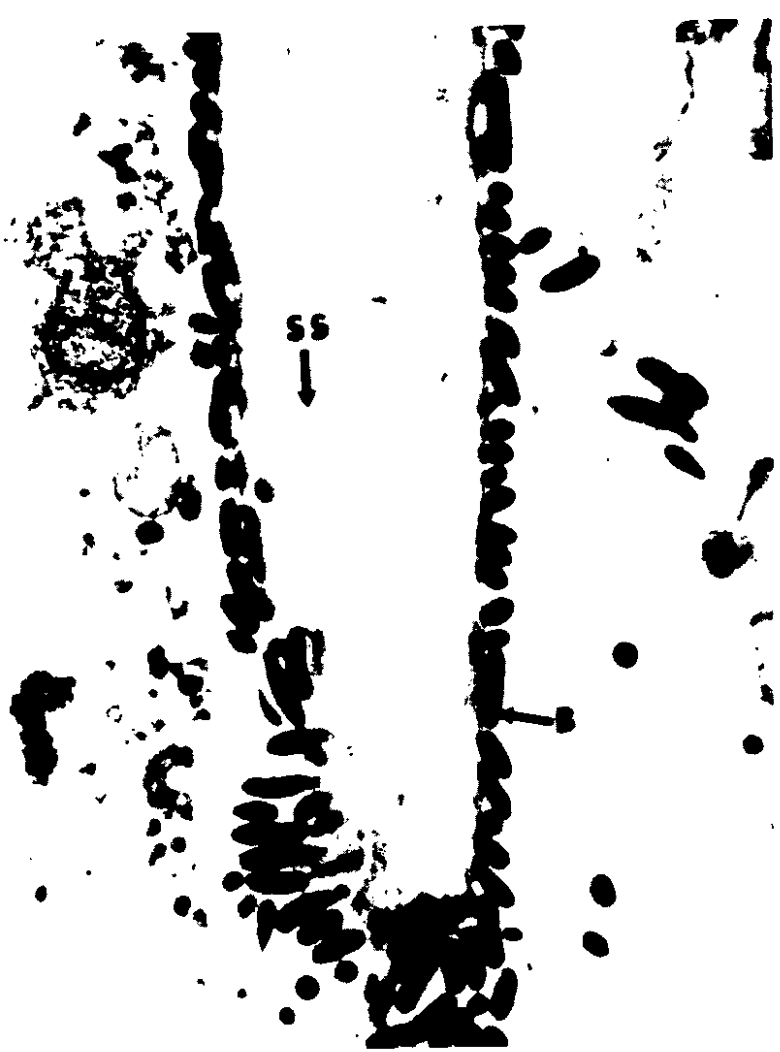

FIGURE 2. Transmission Electronmicrograph of Epistylis sp. from a Largemouth Bass Lesion (X 4,250). Stalk is in longitudinal section. SS = striated stalk fibers. B = bacteria.

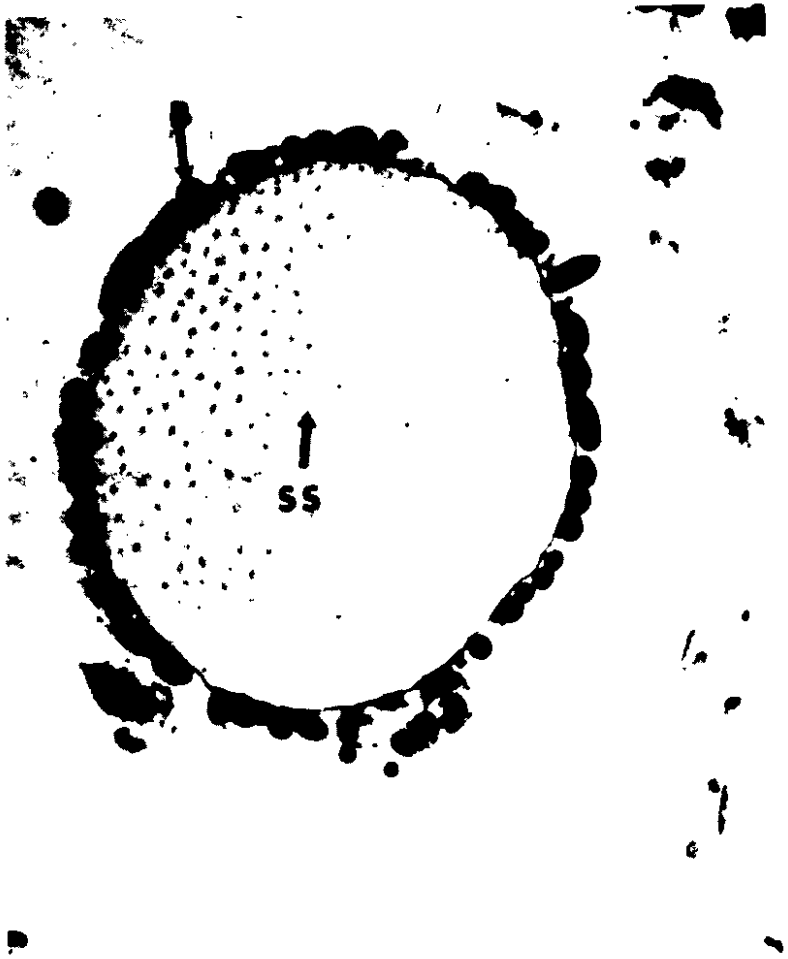

FIGURE 3. Transmission Electronmicrograph of Epistylis sp. from a Largemouth Bass Lesion (X 4,250). Stalk is in transverse section. SS = striated stalk fibers. B = bacteria.

ISOLATION OF Aeromonas Hydrophilia FROM THE AMERICAN ALLIGATOR, Alligator mississippiensis

R. W. Gorden,* T. C. Hazen,* G. W. Esch,* and C. B. Fliermans

Several ponds and swamps were sampled extensively to determine the frequency of isolation of Aeromonas hydrophila. A. hydrophila was isolated from the lungs, hearts, livers, kidneys, and intestines of 16 out of 23 alligators. Although A. hydrophila may be ubiquitous among the sampled alligator populations, under conditions of handling and chemical stress the alligators appear to succumb to the infection.

INTRODUCTION

Aeromonas hydrophila is a pathogen for a wide range of freshwater fish, amphibians and reptiles (Bullock, 1964; Esch, 1976; Marcus, 1971). It has been directly linked with massive fish and alligator kills in Lake Apopka, Florida (Shotts, 1972), and with epizootics of red-sore disease among a variety of fish species in North and South Carolina (Dean, 1974).

During the course of routine bacteriological studies conducted in the spring and summer of 1975, nine SRP Par Pond alligators died suddenly and without apparent cause. Studies in Par Pond indicated that A. hydrophila and red-sore disease are related to temperature induced stress within the largemouth bass (Micropterus salmoides) population (Esch, 1978). The sudden and unexpected mortality among the alligators together with the isolation of A. hydrophila in Par Pond suggested that the bacterium was involved. Since A. hydrophila may require stress conditions to initiate an epizootic disease we suggest that the bacterium is present in or on the alligators and conditions of stress favor a rapid increase in A. hydrophila, contributing to host mortality. Such an hypothesis is in complete agreement with Dubos (1955). A study was conducted on external surfaces, oral cavities, and internal organs of alligators from widely scattered populations in the southeastern United States to determine whether A. hydrophila was commonly present.

* Wake Forest University

MATERIALS AND METHODS

Aseptic techniques were used to sample A. hydrophila from 123 alligators ranging in age from six months to greater than ten years. Samples were taken from internal tissues of recently killed specimens and external samples using sterile cotton applicators. Both swabs and filters were streaked or placed on Rimler-Shotts (RS) medium (Rimler, 1973) and incubated aerobically at 35°C for 18 to 14 hours. Presumptive isolates of A. hydrophila on RS medium were confirmed using the API-20 identification system.

Alligators were obtained from Rockfeller Refuge, LA; South Carolina coastal ponds; Okefenokee Swamp, GA; Orange Lake, FL; and Par Pond, a reactor cooling reservoir at SRP. All animals were captured under federal government permits.

RESULTS AND DISCUSSION

A. hydrophila was isolated from the lungs, hearts, livers, kidneys, and intestines of 69% of the alligators (Table 1). Additional samples were taken from the external surface of 39 live animals. Of the alligators captured in the wild, A. hydrophila was isolated from swabs taken outside of the oral cavity in 50% (35/70) of the animals, while 92% (12/13) of the animals hatched and raised in growth chambers also had the bacterium externally. A. hydrophila was isolated from the oral cavity of 85% (40/47) of the animals sampled in the wild. No data are available for growth chamber animals.

These data indicate that healthy alligators held and raised in captivity, or captured in the field, possess A. hydrophila on the mouth, in the oral cavity and in internal organs. Futher, the high percentage of alligators positive for A. hydrophila, strongly suggests that the bacterium may be ubiquitous among the sampled alligator populations.

While A. hydrophila may not cause disease under normal conditions, during periods of stress the bacterium could be a problem. Recent studies of A. hydrophila in other poikilothermal organisms indicate that a number of factors, i.e. stress and warm water water temperatures, may have contributed to the mortality of Par Pond alligators in the spring and summer of 1975. Groberg (1978) demonstrated a positive correlation between water temperature and the probability of mortality in steelhead trout (Salmo gairdneri) inoculated with low numbers of A. hydrophila. They concluded that higher temperatures (20.5°C) favored rapid proliferation of the bacteria and subsequent host mortality. In this regard, mortality of Par Pond alligators occurred when water temperatures

were in excess of 20°C, and when rapid reproduction of A. hydrophila was favored. However, mortality occurred only among those alligators subjected to handling and not among those which were not trapped or otherwise manipulated, suggesting that stress of handling, in addition to temperature, contributed to their death.

Based on these observations, we suggest that low densities of A. hydrophila in internal organs, coupled with high water temperatures and stress induced by extreme trapping procedures and handling, are sufficient to create physiologic conditions conductive to rapid proliferation of the bacteria. We also suggest that the increases in A. hydrophila within the internal organs result in the production of sufficient quantities of lytic toxins to induce lesions characteristic of red-sore disease (Hazen, 1978), and subsequent mortality.

If A. hydrophila, in combination with stress, does indeed cause death, trapping, handling and manipulation of alligators should be eliminated when water temperatures are warm or when red-sore disease is known to be present among other species.

REFERENCES

G. L. Bullock. "Pseudomonadales as Fish Pathogens." **Dev. Ind. Microbiol. 5**, 101-108 (1964).

J. Dean. "Fish Disease Outbreak." **Wild. in North Carolina**, 18-19 (1974).

R. J. Dubos. "Second Thoughts on the Germ Theory." **Sci. Amer. 192**, 31-35 (1955).

G. W. Esch; T. C. Hazen; R. V. Dimock, Jr.; and J. W. Gibbons. "Thermal Effluents and the Epizootiology of the Ciliate Epistylis and the Bacterium Aeromonas in Association with Centrarchid Fish." **Trans. Am. Micros. Soc. 95**, 687-693 (1976).

G. W. Esch and T. C. Hazen. "Thermal Ecology and Stress: Case History for Red-Sore Disease in Largemouth Bass (Micropterus salmoides)." In: **Energy and Environmental Stress in Aquatic Systems.** DOE Symposium Report CONF-771114, Department of Energy, Washington, DC (1978).

U. J. Groberg, R. H. McCoy, K. S. Pilcher, and J. L. Fryer. "Relation of Water Temperature to Infections of Coho Salmon (Onchorhynchus kisutch), Chinook Salmon (O. tshawytscha) and Steelhead Trout (Salmo gairdneri) with Aeromonas salmonicida snd A. hydrophila." **J. Fish Res. Bd. Can. 35**, 1-7 (1978).

T. C. Hazen, M. L. Raker, G. W. Esch, and C. B. Fliermans. "Ultrastructure of Red-Sore Lesions on Largemouth Bass (Micropterus salmoides): the Association of the Beritrich, Epistylis sp., and the Bacterium, Aeromonas hydrophila." **J. Protozoology 25** (1978).

L. C. Marcus. "Infectious Diseases of Reptiles." **J. Am. Vet. Med. Ass. 159**, 1626-1631 (1971).

R. Rimler. "A Medium for the Isolation of Aeromonas hydrophila." **Appl. Microbiol. 26**, 550-553, (1973).

E. B. Shotts, Jr.; J. L. Gaines; L. Martin; and A. K. Prestwood. "Aeromonas-Induced Deaths Among Fish and Reptiles in an Eutrophic Inland Lake." **J. Am. Vet. Med. Ass. 161**, 603-607 (1972).

TABLE 1. Isolation of A. hydrophila from Alligators Captured in Various Locations in the Southeastern United States

Location	Date	Age	Alligators positive for A. hydrophila/number sampled			Comments
			External	Oral Cavity	Tissue	
Par Pond	Spring/78	Adult[a]	8/8	ND[b]	8/8	Necropsy - intestines and lungs were sampled
Rockefeller[c]	9/23/76	Adult	ND	ND	8/15	Harvest,[d] lung, heart, liver, kidney tissue
Rockefeller[c]	9/24/76	Adult	2/16	ND	ND	Live, wild
Coastal, SC	10/14/76	Juv.[e]	18/22	ND	ND	Live, wild
Rockefeller	2/4/77	Juv. 3 yr	6/7	ND	ND	Live, growth chamber[f]
Rockefeller	2/4/77	Juv., 2 yr	3/3	ND	ND	Live, growth chamber
Rockefeller	2/4/77	Juv., 1 yr	3/3	ND	ND	Live, growth chamber
Coastal, SC	4/12/77	Juv.	2/9	9/9	ND	Live, wild
Coastal, SC	6/21/77	Juv.	3/9	10/11	ND	Live, wild
Okefenokee	7/10/77	Adult	2/6	2/4	ND	Live, wild
Coastal, SC	8/9/77	Juv.	ND	6/6	ND	Live, wild
Orange Lake	8/14/77	Juv., 1 yr	ND	13/17	ND	Live, clutch mates
		Totals	40/75	40/47	16/23	

a. Adult = adult alligator (>6 feet long, 6 years or older).

b. ND = Not Determined.

c. Inadequate incubation facilities for accurate bacterial analyses probably resulted in a conservative number of positive samples.

d. Harvest - animals killed in federally controlled alligator harvest.

e. Juv. = juvenile alligator (<6 feet long, less than 6 years of age).

f. Growth chamber = hatched and raised in growth chambers under controlled temperature conditions.

UPPER TEMPERATURE LIMITS FOR ALGAE IN SRP REACTOR EFFLUENTS

E. W. Wilde

Thermal effluents from the Savannah River Plant nuclear reactors provide an opportunity to study responses of algae to a severe temperature stress. Summer temperatures in reactor discharge canals often range from >75°C, which is higher than the maximum tolerable temperature for all known algae (Castenholz, 1978; Brock, 1967, 1975), to near ambient. Algal communities above 56-60°C consist only of 2 blue-green alga taxa. The communities become increasingly more complex as the water cools; at near ambient, 40 species (6 blue-greens, 15 greens, and 19 diatoms) were observed.

PURPOSE

Primary objectives of current studies are to determine maximal and optimal temperatures at which principal algae grow in the system, and to assess spatial and temporal variability in algal biomass and composition resulting from reactor operation. These studies are in conjunction with a variety of physiological studies of the autotrophic and heterotrophic activities of thermophilic organisms on the SRP site.

METHODS

Fifty-two algal samples collected from a specially designed trough parallel to the P-Area reactor discharge canal were quantitatively analyzed. Sampling sites on the trough represented a gradient of temperatures on each of 11 sampling dates. Core samples were diluted to a known volume and homogenized. An aliquot of each homogenate was examined with an inverted fluorescence microscope, and algae which demonstrated chlorophyll fluorescence were identified and enumerated. Dimensions of all taxa were measured to calculate algal volume per unit area of trough substrate.

RESULTS AND DISCUSSION

Mastigocladus laminosus and Phormidium sp., a pair of cosmopolitan, thermophilic, blue-green algae (Castenholz, 1978), were

the only taxa collected at temperatures above 50°C. They appear to grow at temperatures up to around 60°C in both P-Area reactor and C-Area reactor canal systems. A single species of *Oscillatoria* usually grows along with Mastigocladus and Phormidium between 45 and 50°C. Six blue-green and one green alga (Cosmarium sp.) were collected from water exceeding 40°C in the P-Reactor canal system (Table 1). At successively lower temperatures, a distinctive shift in dominance from blue-green algae to green algae to diatoms occurred along with a dramatic increase in species diversity (Table 2). A similar phenomenon has been reported for other systems (Patrick, 1969).

The volume of attached, chlorophyll-containing algal material per unit area of substrate was measured at temperatures of 50, 45, 40, 35 and 30°C during three different reactor cycles. Figure 1 shows mean values for total algal volume and Mastigocladus-Phormidium volume. The data show that the diverse nature of the mat at 30 and 35°C results in a substantially larger quantity of chlorophyll-containing algal material per unit area than does the blue-green dominated mat at 40-50°C. Gross structure of the algal mat at temperatures of 40-50°C is conspicuously different than the mat at 35 and 30°C. At the higher temperatures, a very thin layer of interwoven, viable, blue-green algal filaments overlies a thick mass of "dead" (non-chlorophyllous) blue-green algal filaments. At 35 and 30°C, the mat is much less compacted and lacks both the large quantity of dead algal material and the thin, leathery, light-inhibiting cover of blue-green algae present at the higher temperatures.

REFERENCES

T. D. Brock. "Life at High Temperatures." **Science 158,** 1012-1018 (1967).

T. D. Brock. **Predicting the Ecological Consequences of Thermal Pollution from Observations on Geothermal Habitats.** Proceedings of the Symposium on Environmental Effects of Cooling Systems of Nuclear Power Plants, IAEA, 599-622, Vienna, Austria (1975).

R. W. Castenholz. "Thermophilic Blue-Green Algae and the Thermal Environment." **Bact. Rev. 33** (4), 476-504 (1975).

R. W. Castenholz. "The Biogeography of Hot Spring Algae Through Enrichment Cultures." **Mitt. Internat. Verein. Limnol. 21,** 296-315 (1978).

R. Patrick. **Some Effects of Temperature on Freshwater Algae.** Biological Aspects of Thermal Pollution, Vanderbilt University Press, Nashville, TN, 161 (1969).

TABLE 1

Thermophilic Algae Collected from the P-Area Reactor Canal System

Temperature >50°C	Temperature >45°C	Temperature >40°C
Mastigocladus laminosus	*Mastigocladus laminosus*	*Mastigocladus laminosus*
Phormidium sp.	*Phormidium* sp.	*Phormidium* sp.
	Oscillatoria sp.	*Oscillatoria* sp.
		Anabaena sp.
		Chroococcus sp.
		Colonial blue-green sp.
		Cosmarium sp.

TABLE 2

Distribution of Algae at Various Temperature Increments in the P-Area Reactor Effluent Canal System

Temperature °C	Number of Species Observed			
	Blue-Greens	Greens	Dias	Total
56-60	2	0	0	2
51-55	2	0	0	2
46-50	3	0	0	3
41-45	6	1	0	7
36-40	6	3	0	9
31-35	6	11	6	23
26-30	6	15	19	40

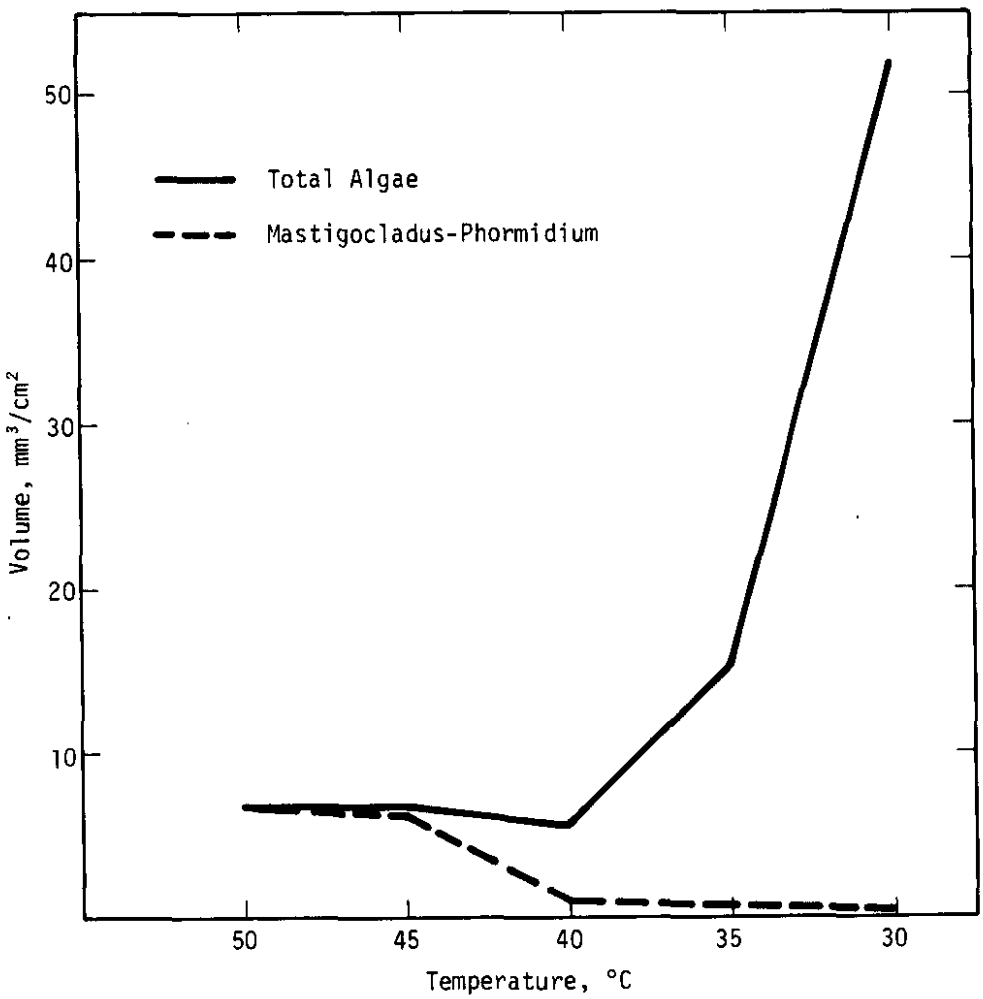

FIGURE 1. Volume of Attached Chlorophyll-Containing Algae at Various Temperatures. Data points represent mean values for three sampling dates during three different reactor cycles.

SEASONAL RESPONSE OF PERIPHYTON TO TEMPERATURE ELEVATION

D. C. Brown*

The Flowing Streams Laboratory consists of streams maintained at temperatures of 2.5, 5, 7.5, and 12.5°C above ambient. As Wilde (1978) has reported, the taxonomic composition of algal communities from elevated temperature streams differs from that of the ambient temperature streams. Algal biomass (as measured by chlorophyll a per slide) and productivity (as measured by ^{14}C-uptake per slide per hr) were measured in ambient temperature, +5°C, and +12.5°C streams for 1 year. The communities in the 3 streams differed significantly. The elevated temperature changed the seasonal pattern of biomass and productivity of the periphyton.

METHODS

Glass slides were held in clear plastic troughs so that the water flow was parallel to their long axis. Fourteen days were allowed for colonization by periphyton before samples were processed. Chlorophyll a was determined by extracting the chlorophyll from the slides with 90% acetone (buffered with $MgCO_3$) and reading the extractions in a Beckman spectrophotometer (Strickland 1972). ^{14}C-uptake was determined by 1.5 hour incubations of colonized slides with $NaH^{14}CO_3$ in closed incubation bottles. The contents of each bottle were stirred with a magnetic stirring bar.

RESULTS

Figures 1 and 2 show chlorophyll a per slide and carbon uptake per slide per hr, respectively, over the year. The 3 communities differed greatly in their pattern of biomass content over the year. The ambient temperature communities had a lower biomass in winter, exhibited a small peak at the end of March and a large one in June and July. The +12.5°C communities had more biomass in winter than did the ambient temperature communities, peaked at the beginning of June, and were very low in July and August. The +5°C communities were generally intermediate in biomass, peaking in May and at the end of July, and showing a surge in November.

* SRL Graduate Participant from the University of South Carolina.

Carbon-uptake per slide per hr was similar to the chlorophyll data. The uptake by the ambient temperature communities was low in winter and high in summer. The uptake by the +12.5°C communities slumped in summer. Productivity generally peaked later than chlorophyll peaks.

DISCUSSION

Elevating the temperature of an aquatic system changes the seasonal pattern of biomass and productivity of the periphytic communities. This is shown in this study by chlorophyll a per slide, with elevated temperature communities having more chlorophyll a per slide in winter and less in summer than ambient temperature communities. Productivity is more variable from week to week than chlorophyll a. Carbon uptake depends on the precise conditions at the time of incubation as well as the conditions during the two-week colonization period. Varying nutrients, pH, and available carbon may blur the seasonal and temperature effect on carbon uptake.

REFERENCES

T. V. Crawford, et al. "Periphytic Algal Species Composition Differences in Thermally Altered Artificial Streams." **Savannah River Laboratory Environmental Transport and Effects Annual Report - 1977.** USERDA Report DP-1489, E. I. du Pont de Nemours & Co., Savannah River Laboratory, Aiken, SC (1978).

J. D. H. Strickland and T. R. Parsons. A Practical Handbook of Seawater Analysis. **Fish, Res. Bd. Can. 167**, 311 (1972).

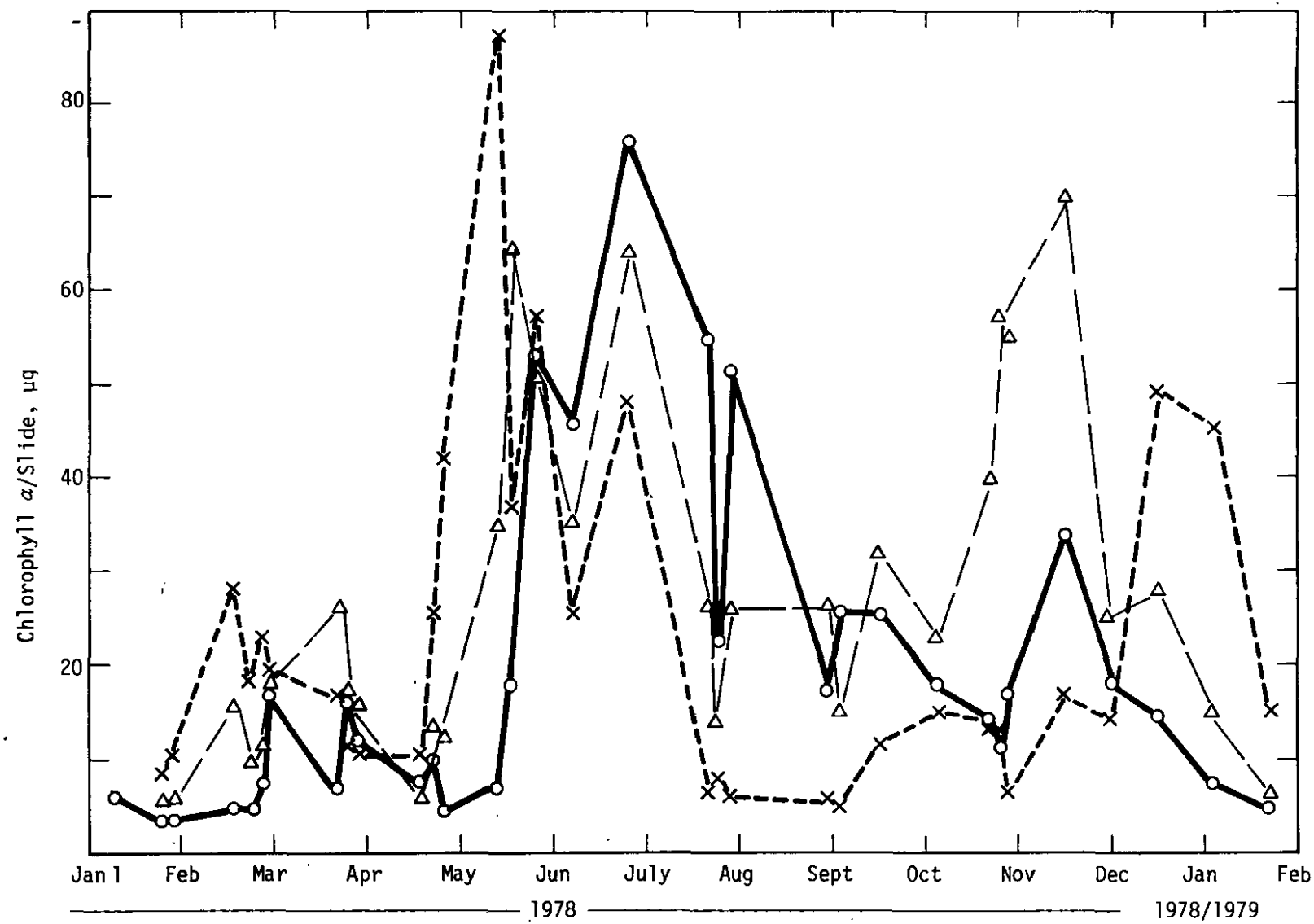

FIGURE 1. Chlorophyll a/Slide vs. Season. O: ambient temperature. Δ: +5°C. X: 12°C. Means of 3 to 6 replicates shown.

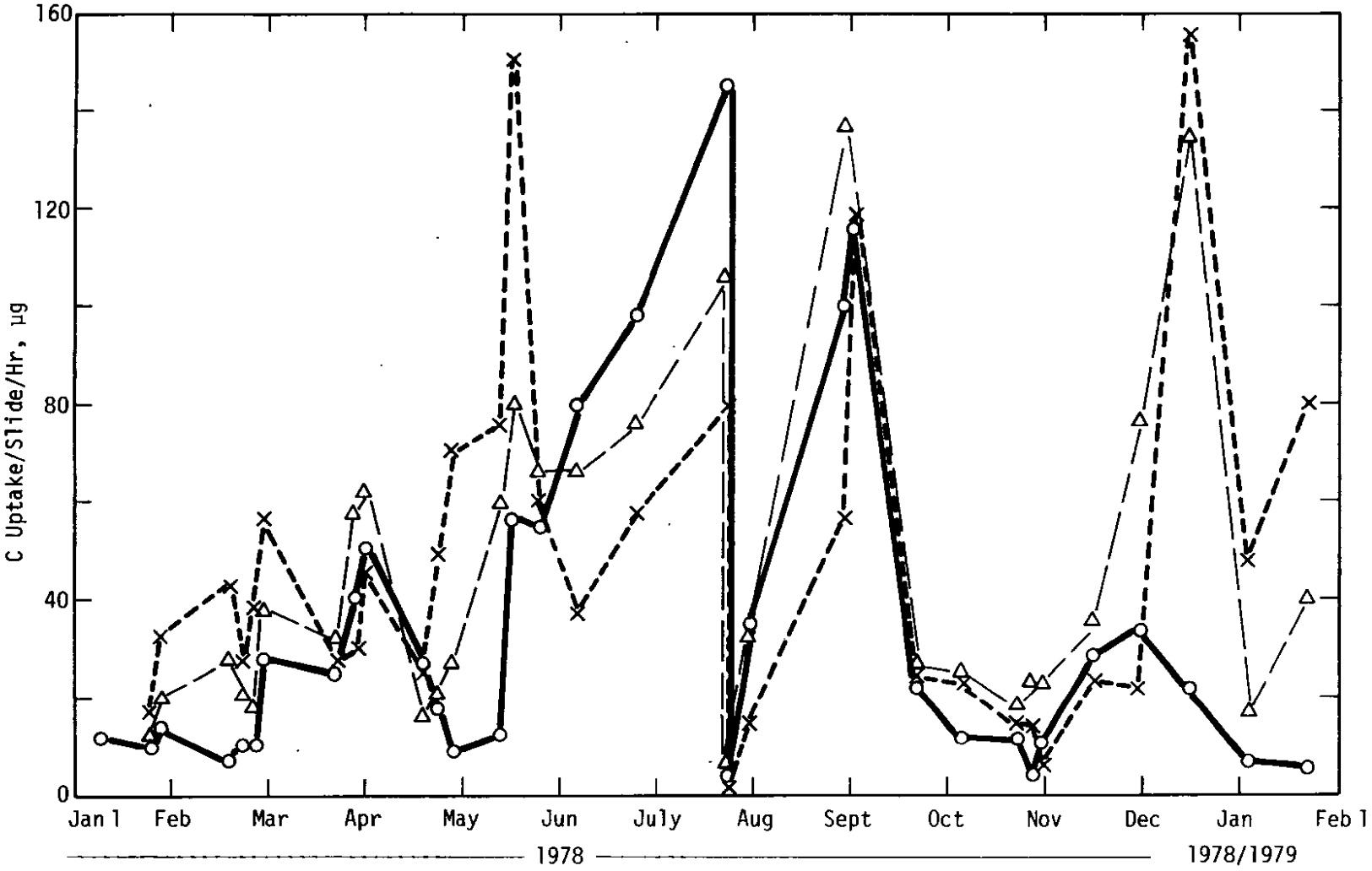

FIGURE 2. Carbon-Uptake/Slide/Hr vs. Season. O: ambient temperature. Δ: +5°C. X: 12°C. Means of 3 to 6 replicates shown.

EFFECT OF TEMPERATURE ELEVATION ON PERIPHYTON COMMUNITIES FROM ENRICHED AND UNENRICHED "STREAMS"

D. C. Brown*

The interactions of elevated temperature and nutrient addition can affect both the species' composition and the productivity of algal communities (McCombie, 1960; Patrick, 1969) in patterns which differ from single-factor effects. Periphyton communities from Upper Three Runs Creek were used to investigate this interaction at the Flowing Streams Lab. The hypothesis was that unenriched (oligotrophic) and enriched (simulated eutrophic) periphyton communities would differ in biomass and rate of primary productivity under different temperature regimes. In general, the experiments indicated that increased nutrient concentration stimulated periphyton growth and production in July with the +12°C community, and in January with the ambient temperature community.

METHODS

A 3 x 3 array of clear plastic troughs contained the slide racks for the glass slide periphyton communities. Three sequential troughs were at ambient, +5°C and +12°C temperatures. Nitrate, phosphate, calcium, manganese, molybdenum, and cobalt were added to one or both downstream troughs at each temperature. Samples of periphyton were taken, after a 14-day colonization period for chlorophyll a (Strickland, 1972), ash-free dry weight (Standard Methods, 1975), protein (Lowry, 1951), and carbon-uptake (See Brown, p. 163). Three replicate experiments were conducted during an 8-day period in April, July, and October 1978, and in January 1979. Each experiment lasted for 2 days. An increase in biomass parameters or in rate of carbon-uptake is taken to indicate stimulation.

RESULTS AND DISCUSSION

Although a more thorough computer analysis is not yet available, the basic results of the three experiments for each season are shown in Table 1. The most consistent stimulatory effect of nutrient addition to these communities occurred in July and January, months with typically less variable light and temperature conditions.

* SRL Graduate Participant from the University of South Carolina.

Chlorophyll a and carbon uptake are the parameters which are directly involved with the periphyton; dry weights and protein measurements involve animal and detrital matter as well as plant matter. The chlorophyll a and carbon uptake results are therefore considered more important in evaluating stimulation. These two parameters were greater under enriched conditions for ambient temperature communities in July and January, for +5°C communities in January, and for +12°C communities in July and in January. When nutrients were added, the ash-free dry weight and protein increased in July at all three temperatures, in October for +12°C communities, and in January for +5°C communities.

These results suggest that, although the nutrient concentrations in Upper Three Runs are very low, the addition of nutrients does not always increase periphyton growth and production. In the hot summer months and during winter, increased nutrient levels stimulate periphyton communities. During spring and fall, when temperatures are fluctuating, results are less consistent and other factors (temperature, photoperiod, pH) may be more important in controlling periphyton growth than nutrient levels.

REFERENCES

O. Lowry, N. J. Rosebrough, A. L. Farr, and R. J. Randall. "Protein Measurement with the Folin Phenol Reagent," **J. Biol. Chem. 193**, 265-275 (1951).

A. M. McCombie. "Actions and Interactions of Temperature, Light Intensity, and Nutrient Concentration on the Growth of the Green Alga, Chlamydomonas reinhardi Dangeard," **J. Fish. Res. Bd. Can. 17**, 871-894 (1960).

R. Patrick, B. Crum, and J. Coles. "Temperature and Manganese as Determining Factors in the Presence of Diatom or Blue-Green Algal Floras in Streams," **Proc. Nat. Acad. Sci. USA 64**, 472-478 (1969).

Standard Methods for the Examination of Water and Wastewater. **Am. Public Health Assn.**, 1193 (1975).

J. D. H. Strickland and T. R. Parsons. "A Practical Handbook of Seawater Analysis," **Fish. Res. Bd. Can. 167**, 311 (1972).

TABLE 1. Effect of Added Nutrients on Periphyton Communities at Ambient, +5°C, and +12°C
(+ indicates increase in parameter; 0 indicates no effect or decrease)

	Ambient			+5°C			+12°C		
Experiments:	1	2	3	1	2	3	1	2	3
April 1978									
Chlorophyll *a*	0	0	+	+	0	0	0	0	+
Carbon Uptake	0	0	+	+	0	+	0	0	0
Ash-free Dry Weight	0	+	+	0	0	+	+	+	+
July 1978									
Chlorophyll *a*	0	+	+	0	0	0	+	+	+
Carbon Uptake	+	+	0	+	0	+	+	+	+
Ash-free Dry Weight	+	+	+	+	0	+	+	+	+
Protein	0	+	0	+	0	+	+	0	+
October 1978									
Chlorophyll *a*	0	0	0	0	0	0	0	0	+
Carbon Uptake	0	+	0	0	0	0	0	0	0
Ash-free Dry Weight	0	0	0	0	+	+	+	+	+
Protein	0	+	0	+	0	0	+	+	0
January 1979									
Chlorophyll *a*	+	+	+	+	+	+	+	+	+
Carbon Uptake	+	+	+	+	+	0	0	0	+
Ash-free Dry Weight	0	0	0	+	+	+	0	0	0
Protein	0	+	0	0	+	0	0	0	0

TERRESTIAL STUDIES

EFFECT OF DISKING AND OTHER AGRICULTURAL PRACTICES ON THE DISTRIBUTION OF SURFACE DEPOSITED PLUTONIUM IN SOIL

J. C. Corey, J. E. Pinder,* and D. C. Adriano*

Two old fields near a chemical separations facility were recently farmed to determine the behavior of Pu deposited on the soil surface due to routine low-level stack releases during the last 20 years. The soil was disked thoroughly in preparation for a wheat crop in 1974 and a soybean crop in 1975. The agricultural practices did not materially increase the plutonium concentration in the 15 to 30 cm depth nor reduce the plutonium in the surface 0 to 5 cm depth. There was a considerable increase in the 5 to 15 cm depth.

METHODS

To determine the redistribution of Pu by agricultural cultivation, samples of soil were collected at various periods on two agricultural fields adjacent to the H-Area facility: while the field was in its old field condition, after soil preparation for a wheat crop, after the wheat harvest, and after a soybean harvest. Plutonium is being deposited on the two fields by global fall-out and stack releases from H Area. When the study began in 1974, approximately 1.2 Ci of $^{238,239,240}Pu$ had been released by the H-Area stack since operations began in 1955. During 1974 and 1975 a total of 8 mCi were released from the stack. Thus, stack releases during the study had a negligible influence upon Pu concentrations in the soil.

RESULTS

Downward movement of Pu was very slow during the 20 years in which the Pu was deposited on the soil surface since, as shown in Table 1, the Pu concentration in both fields was much higher in the 0 to 5 cm depth than in either the 5 to 15 cm or 15 to 30 cm depth before tillage. Tillage did produce increases in the 5 to 15 cm depth of soil in both fields indicating some mixing of the 0 to 5 cm and 5 to 15 cm depths, but the amount of mixing was surprisingly small. This observation suggests that agricultural practices will not rapidly reduce the plutonium concentration of the top 15 cm of soil. The other significant change was a reduction of the Pu concentration in the 15 to 30 cm depth of soil in Field 1. There is no apparent explanation for this change.

* Savannah River Ecology Laboratory

TABLE 1

Plutonium in Soil (pCi/g)[a]

Sampling Time	Field 1 depth (cm) 0 to 5	5 to 15	15 to 30	F Test[b]
Before Tillage	2.5 (2.6)	0.08 (2.5)	0.10 (3.2)	**
After Wheat Planting	4.3 (2.2)	0.33 (4.3)	--	**
After Wheat Harvest	2.6 (3.2)	0.22 (3.5)	0.02 (1.8)	**
After Soybean Harvest	3.6 (2.3)	0.67 (2.5)	0.04 (2.8)	**
F Test[b]	NSD	**	**	
	Field 2 depth (cm)			
Before Tillage	0.87 (1.4)	0.10 (3.2)	0.029 (1.8)	**
After First Tillage	0.61 (1.6)	0.12 (2.4)	—	**
After Wheat Harvest	0.64 (1.6)	0.26 (2.6)	0.019 (2.4)	**
After Soybean Harvest	0.91 (1.8)	0.32 (2.5)	0.013 (2.4)	**
F Test[b]	NSD	*	NSD	

a. The data are log-normally distributed so the reported values are geometric means. The values in ( ) are geometric standard deviations.

b. * Significant difference at the 0.05 level of confidence.
** Significant difference at the 0.01 level of confidence.

LEACHATE CONCENTRATIONS OF HEAVY METALS FROM COAL ASH FOLLOWING SEWAGE EFFLUENT APPLICATION

J. H. Horton,* T. R. Fawcett,** and J. C. Corey

Secondarily treated sewage effluent is currently being applied to an ash-filled basin on SRP. The purpose of this study was to determine the leachate concentrations of As, Cd, Co, Cu, Hg, Pb, and Zn for ash columns to which distilled water or sewage effluent was applied. Sewage effluent application did not increase the concentration of the heavy metals in the effluent over those observed with distilled water.

DISCUSSION

Eight columns, each 75 cm long, were filled with ashes from the 400-D Area ash basin. Once a week, 100 mL of deionized water were added to each of four columns, and 100 mL of treated sewage from 400-D Area were added to each of the remaining four columns.

Results of the laboratory leaching studies are shown in Figures 1 and 2. There were no major differences in the effluent concentrations from ash columns treated with distilled water or sewage effluent except for As. The effluent concentration of As from the columns receiving distilled water were significantly greater than those receiving sewage effluent. Drinking water standards for As, Cd, Pb, and Hg in drinking water are 50, 10, 50, and 2 ppb, respectively. In all cases the observed concentrations were less than the standards for these inorganic elements.

* Deceased.
** Co-op student from Clemson University.

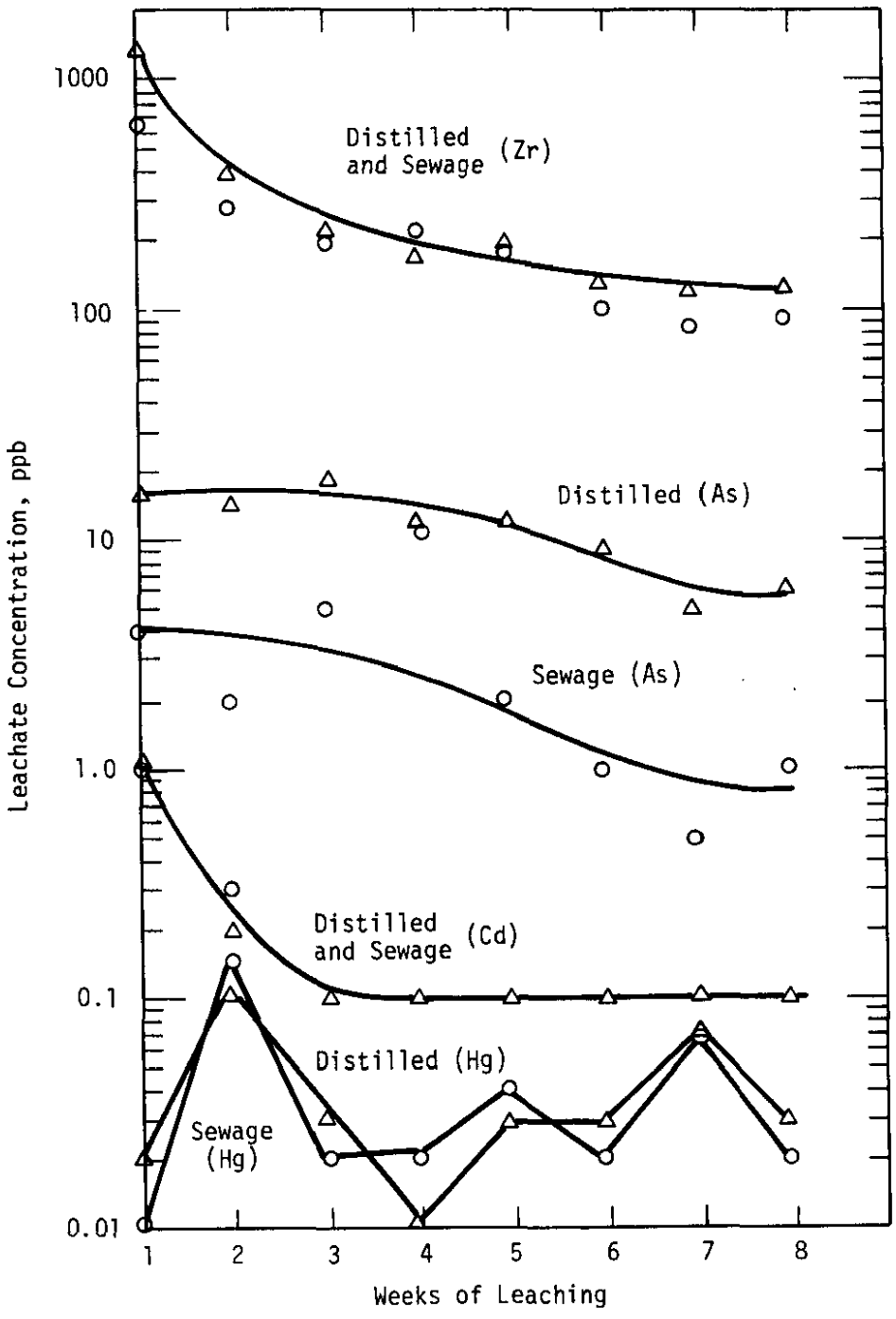

FIGURE 1. Leachate Concentrations Following Application of 100 mL per Week of Distilled Water or Sewage Effluent to Ash-Filled Columns (Zr, As, Cd, and Hg)

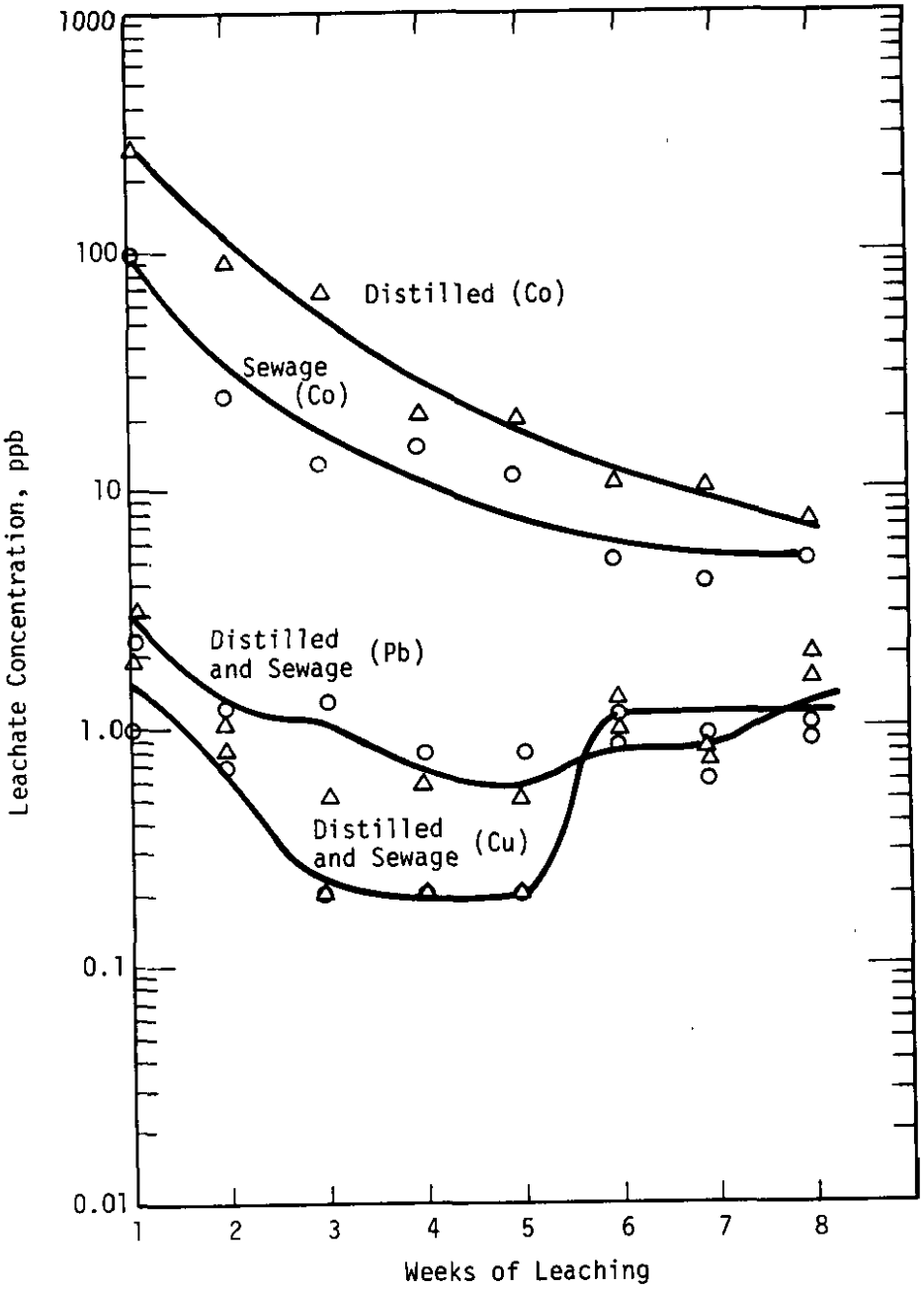

FIGURE 2. Leachate Concentrations Following Application of 100 mL per Week of Distilled Water or Sewage Effluent to Ash-Filled Columns (Co, Pb, and Cu)

TRITIUM CYCLING IN A TREE SPIKED WITH TRITIATED WATER

C. E. Murphy, Jr., and J. C. Luvall*

Transfer and turnover rates in forests are important to compute the residence time of tritiated water in an area following an accidental release (Watts, 1978). In this study tritium was injected in the base of 7 year old, loblolly pine (Pinus taeda, L) trees to determine the rate of transfer through the trees and the turnover in the trees independent of the soil. The results indicate the flow rates depend on the rate of water movement through the tree, which is influenced by the microclimate, and exchange of tritium with hydrogen exchange sites in the tree. The initial pulse of tritium appears to move through the tree in about four days. The descending portion of the curve can be described as a two compartment model with half-lives of 1.41 and 21.7 days. There is some evidence that a longer turnover compartment is associated with metabolically fixed tritium.

METHODS

Tritiated water (8.37 mCi/mL) was injected into each of three holes drilled in the base of four loblolly pine trees. Four branch tips were bagged in polyethylene bags. The water condensing in the bags was collected for the next four mornings and then less frequently until the seventeenth day. Simultaneously the needles and a section of branch from the bagged branch tip and adjacent branch tip were sampled and stored in glass containers. After each sampling, new branch tips were bagged for the next sample to be collected. Water was obtained from the needles and branches by vacuum distillation. The dry needles and branches were burned and the water of combustion collected. Water from each type of sample was counted for tritium by liquid scintillation.

RESULTS

Figure 1 shows the concentration of tritium in the water collected by freeze drying for one of the four trees injected. The primary difference in the concentrations is that the water

*Savannah River Ecology Laboratory

collected from the bags peaks at a much higher level. Freeze drying methods might not have determined the peak concentration because they measure the concentration taken over a short period of time, while the bags collect an integrated sample. After the initial period of three days, the decrease in concentration is about the same for all the sampling methods. By fitting a straight line to two segments of the descending section of the curve, the turnover rate of two compartments can be approximated as 1.41 and 21.7 days.

At the end of the measurement period the water concentration had decreased to 0.2 nCi/mL while the combusted sample averaged 1.0 nCi/mL. Immediately after the injection of tritiated water, the concentration in the water of combustion rose and fell with the water concentration at a level of about 30% of the equilibrium value in the water. The value of 30% is close to the value of the exchangeable hydrogen expected in wood (Taniguchi, 1978). The maintenance of tritium above the level of the exchangeable equilibrium suggests that a small part of the tritium has entered tightly bound compartments.

REFERENCES

T. Taniguchi, H. Harada, and K. Nakato, "Determination of Water Adsorption Sites in Wood by a Hydrogen - Deuterium Exchange." **Nature 72**, 230-231 (1978).

J. R. Watts and C. E. Murphy, Jr. "Assessment of Potential Radiation Dose to Man from an Acute Tritium Release into a Forest Ecosystem." **Health Physics 35**, 278-291 (1978).

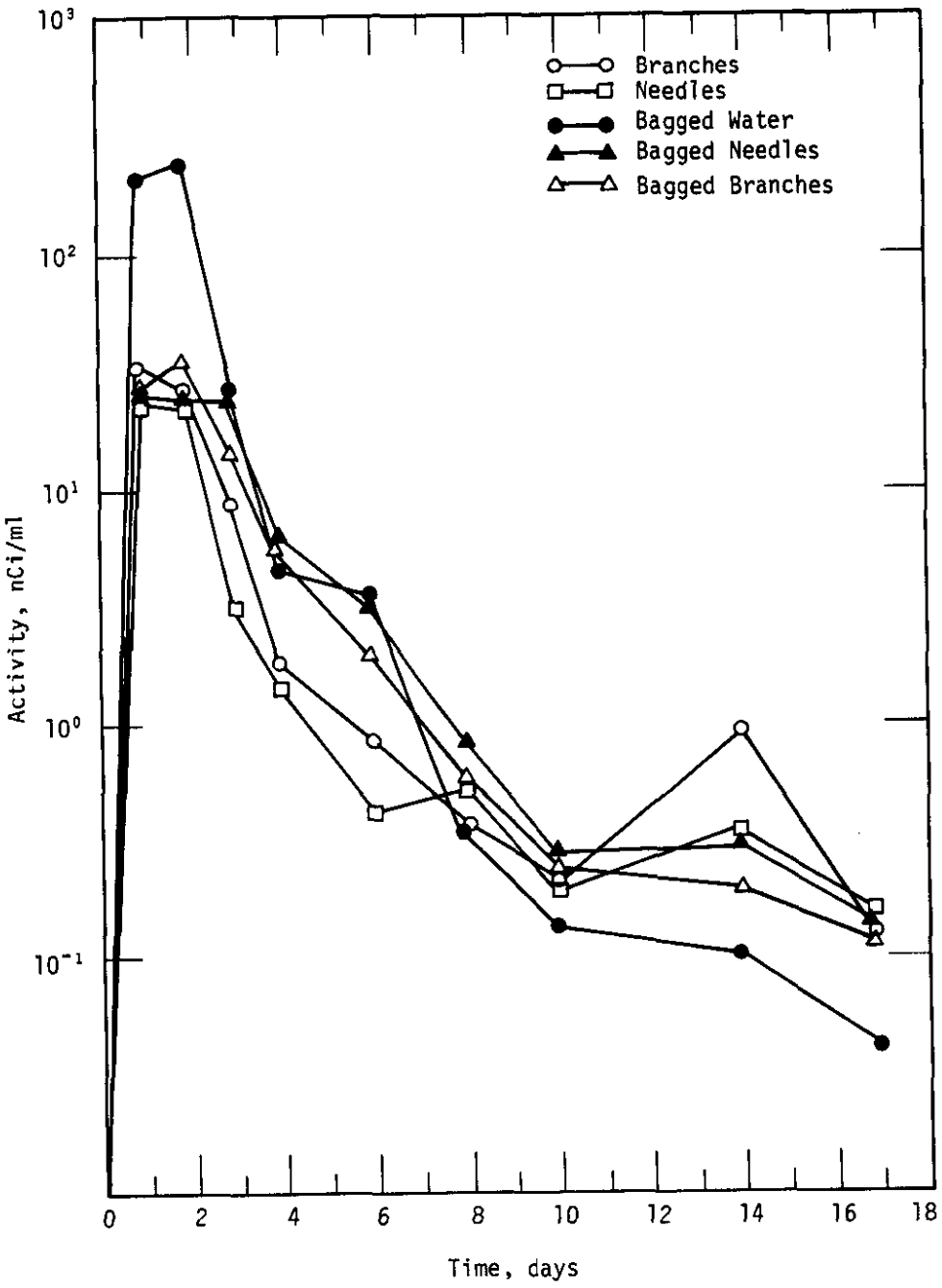

FIGURE 1. Concentration of Tritiated Water in a Pine Tree Following Basal Injection

THE MEASUREMENT OF THERMAL CONDUCTIVITY AND HEAT FLUX IN SOIL

C. E. Murphy, Jr., and S. Kaplan*

Energy balance techniques are being employed to determine the heat and mass transfer characteristics of a typical SRP pine forest. One term of the energy balance of the forest is the heat transfer to the ground under the canopy. Knowledge of the heat transfer characteristics of the soil allows determination of the magnitude of the soil heat transfer. Measurement indicated the thermal conductivity is 0.00882 cal/cm-sec-°C and the thermal diffusivity is 0.0145 cm^2/sec.

METHOD

An in situ method of measuring heat flux characteristics is the most desirable to obtain reliable heat transfer characteristics because obtaining undisturbed soil samples for laboratory analysis is difficult. In this study, the diurnal variation of soil temperature was measured at four depths (2.5, 5.1, 12.7, and 25.4 cm) with two junction copper-constantan thermocouples. The temperatures were recorded every half hour and the resulting time series was subjected to Fourier analysis. The base period was 24 hours. Amplitudes (T_a) and phase angles (ϕ) were computed for five harmonics (periods 24, 12, 6, 3, and 1.5 hours). Heat transfer theory predicts the slope of the phase angle vs. the depth (Z) of measurement, or the slope of the logarithm of the amplitude vs. depth will define the damping depth (D).

$$D = \sqrt{\frac{w}{2a}} = \frac{Z}{\phi} \qquad (1)$$

w = angular frequency

a = thermal diffusivity

The damping depth can be used to solve for the thermal diffusivity. The heat flux at the surface can be approximated from the Fourier series at the measurement depth extrapolated to the surface according to Equation 2 (Van Wijk, 1966).

* Co-op student from Georgia Tech.

$$H_s = -\lambda \frac{\partial T}{\partial Z} + \sum_{k=i}^{\infty} T_{Ak} (\lambda C k w)^{1/2} \sin (kwt + \phi_k + 1/4\,\pi) \qquad (2)$$

C = heat capacity

T_{Ak} = temperature amplitude of harmonic number k

λ = thermal conductivity

T = average temperature

t = time

ϕ_k = phase angle of periodic temperature wave of number k

RESULTS

Figure 1 illustrates the results of plotting the logarithm of amplitude vs. depth for the first five harmonics. The results of the three lowest frequency harmonics are consistent and give an average damping depth of 19.9 cm and a corresponding thermal diffusivity of 0.0145 cm^2/sec. Using a value of 0.61 $cal/cm^2-°C$ for heat capacity derived from bulk density and water content data (De Vries, 1966), the thermal conductivity is 0.00882 cal/cm-sec-°C.

Figure 2 shows the results of using equation (2) to calculate the heat flux at the surface. The heat flux accounts for the contribution of surface heating or cooling processes with periods greater than 1.5 hours. Shorter periodic effects require that higher frequency amplitudes and longer phase lags be calculated, which would be difficult in this experiment because of system noise.

REFERENCES

D. A. De Vries. "Thermal Properties of Soils", **Physics of Plant Environment.** North Holland Publ. Co., Amsterdam, 210-235 (1966).

W. R. Van Wikj and D. A. De Vries. "Periodic Temperature Variations in Homogeneous Soil in Physics of Plant Environment." **Physics of Plant Environment.** North Holland Publ. Co., Amsterdam, 102-140 (1966).

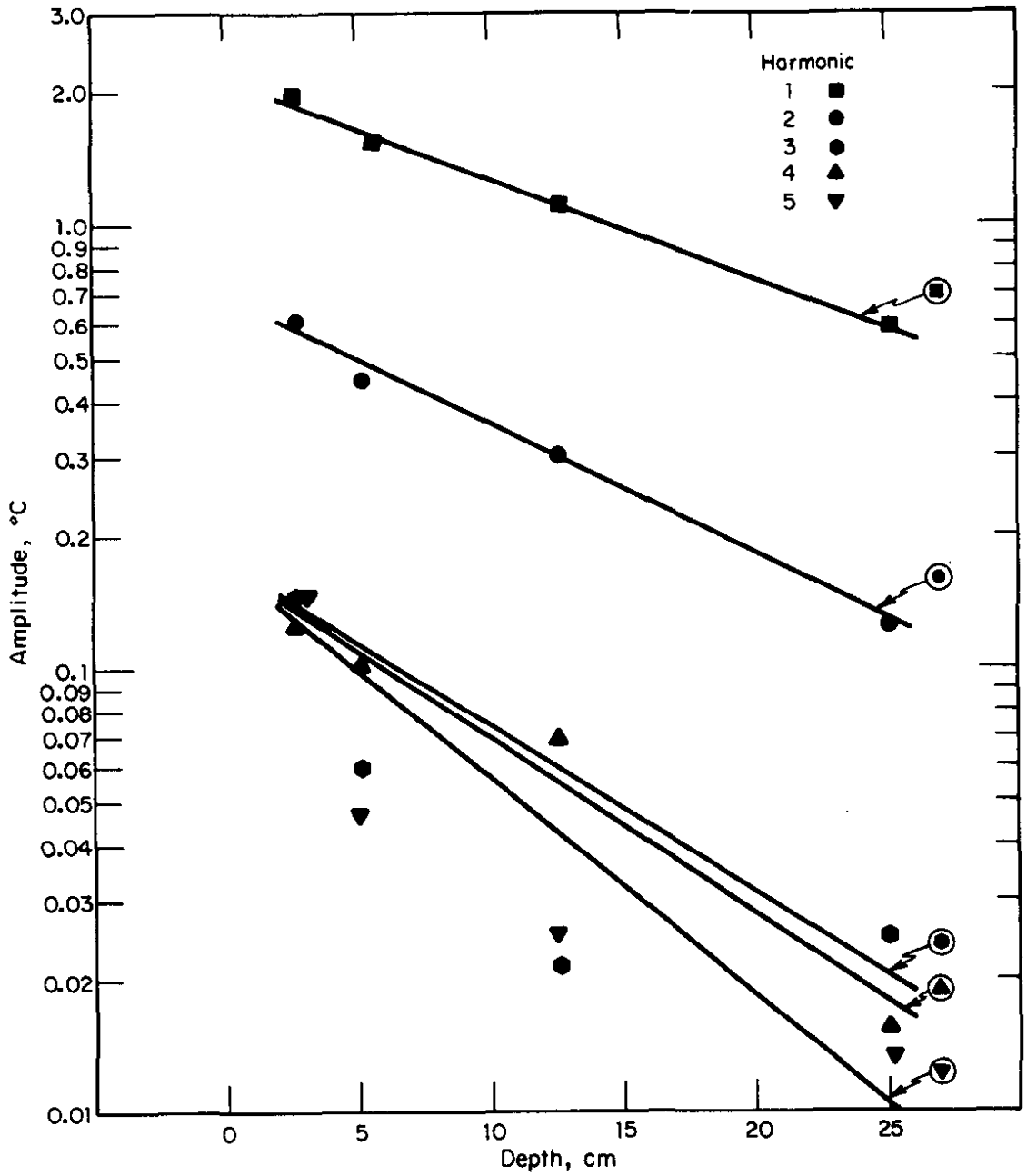

FIGURE 1. Amplitude of the First Five Harmonics of Temperature vs. Depth

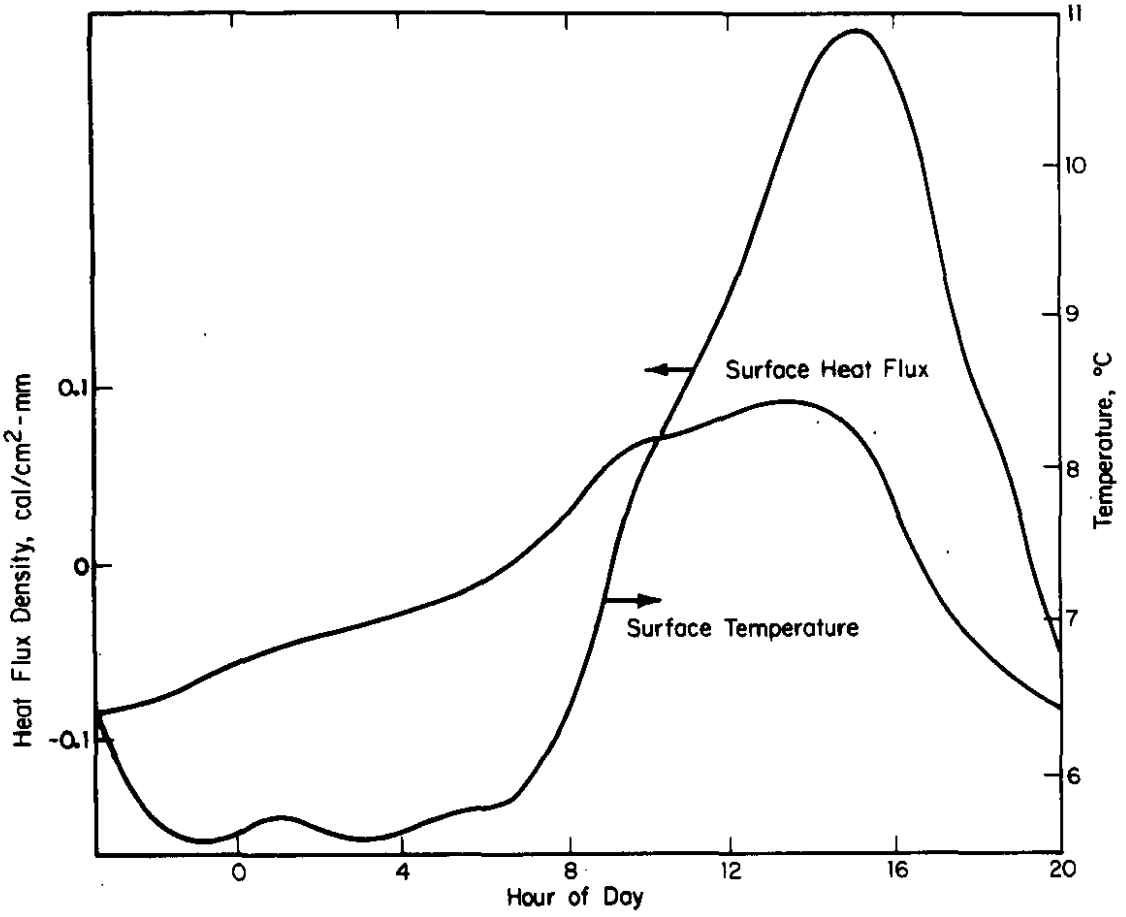

FIGURE 2. Calculated Surface Heat Flux and Surface Temperature

MEASUREMENT OF LIGHT PENETRATION IN A FOREST

C. E. Murphy, Jr., and J. E. Suich

Energy and water balance studies are being conducted at SRL to help better understand vegetative cycling of air pollutants. A critical parameter for models of pollutant uptake is the surface area of the vegetation. Measurements of vegetation surface area by dissection and planimetry of vegetation parts are very time consuming. Therefore, it was decided to attempt to calculate the surface area from sunlight penetration measurements. The results of a single winter's measurements have indicated that the needle surface area of a pine forest can be related to the light penetration.

INTRODUCTION

Light penetrates a forest through a random process of beam interception by discrete tree elements. Since the greatest amount of surface in most trees is contained in the leaves or needles, interception by a needle is more likely than interception by branches or the trunk. This random process is best described by a Poisson statistical distribution. The Poisson distribution leads to the Beer's extinction law:

$$S = S_o \exp(-aA) \qquad (1)$$

S = the average flux density at some point below the tree canopy

S_o = the flux density of radiation above the strand

a = the extinction coefficient

A = the projected leaf area divided by the ground surface area (leaf area index)

If the process of interception is truly random, the extinction coefficient for loblolly pine should be:

$$a = (0.5)(0.163)/\sin(\alpha) \qquad (2)$$

0.5 = decrease in needle area because of average angle of needle to direction of incident light (assumed 60°)

0.163 = relationship of projected area to total surface area in needled pines based on needle shape of a needle perpendicular to the incident light

α = solar elevation angle

Since light penetration in a forest is largely through sun flecks, the variability is great. An average penetration was determined by moving a light sensor along a 14-m track under the forest canopy. A photocell sensor was used as a sensor because it is sensitive to a part of the solar spectrum (400-700 nm) which is strongly absorbed by the vegetation. The strong absorption decreases the calculational problems caused by multiple reflections.

RESULTS

Figure 1 shows a plot of extinction coefficient versus the frequency of measurement for two periods of the day. Near noon more of the light reaches the level of the light sensor directly than in the morning as evidenced by the high occurrence of low extinction coefficients. However, there are also some instances of high extinction coefficients during the noon measurements. The absence of high values of extinction at the lower solar elevation angles may be because of the larger amount of diffuse light or may result from the clumping pattern of the vegetation.

The average extinction coefficient is 0.53. This corresponds to a leaf area of 6.53 cm^2 per cm^2 of ground surface. While this is a reasonable value of leaf area for this stand, the true test of the method will come in observing leaf area through a season.

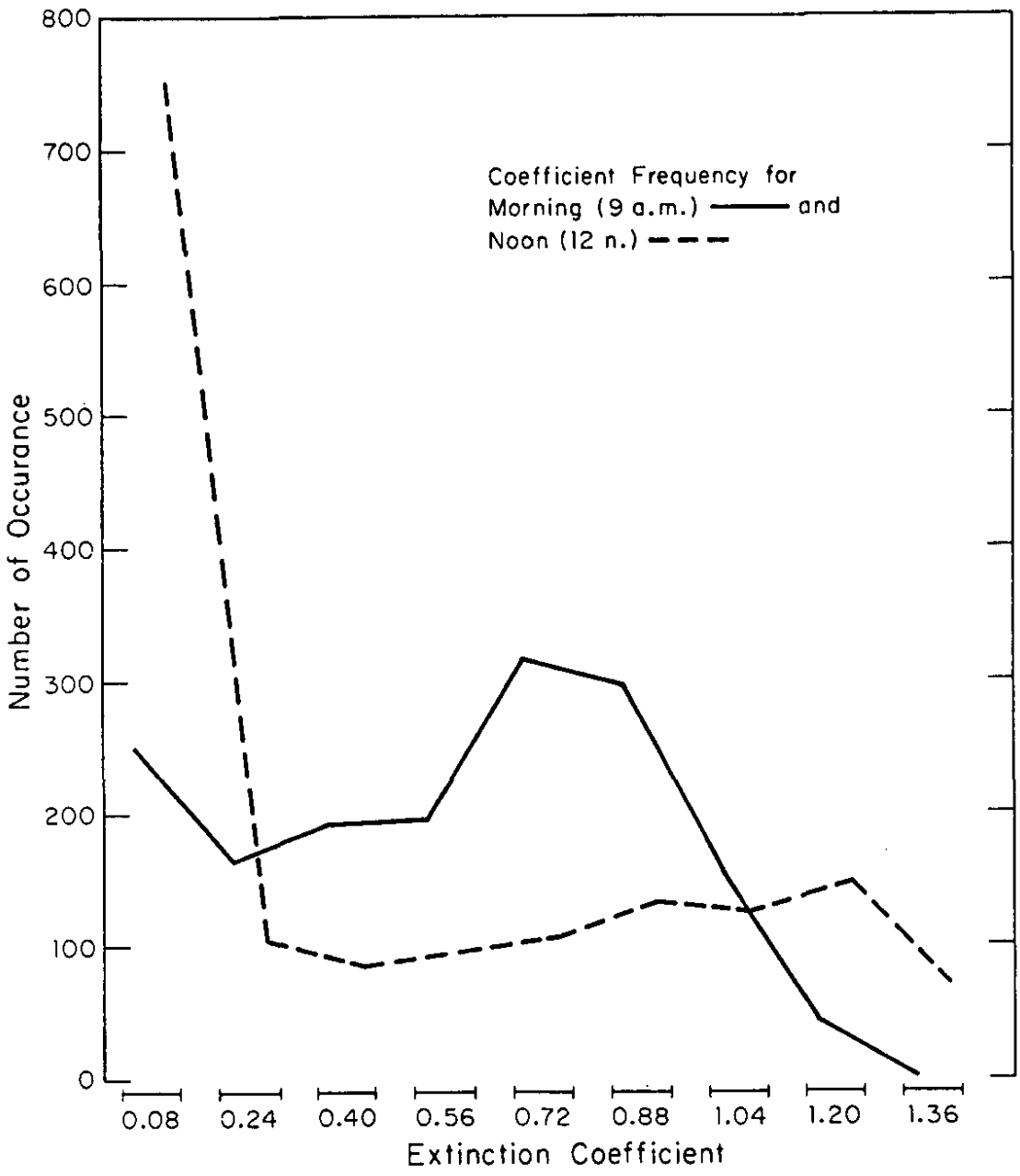

FIGURE 1. Histogram of Extinction

A MODEL OF TRITIUM CYCLING IN THE VICINITY OF SRP

C. E. Murphy, Jr., and M. M. Pendergast

Patterns of tritium dispersion in the environment surrounding SRP indicate a power-law relationship between air concentration and distance from the source. The relationship between the concentration of tritiated water in vegetation and distance is more complex. A model of the tritium dispersion and cycling in the environment explains the dispersion patterns in terms of the ratio of tritiated hydrogen to tritiated water, climate, and vegetation characteristics. The annual variation in the environmental patterns around the SRP is almost completely determined by the source strength and the fraction of tritiated hydrogen (HT) in the release, as mediated by the conversion of tritiated hydrogen to tritiated water (HTO) in the vegetation and soil.

METHODS

A mathematical model of tritium dispersion and cycling was developed which contains mathematical statements expressing the processes of 1) atmospheric dispersion of HT and HTO, 2) wet and dry deposition (uptake) of HT and HTO by vegetation and soil, 3) movement of HTO in soil, and 4) HTO absorption by vegetation roots from soil and flow through the vegetation. A steady-state model was developed because it was appropriate for comparing averages of environmental samples taken over a year's time.

The annual dispersion by wind is nearly radial and the concentration should vary inversely with the radial distance from the plant. The expression used in our model is:

$$X = (Q/uL2\pi r) \qquad (1)$$

where

X = concentration in air (pCi/m^3)

Q = source strength (pCi/s)

u = wind speed (m/s)

L = mixing depth of the atmosphere for HT and HTO (m)

r = radial distance from SRP (m)

Dry deposition is expressed by the equation:

$$F = V_d (X - C) \qquad (2)$$

where

F = flux density of material (pCi/m^2-d)

V_d = deposition velocity (m/d)

C = surface concentration (pCi/m^3)

The classical use of deposition velocity assumes that the surface concentration is zero. This is appropriate when HT is converted to HTO at the surface. However, a zero surface concentration is not appropriate for HTO which may accumulate at the surface. Equations of the form of Equation 2 are used for deposition of HTO and HT to both the soil and the vegetation. The values of deposition velocity used in these calculations (Table 1) were derived from independent field, leaf chamber, and laboratory soil chamber experiments adjusted for the conditions found at SRP by atmospheric diffusion theory.

TABLE 1

Deposit Velocities Used in Model Calculations (cm/sec)

Tritium Form	Vegetation	Soil
HTO	0.6	0.1
HT	0.2	0.2

Wet deposition of HTO is calculated by assuming that rainfall is in equilibrium with air HTO concentration. This probably overestimates wet deposition because much of the rainwater comes from heights in the atmosphere above the direct influence of SRP emissions. Wet deposition of HT is ignored because of the low solubility of hydrogen.

Soil-movement is described by a mass balance equation for a surface soil layer and a deep soil layer. The soil HTO concentrations calculated must be looked at as long-term averages. The balance equation for the surface soil is:

$$V_{ds} (X_H - C_s H) + V_{dTs}\left(X_T\right) + R_R\left(X_H/H\right) - T\, C_s - (R_R - T)\, C_s = 0 \qquad (3)$$

where

V_{ds} = deposition velocity of HTO to soil

X_H = concentration of HTO

C = soil HTO concentration

H = Henry's law constant for HTO

V_{dTs} = deposition velocity of HT to soil

X_T = concentration of HT

R_R = rainfall rate

T = transpiration rate

Equations 2 and 3 are coupled to Equation 1 by the mass balance equations

$$\frac{dQ_{HTO}}{dr} = D_{HTOs} + D_{HTOv} \tag{4}$$

$$\frac{dQ_{HT}}{dr} = D_{HTs} + D_{HTv} \tag{5}$$

$$D_{HTOv} + D_{HTv} + F_{s-v} = 0 \tag{6}$$

where

Q_{HTO} = source strength for HTO

Q_{HT} = source strength for HT

D_{HTOs} = deposition of HTO to soil

D_{HTs} = deposition of HT to soil

D_{HTOv} = deposition of HTO to vegetation

D_{HTv} = deposition of HT to vegetation

F_{s-v} = transpirational flux of HTO from soil to vegetation

The equations were coded in the IBM simulation language CSMP and solved using annual average climatic and deposition parameters.

RESULTS

Figure 1 shows the calculations of X_{HTO}/Q_{HTO} for a mixing depth of 700 m. The experimentally determined values of X_{HTO}/Q_{HTO} for the years 1974-1977 are plotted on the same figure.

The plot is not an exactly straight line because of incomplete mixing through the surface layer near the stacks and the addition of HTO converted from HT, which increases the amount of HTO as the air moves downwind. The effect of changing HT/HTO at the source on the ratio X_{HTO}/Q_{HTO} is shown as dashed lines in Figure 2.

The percent of HT in the releases is known for 1977 only (16% HT). However, an estimate of the HT percentage can be made for 1974 and 1975. In 1974, 479,000 Ci of the total release were more than 99% HT because of an incident at the tritium separations area. If we assume that the chronic releases contained 16% HT as in 1977, then 40% of the 1974 release was in the form HT. Similar calculation for the 182,000 Ci inadvertently released in 1975 indicates that 47% of the released tritium for the year was HT. We must assume 1976 was a normal year. The inclusion of the HT/HTO ratio brings the dispersion estimates into a better agreement with the measurements.

It might be expected that the variation in vegetation HTO concentration is also related to the percentage of HT in the source release. This can be studied by looking at the ratio of vegetation/air HTO versus percent HT in the source air. Figure 2 shows the model calculation and the average ratios from data for the years 1974-1977. The ratios calculated above have been changed so that the 1975 inadvertent release will be credited to 1976 since the release took place late on December 31, 1975, and the vegetative effects would be expected over the first months of 1976. The results are surprisingly good. It seems most of the variation in the ratio of leaf HTO to air HTO is due to the HT percentage.

REFERENCES

Waste Management Operations, ERDA-1537, E. I. du Pont de Nemours & Co., Savannah River Laboratory, Aiken, SC (1977).

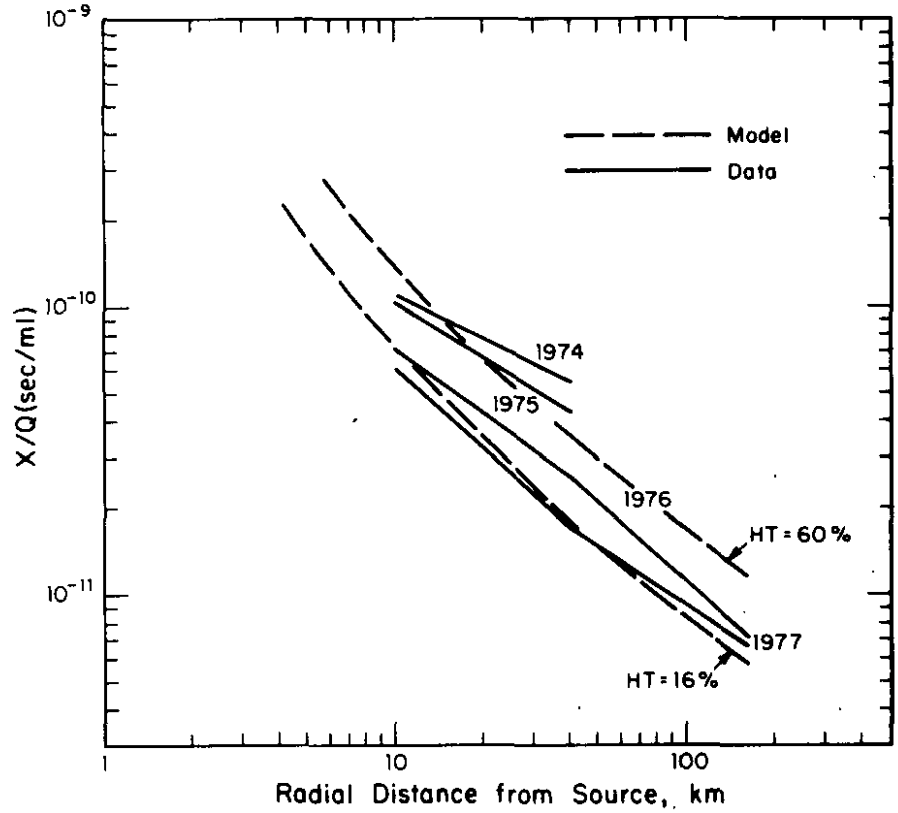

FIGURE 1. Model and Measured Tritium Concentrations in Air Moisture. Mixing Layer is 700 m.

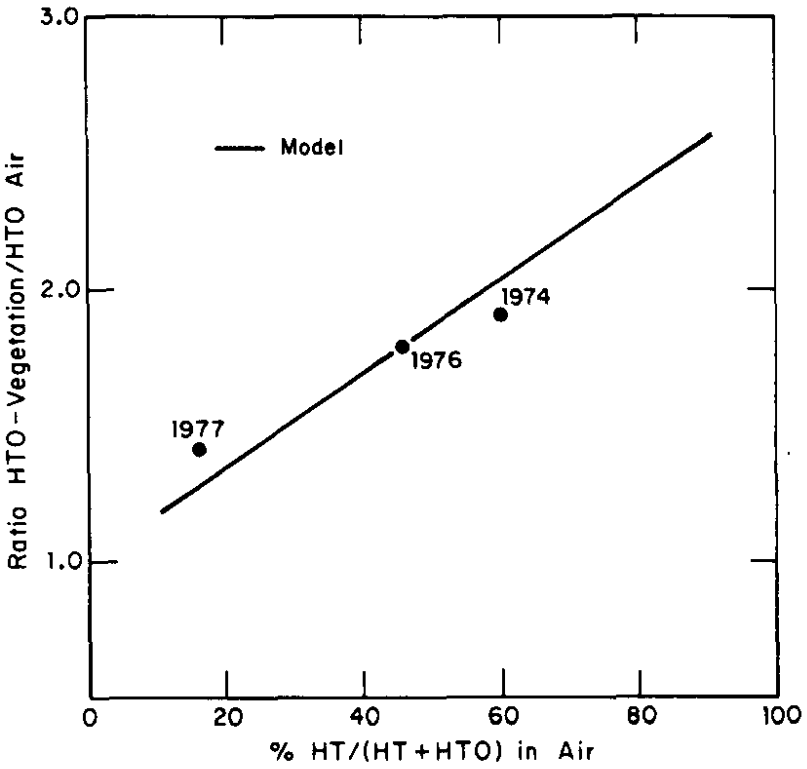

FIGURE 2. Comparison of Model and Measured Tritium Concentration in Vegetation Water as Affected by Tritiated Hydrogen Content

WATER MOVEMENT IN A PINE FOREST

A. H. Dexter and C. E. Murphy, Jr.

The cycling of pollutants within a pine forest must take into account the soil water movement because most pollutants move through soils in the aqueous phase. The results for a slash pine forest on the SRP site indicate that evapo-transpiration and drainage each account for approximately 60 cm/year of water movement out of the soil profile.

INTRODUCTION

A 25-year-old pine forest located in A Area was the focus of a year long study of water movement. Weekly measurements of the water content of the soil were made in this slash-pine stand with commercially available instruments (Depth Moisture Gauge) that employed gamma-ray transmission and neutron scattering, as described in a previous report (Crawford, 1978). A comparison of successive measurements of the water content provided the change in water content, a term of the conservation equation which may be written:

$$P \pm \Delta\theta - D - \int Edt = 0$$

where

P = precipitation received in the area
$\Delta\theta$ = change in water content of the soil
D = drainage from both surface run off and deep seepage
$\int Edt$ = total evaporation over the period t

RESULTS

The soil-water measurements taken during the year were reduced to average soil moisture changes for the plot, and total precipitation was determined for the intervals between the soil-water measurements from local meteorological data. The total evaporation for each of the weekly periods was calculated by a previous method (Monteith, 1964) which employed both local meteorological data and values of stomatal resistance as determined locally in a separate investigation (Murphy, 1978). Drainage is calculated from substitution of the other three quantities.

Figure 1 presents accumulative values of precipitation, evaporation, and drainage as a function of time for the one year period.

For this pine forest and its conditions during the year-long measurements, evaporation and drainage were roughly comparable. During late winter and spring, when rainfalls are normally greater, drainage predominated; during summer and fall when periods of high evaporative demand occurred, evaporation predominated.

REFERENCES

T. V. Crawford, et al. "Soil Water Measurements with Gamma and Neutron Probes," **Savannah River Laboratory Environmental Transport and Effects Research, Annual Report - 1977.** Report DP-1489, E. I. du Pont de Nemours & Co., Savannah River Laboratory, Aiken, SC (1978).

Depth Moisture Gauge, Model 1255SN852, and **Two-Probe Density Gauge,** Model 2376, Manufactured by Troxler Electronic Laboratories, Inc., Raleigh, NC.

J. L. Monteith, "Evaporation and Environment in the State and Movement of Water in Living Organism." **19th Symp. Soc. Exp. Biol. 205** (1964).

C. E. Murphy, J. F. Schubert, and A. H. Dexter. "The Energy and Mass Exchange Characteristics of a Loblolly Pine (Pinus teeda) Plantation. Submitted to **J. of Appl. Ecol.** (1978).

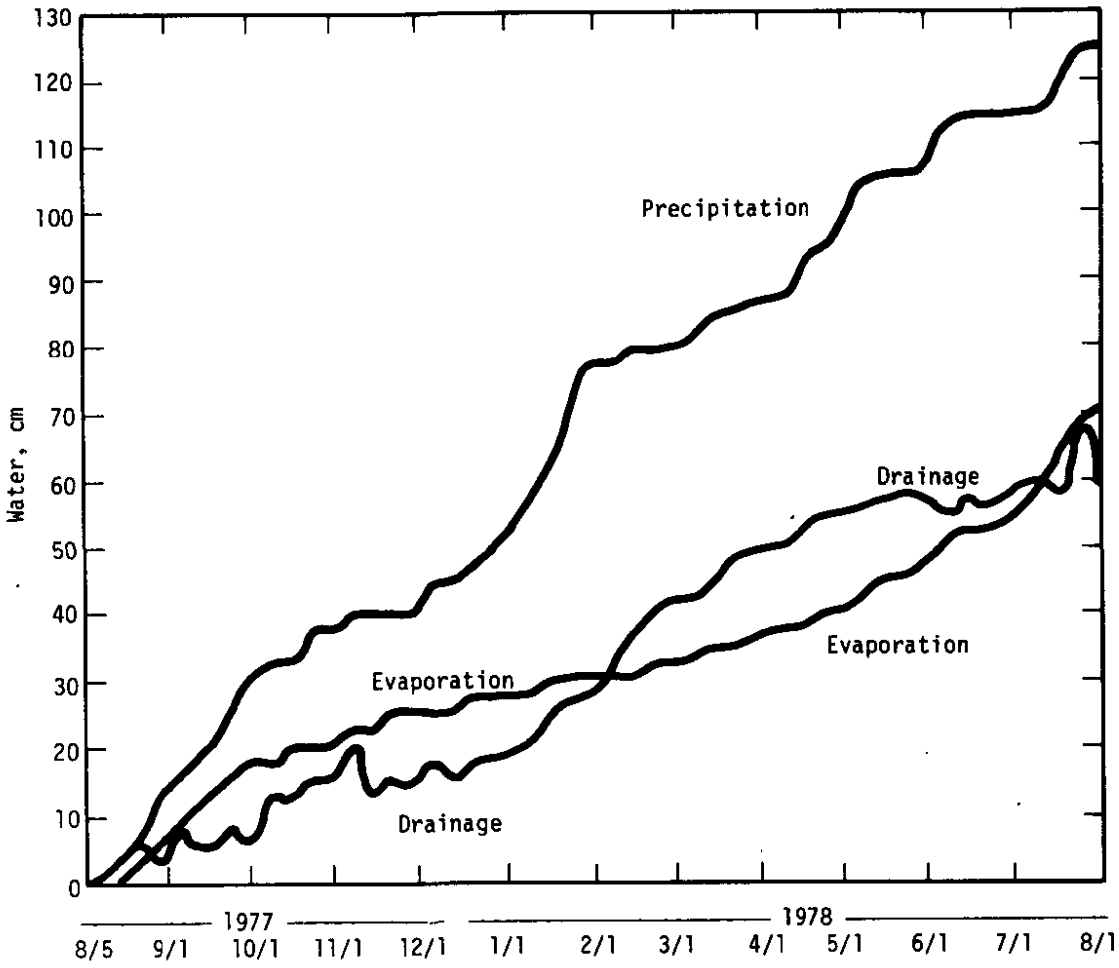

FIGURE 1. Water Balance in A-Area Slash Pine Stand

GEOLOGY STUDIES

PROPERTIES OF GEOLOGIC MEMBRANES AFFECTING THE MAGNITUDE OF OSMOTIC PRESSURE

S. J. Fritz

It has been demonstrated that geologic material can act as an osmotic membrane when clays separate fluids of different salinity. The effect of the fluid characteristics on this phenomena are well known (Fritz, 1978), but geologic materials have not been well studied. Four clays are used in this study to show that osmotic efficiency is controlled by clay mineralogy and its porosity, as well as solution properties.

DISCUSSION

If a membrane separates two aqueous solutions of unequal concentration, water flows from the low concentration solution to the high concentration solution. This results in a build-up of hydrostatic pressure, which at equilibrium, is defined as the osmotic pressure. If no salt is transmitted through the membrane, the hydrostatic pressure equals the theoretical osmotic pressure given by

$$\Delta\pi = \frac{RT}{\overline{V}} \Delta \ln a_w$$

where $\Delta\pi$ = differential osmotic pressure (atm.)

R = gas constant (.082 lit-atm/mole-deg)

T = T°K

$\overline{V}$ = partial molar volume of water in liters/mole

$\Delta \ln a_w$ = difference of natural logarithms of water activities in solutions on either side of the membrane

If the membrane is non-ideal, the developed osmotic pressure is less than the theoretical osmotic pressure. At osmotic equilibrium, the ratio of observed to theoretical osmotic pressure is defined as the osmotic efficiency.

OSMOTIC EFFICIENCY

The osmotic efficiency of clay membranes is largely governed by three factors: 1) the exchange capacity of minerals comprising the membrane; 2) porosity of the membrane; and 3) the concentration gradient across the membrane.

Figure 1 shows the relation between these three factors and membrane efficiency. Quantitative expressions relating these parameters were directly abstracted from separate equations involving concentration gradients (Caplan, 1966) and mineralogy and porosity (Hanshaw, 1962). Membrane efficiency (σ) is thus calculated by

$$\sigma = \frac{CX}{C^2-X^2} + 1$$

where X = exchange capacity per cc pore volume and
C = mean concentration difference across the membrane in moles per cc.

Membranes composed of montmorillonite, chlorite, illite, and kaolinite, having average exchange capacities of 1, 0.3, 0.2, and 0.08 meq/gram are shown in Figure 1 at various porosities. Also shown are osmotic conditions occurring when these membranes separate pure water and various concentrations of NaCl solutions. A mineral's exchange capacity influences membrane efficiency. For a given porosity and concentration gradient, membrane efficiency varies greatly, depending upon membrane mineralogy. The efficiency of membranes composed of clays with low exchange capacities is especially sensitive to concentration gradients. However, even an inherently efficient montmorillonite membrane can exhibit relatively low efficiencies if the concentration gradient is sufficiently high. Decreased porosity results in higher membrane efficiencies, although the rate of increase is not constant and varies with mineralogy.

REFERENCES

S. R. Caplan and D. C. Mikulecky. **Transport Processes in Membranes.** Ion Exchange, Vol. I, 1-64, Marcel Dekker, Inc., New York (1966).

T. V. Crawford, et al. "Dependence of Osmotic Pressure on Solution Properties." **Savannah River Laboratory Environmental Transportation and Effects Research Annual Report - 1977.** Report DP-1489, E. I. du Pont de Nemours & Company, Savannah River Laboratory, Aiken, SC (1977).

B. B. Hanshaw. Membrane Properties of Compacted Clays. Ph.D. Dissertation, Harvard University, Cambridge, MA (1962).

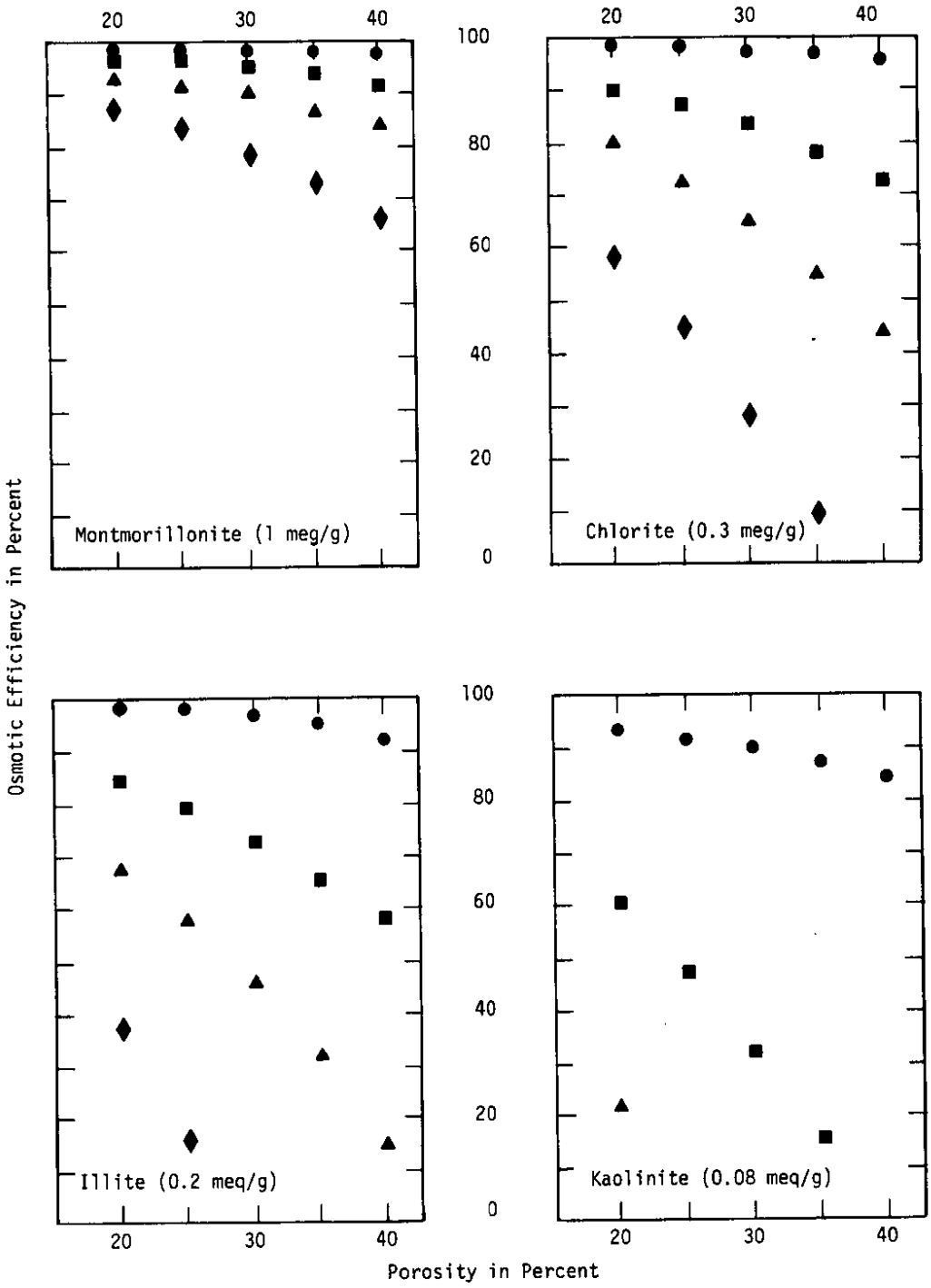

FIGURE 1. Osmotic Efficiencies of Various Clay Membranes at Selected Differential Concentrations. Circles represent osmotic conditions occurring when the membrane separates pure water and 0.1 molal NaCl; squares, 0.25 molal NaCl; triangles, 0.5 molal; and hexagons 1.0 molal. A 1.0 molal NaCl solution is about 55,000 parts per million.

SUBSURFACE HYDROLOGY OF COASTAL PLAIN SEDIMENTS IN THE SRP SEPARATIONS AREAS

R. W. Root, Jr.

An understanding of the three-dimensional flow of ground water beneath the Savannah River Plant separations areas requires a complete knowledge of hydraulic head in the area. The water table occurs primarily within the Barnwell Formation. As would be expected, the water table (Figure 1) map shows the greatest relief of the three hydraulic head maps and also shows the highest gradient, as it is influenced by many small tributaries. Both the water table and the potentiometric surface of the McBean Formation (Figure 2) show large depressions caused by their drainage to both Upper Three Runs Creek and Four Mile Creek. On the other hand, the potentiometric surface of the Congaree Formation (Figure 3), which is not intersected by the valley of Four Mile Creek, shows only a depression caused by Upper Three Runs Creek. The gradient in the Congaree is also low compared to the gradient of the water table and the McBean Formation.

DISCUSSION

SRP is underlain by unconsolidated Coastal Plain deposits to a depth of about 290 m (Figure 1). From the surface down, the hydrologic units are 1) the Barnwell Formation, which consists of clays, sandy clays, and clayey sands; 2) a tan clay; 3) the McBean Formation, which consists of an upper layer of clayey sand and a lower calcareous clay and clayey sand containing small cavities; 4) a green clay; 5) the Congaree Formation, which consists of layers of sand interbedded with layers of clay; 6) the Ellenton Formation, which consists of lignitic micaceous clay and coarse sand; and 7) the Tuscaloosa Formation, which consists of interbedded sand, gravel, and clay. The hydraulic heads at seven different levels in this sedimentary section are shown on Figure 4.

Figure 4 illustrates that the head in each formation is lower than that in the overlying formation, until the Congaree Formation is reached; below this formation, the head increases with depth. The change in hydraulic head with depth may be due to two factors. First, the tan clay, between the Barnwell and McBean formations, and the green clay, between the McBean and Congaree formations, retard the downward movement of water. This causes a head gradient to develop between points above and below each clay layer.

Second, because the clay content of the Congaree Formation is less than that of the Barnwell and McBean formations, the Congaree Formation conducts water more rapidly towards Upper Three Runs Creek, where the water is discharged from the formation (Figure 3). This water discharge from the Congaree Formation contributes to the large head difference across the green clay.

HYDROLOGY

Figures 2, 3, and 4 show contour maps of the hydraulic head at the water table, in the upper McBean Formation, and in the upper Congaree Formation. A map of the hydraulic head in the Tuscaloosa Formation is not shown because the head is relatively constant at 56 to 58 m beneath the entire area.

The head gradient can be determined by comparing the contour maps. The water table in the Barnwell Formation and the hydraulic heads in the upper McBean and upper Congaree formations converge at Upper Three Runs Creek, where waters from all three formations are discharged on the north side of the separations areas. Both the water table in the Barnwell Formation and the hydraulic head in the upper McBean Formation converge at Four Mile Creek, where water from both formations is discharged on the south side of the separations areas. Because Four Mile Creek has not eroded down into the Congaree Formation, this formation is not affected by this creek. The Tuscaloosa Formation head is not affected by either creek, but is controlled by the level of discharge into the Savannah River.

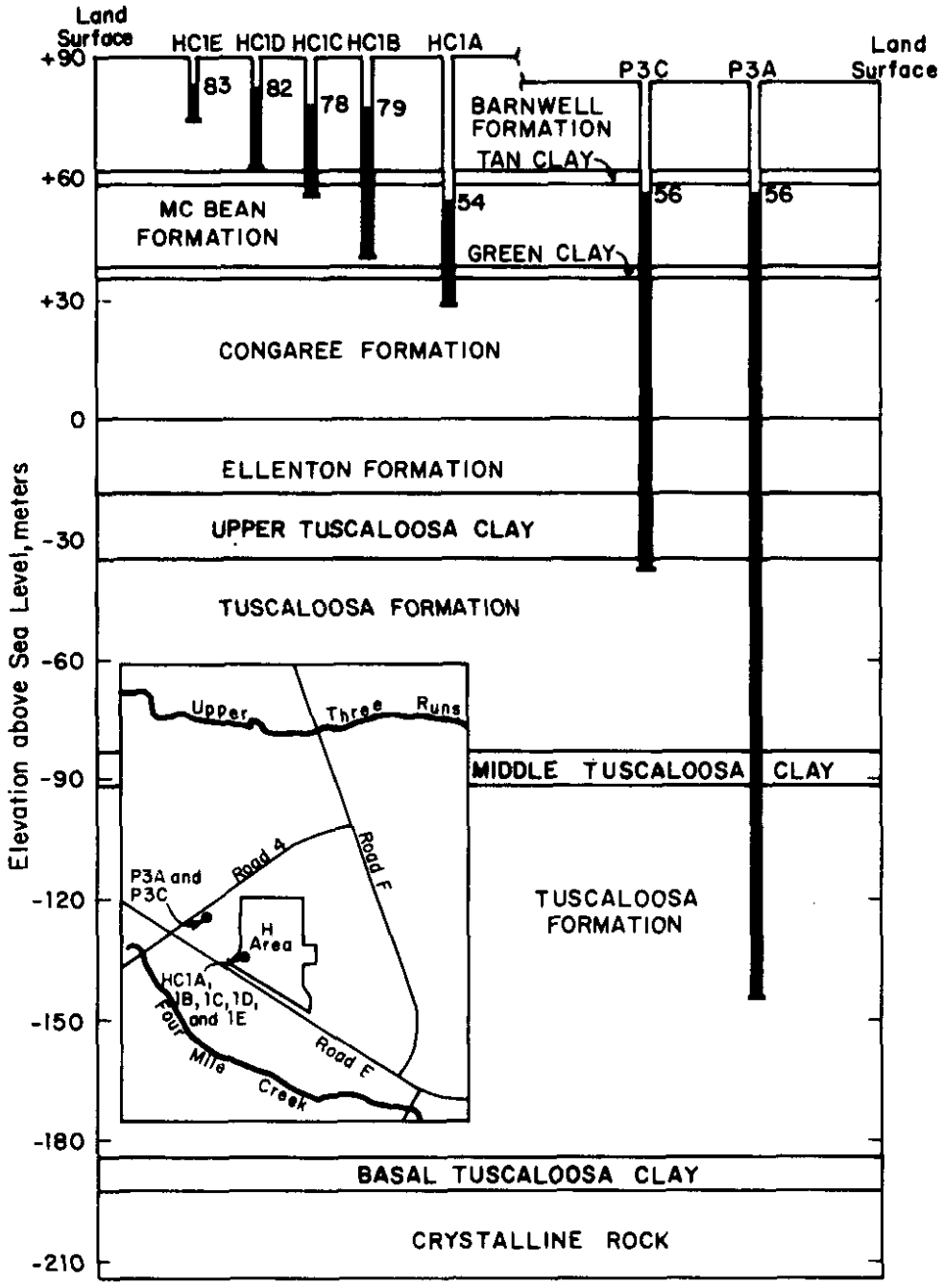

FIGURE 1. Geology and Hydrostatic Head in Ground Water Near the Center of SRP (Insert shows location of wells)

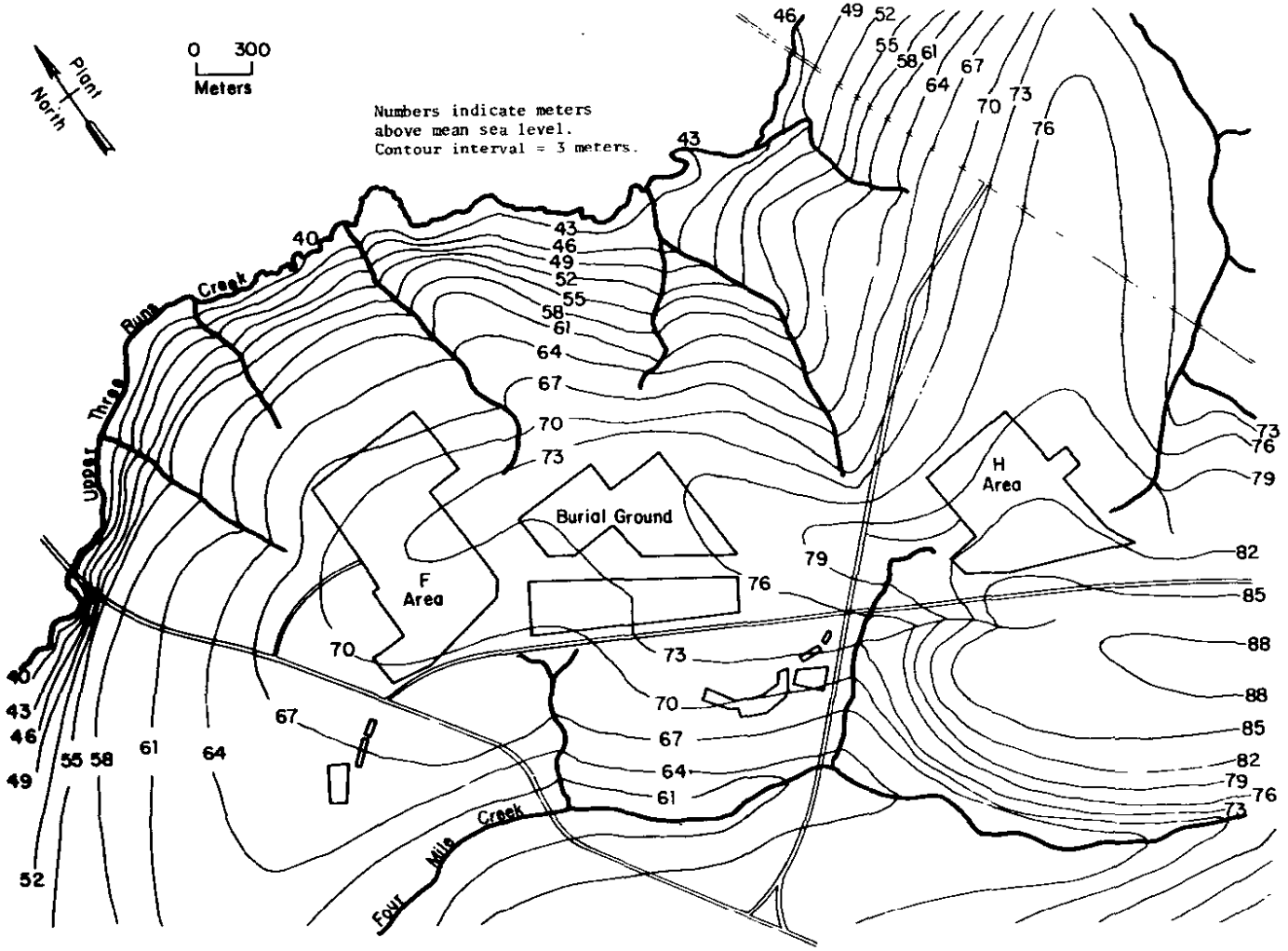

FIGURE 2. Average Elevation of the Water Table at SRP During 1968

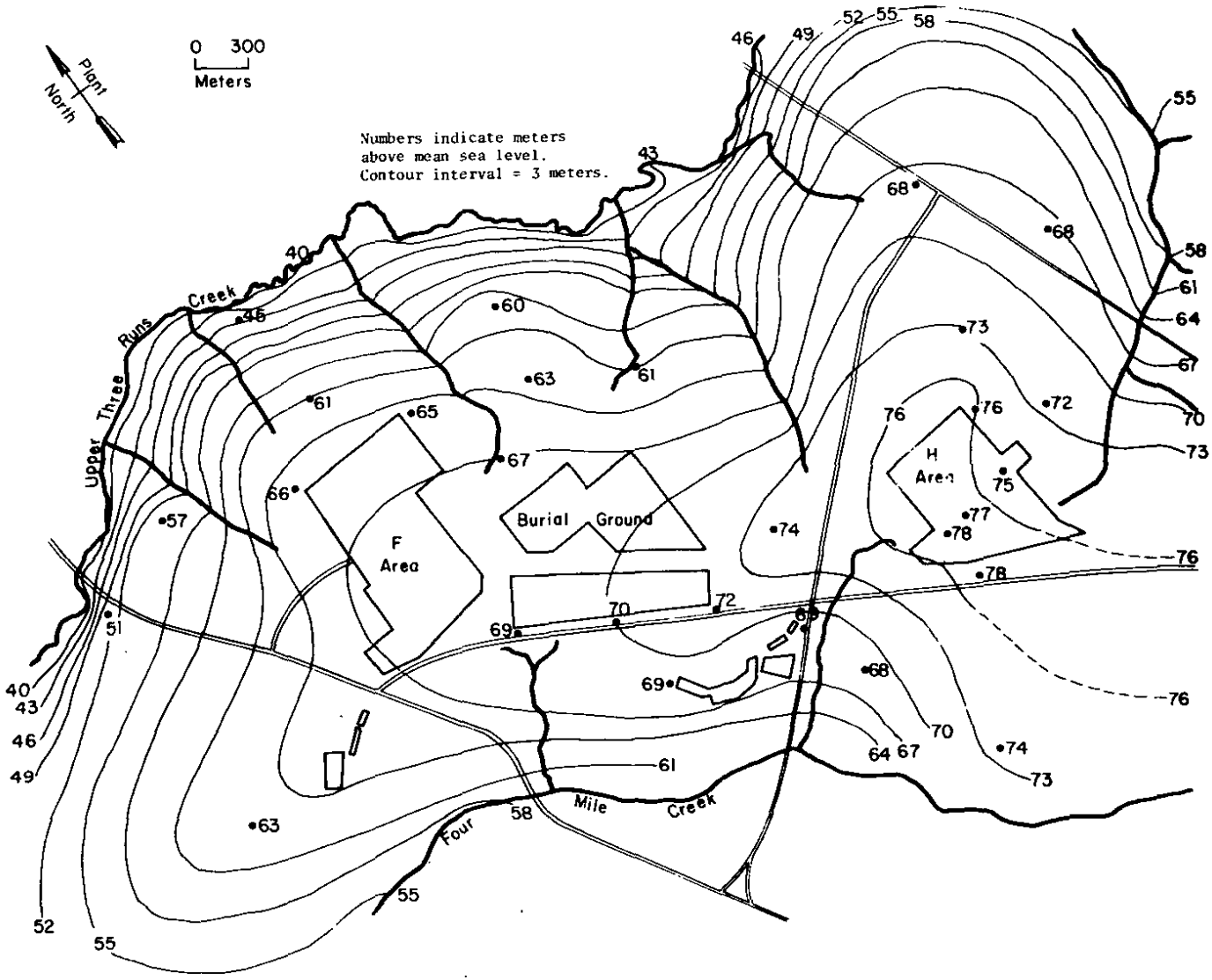

FIGURE 3. Elevation of the Hydraulic Head in the Upper Part of the McBean Formation (measured 8/29/77)

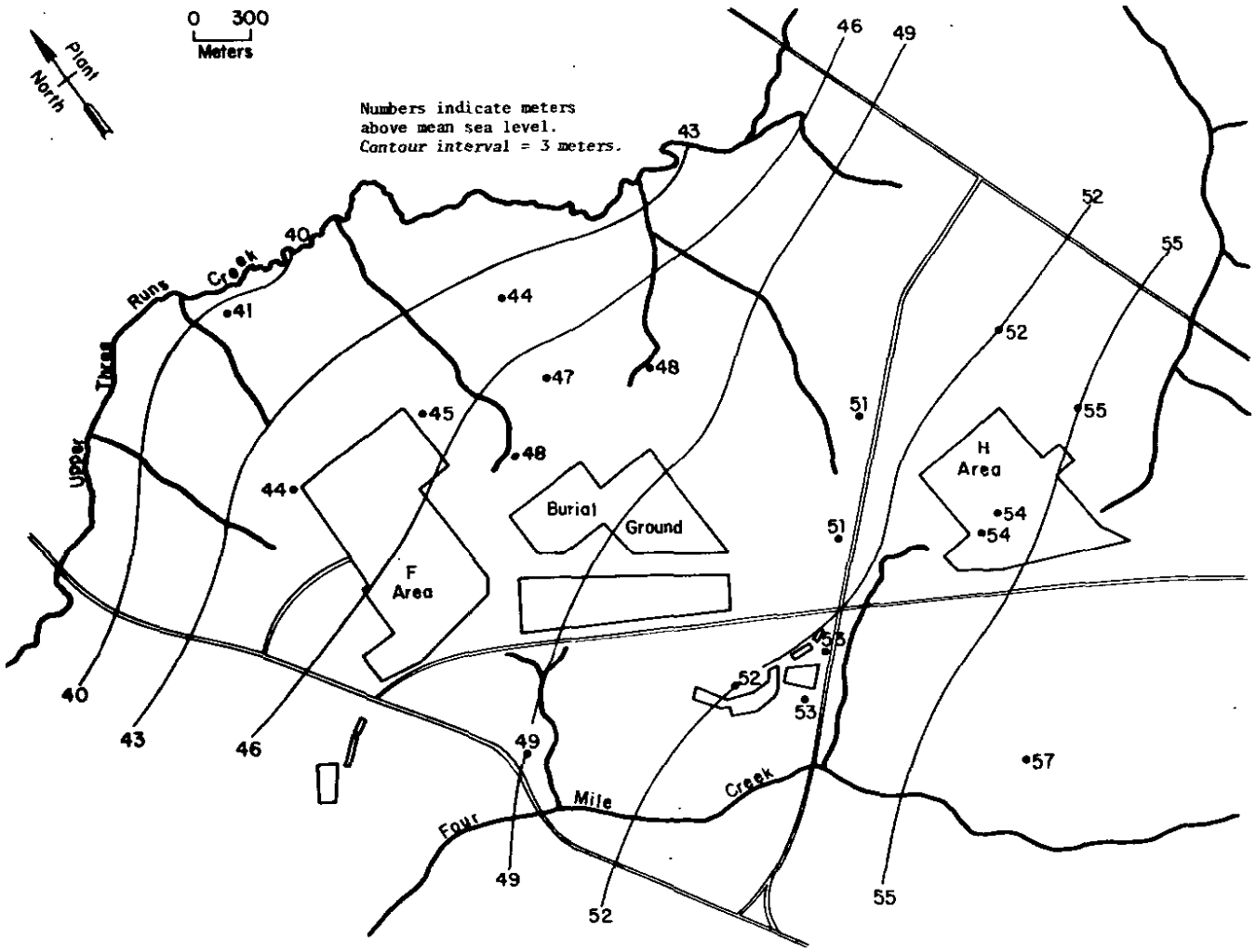

FIGURE 4. Elevation of the Hydraulic Head in the Upper Part of the Congaree Formation (measured 8/29/77)

RESULTS OF DRILLING A WELL CLUSTER NEAR F AREA AT SRP

R. W. Root, Jr.

A cluster of five wells was drilled on the bluff above Upper Three Runs Creek in the northwestern part of the Savannah River Plant separations areas to confirm the conceptual geohydrologic model in this area (Root, 1976). This well cluster confirmed the existence of the tan and green clays at this site, the downward gradient of hydraulic heads in the Barnwell and McBean formations, and the upward gradient of hydraulic heads in the Congaree and Ellenton formations. The upward head gradient in the Congaree and Ellenton formations suggests that water is discharging into Upper Three Runs Creek from these formations. This information is useful in developing a three-dimensional model of ground water movement and potential contaminant transport.

DISCUSSION

Three well clusters totaling 16 wells have been drilled near F Area (Root, 1978) (Figure 1). Well Cluster FC4, located approximately 1 km northwest of F Area on the bluff above Upper Three Runs Creek (Figure 1), provides geologic and hydrologic information and determines the water level distribution in the Congaree Formation.

Prior to casing installation in Well FC4A, an off-site consulting firm conducted geophysical logging in the hole. Caliper, electrical resistivity, spontaneous potential, and gamma logs are shown in Figure 2. The wells in Cluster 4 are finished at the following depths: FC4A-83.5 m, FC4B-50 m, FC4C-37.5 m, FC4D-28.3 m, and FC4E-19.2 m.

RESULTS

The geological information provided by the continous split-barrel sampling is shown in Figure 2. The two clay layers at depths of 13 m and 34 m represent the tan and green clays, respectively. These two clay layers are apparently continuous beneath the separations areas. A small amount of calcareous material was found at a depth of 14.6 m that may represent the calcareous zone that is also areally extensive beneath the area.

Figure 3 shows the total depths of the wells in Cluster FC4 and their water levels. The water in Wells FC4E, FC4D, and FC4C stand at progressively greater depths, defining a hydraulic gradient vertically downward. However, this trend is reversed in Wells FC4B and FC4A, defining a gradient vertically upward. This may be evidence that ground water which flows laterally in the Congaree Formation begins moving upward to discharge into Upper Three Runs Creek.

The water level in FC4D stands in the middle of the screen indicating that the screen is set at the water table, the boundary between the saturated and the unsaturated zones. However, FC4E, at a shallower depth, has a water level that stands above the top of the screen. Apparently FC4E is screened in a perched water body, held up by the clay layers at a depth of about 22 m (Figure 2).

REFERENCES

R. W. Root, Jr., and I. W. Marine. "A Conceptual Geohydraulogical Model of the Separations Area." **Savannah River Laboratory Environmental Transport and Effects, Annual Report - 1976.** Report DP-1455, E. I. du Pont de Nemours and Company, Savannah River Laboratory, Aiken, SC (1976).

R. W. Root, Jr. "A Summary of Exploration Drilling in F Area for Hydrogeologic Information." **Savannah River Laboratory Environmental Transport and Effects Research, Annual Report - 1977.** USDOE Report DP-1489, E. I. du Pont de Nemours and Company, Savannah River Laboratory, Aiken, SC (1978).

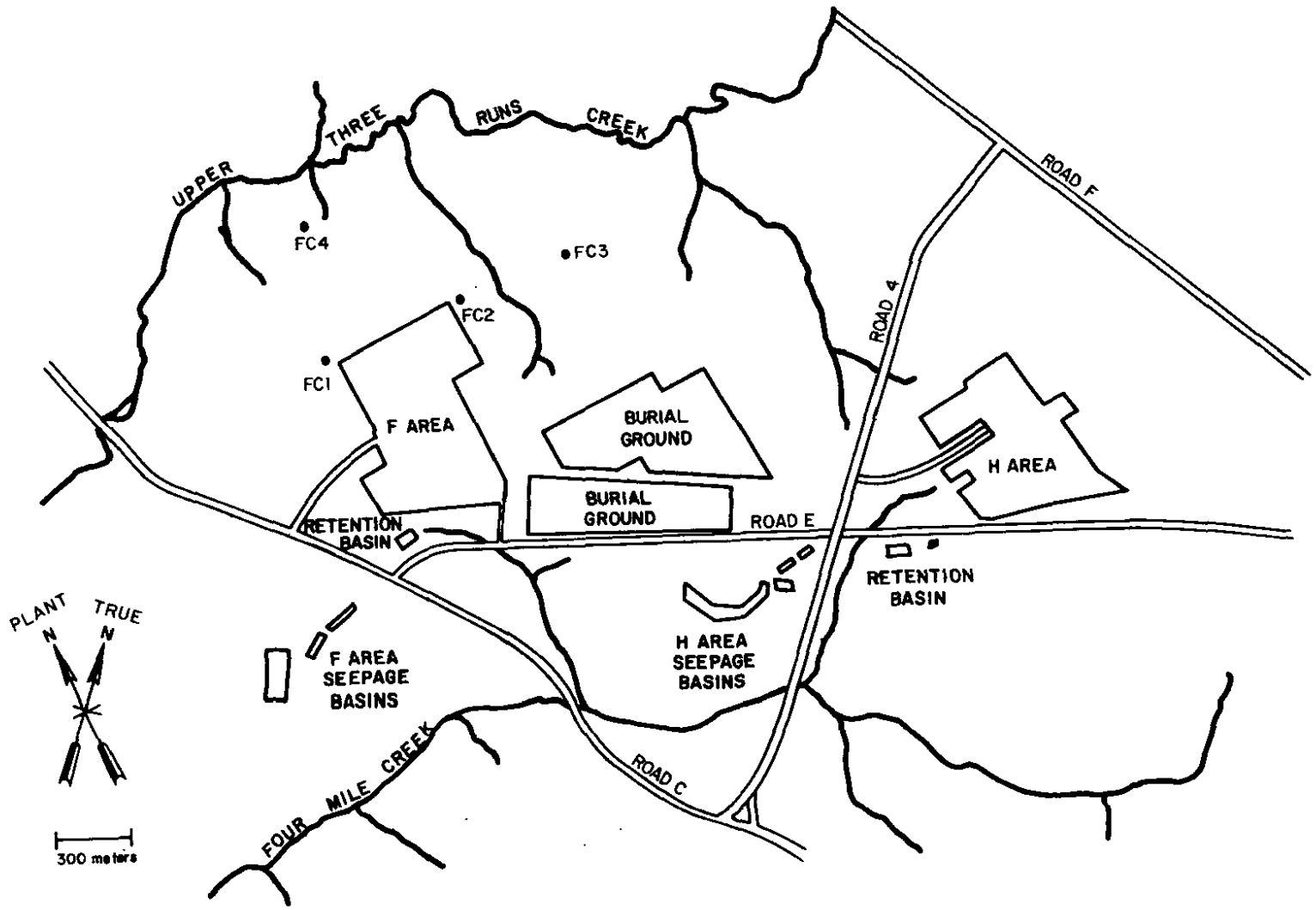

FIGURE 1. Location of FC Well Clusters

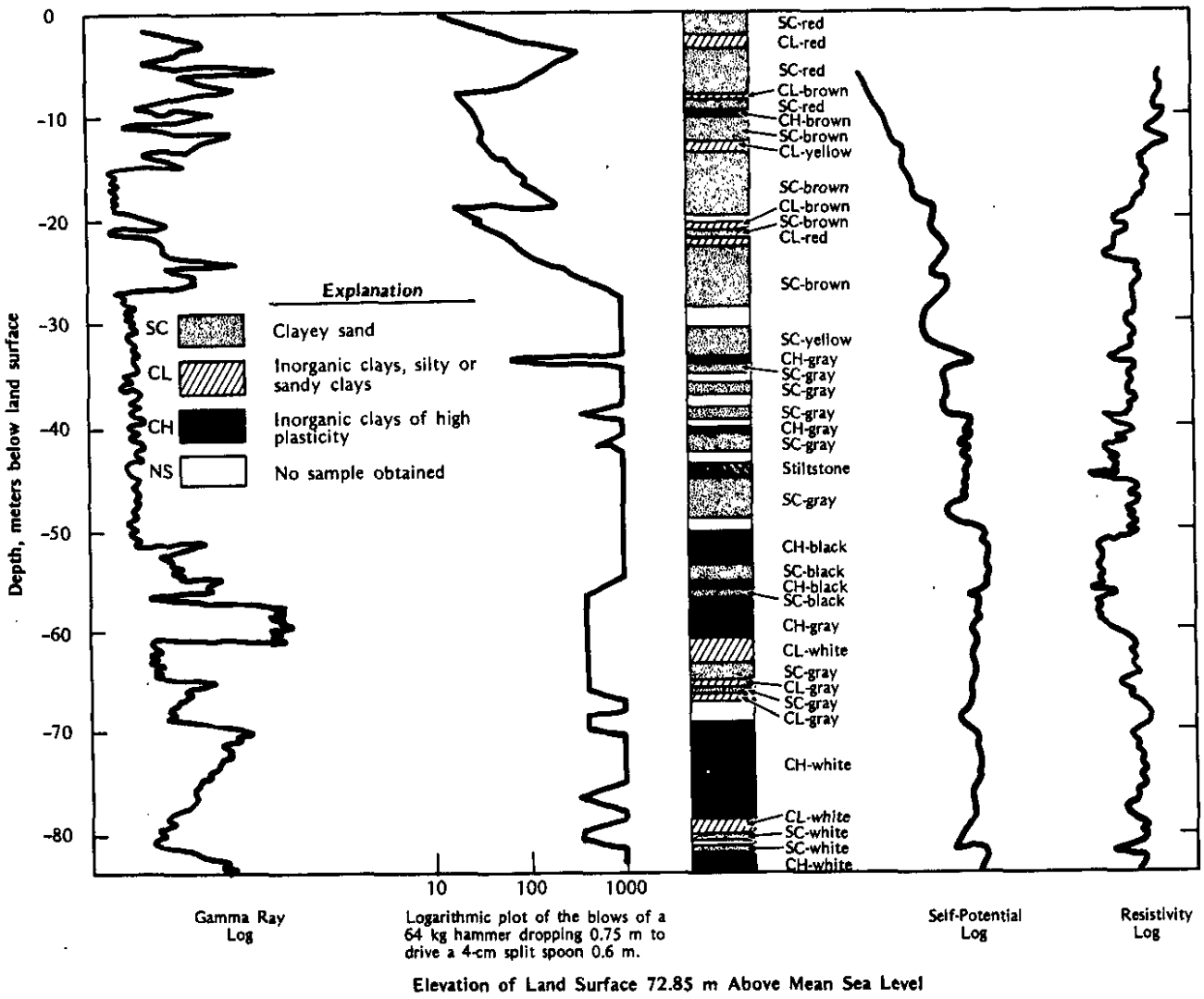

FIGURE 2. Logs Obtained at Well Cluster FC4

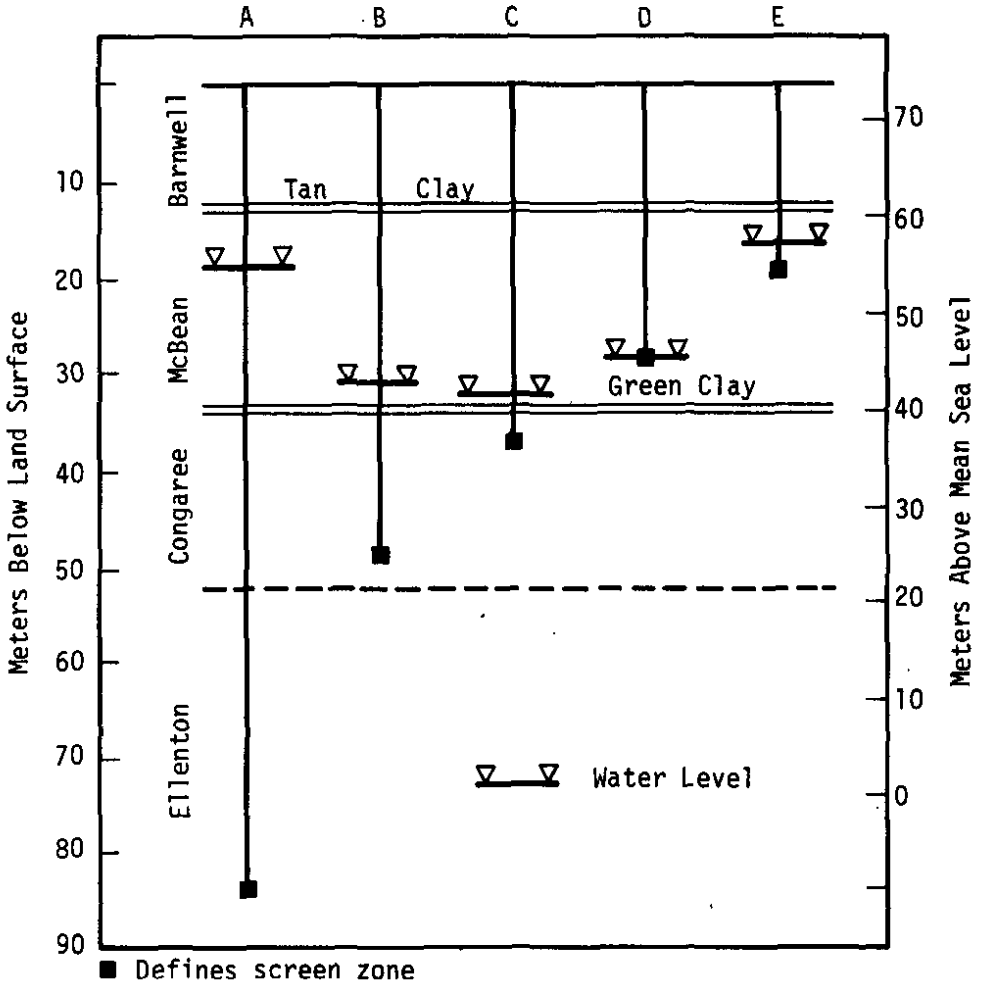

FIGURE 3. Schematic Diagram of Well Cluster FC4 Showing Well Depths and Water Levels

WELL DATA COMPUTER FILE

C. W. Krapp and J. E. Suich

A computer file is currently being developed to provide a centralized access to pertinent data for SRP wells. Obtaining this data requires searching the files of six departments onsite and in Wilmington, DE. The computer file will include data on industrial, domestic, construction, monitoring, and exploratory wells drilled on SRP.

WELL DATA

The Well Data Computer File currently contains information on more than 2300 out of the 5000 wells on the SRP site. The accuracy of the data will be verified by each source department. To date none of these verifications have been completed. However, the file has been queried about eight times for various purposes, including the disposition of water production wells, location of the depth to water for a battery acid disposal area, and the location of wells in areas where new construction is proposed.

Up to 64 variables can be entered for each well which describe the condition, physical construction, and geology of the individual well. The data is entered under: 1) identification, 2) remarks, 3) well hole, 4) casing, 5) finish, 6) water level, 7) yield, and 8) other files. These sections make up a hierarchical record structure as shown in Figure 1. Note that the identification section is the only record segment required. Depending on the purpose and age of the well, the data available may be plentiful or sparse.

COMPUTER PROGRAM

A hierarchical record structure is maintained by the Mark IV File Management System. Data checks and coordinate conversion are handled by OWNCODE using Fortran IV language coding. Coordinates that may be on several different grid systems are converted to latitude and longitude and both are stored in the file. A flow chart (Figure 2) shows the processing of transactions or record segments in the Mark IV System.

A query to the file is handled in a similar manner. The major difference is that no new master is created. The Processing Request limits the file based on the specific query and a report is produced at the end showing those records satisfying the query.

TYPICAL OUTPUT

Data is retrieved from the file by a suitable selection of logical IF statements using a standard Mark IV Information Request. The results of this query can be provided in tabular format, which lists many wells per page or in a one page per well format. The latter format is useful when data from only a few wells is needed. Figure 3 shows such output for a production well, PW-54-P.

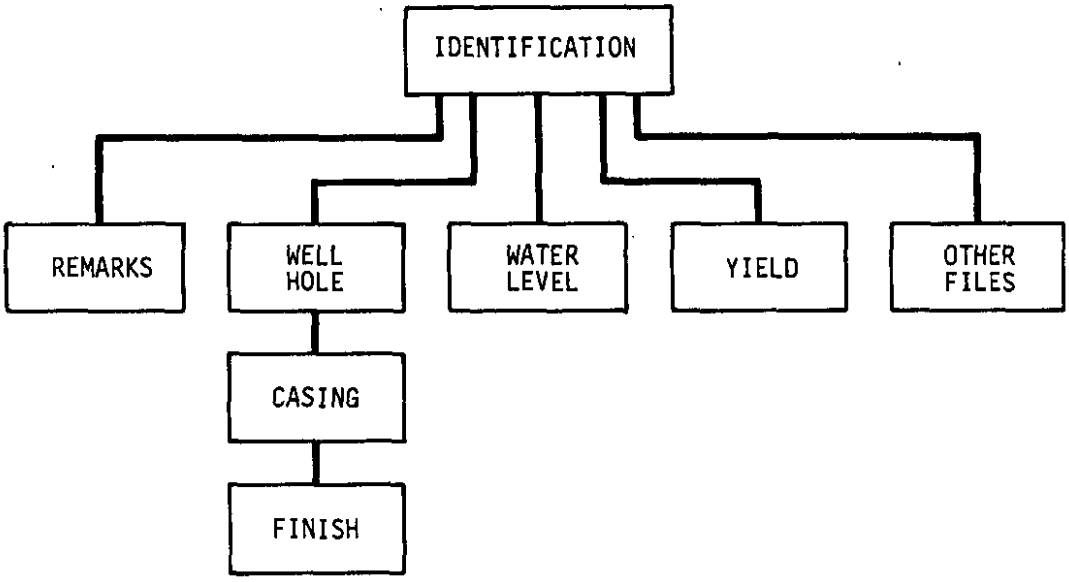

FIGURE 1. Hierarchical Record Structure Used in Mark IV File Management System for the Well Data Computer File

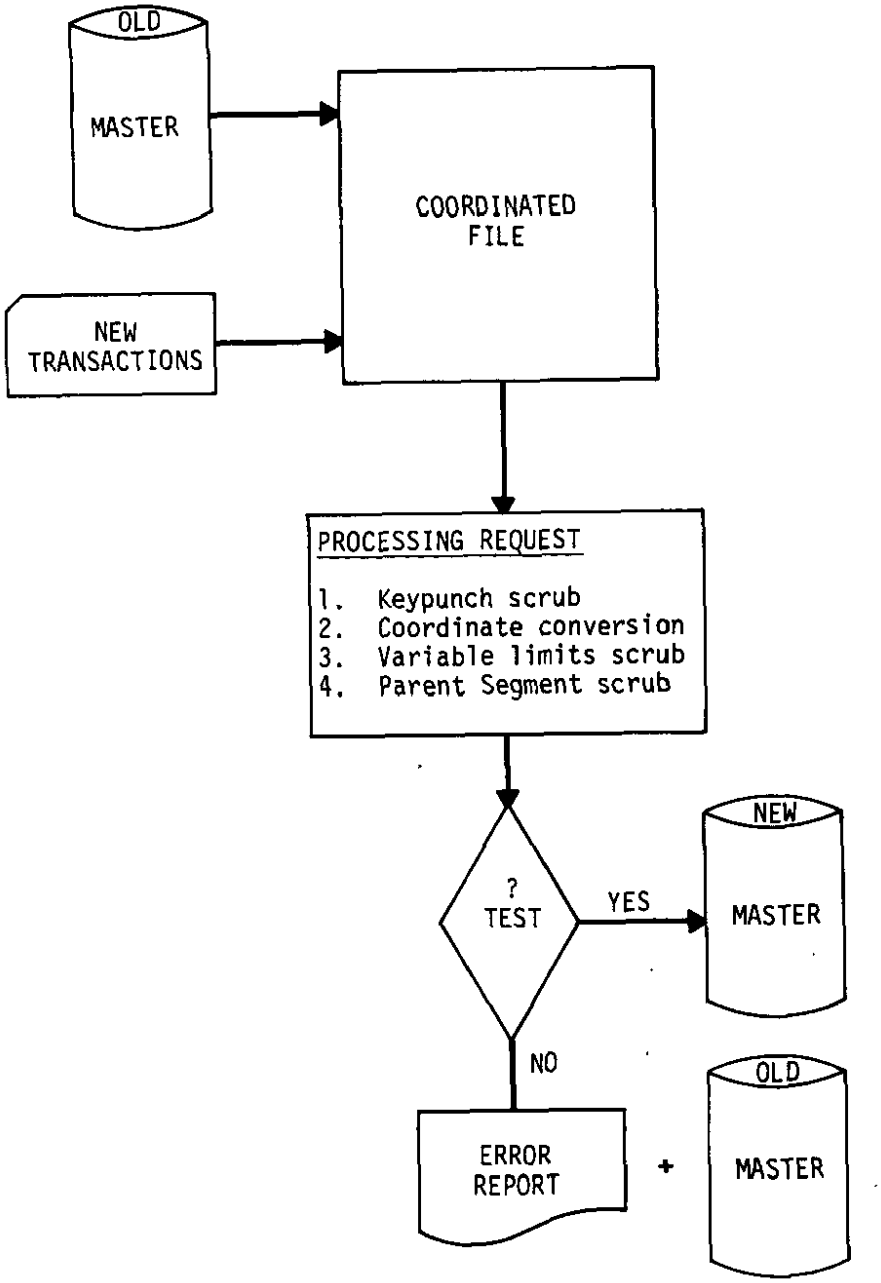

FIGURE 2. Flow Chart of MK IV Transaction Processing Used in Well Data Computer File

```
SRP WELL FILE INFORMATION     FEB 22, 1979


WELL NUMBER  PW  54P     PRODUCTION WELL

LOCATION:
     REACTOR AREA
     SRP GRID SYSTEM                N43,148.0   E65,544.0
     LATITUDE N33.22811696   LONGITUDE E81.57807601
     ELEVATION IS 316.80 FEET ABOVE SEA LEVEL

INFORMATION SOURCE:
     WATER WELL FILE, PROJECTS       , PREPARED BY HUGHES,E.A.                    ON 05/08/78
     W230520

WELL HOLE DATA:
     WELL ABANDONED AS DESCRIBED
     DRILLED ON 09/24/58 USING HYDRAULIC ROTARY BY LAYNE ATLANTIC DRILLING CO., SAVANNAH, GA.
     TO A DEPTH OF    594.0 FEET BELOW GRADE, HOLE DIAMETER OF    .000 INCHES
     TERMINATING IN TUSCALOOSA FORMATION

CASING DATA:
               * CASING TO A DEPTH OF   490.0 FEET BELOW GRADE, I.D.  8.000 INCHES
                                        594.0                         6.000
     TOP OF CASING IS 316.80 FEET ABOVE SEA LEVEL
     CASING HAS PORTLAND CEMENT            GROUTING, BOTTOM TO TOP, TREMIE

FINISH DATA:
     FINISH IS                 *SHUTTER SCREEN
     OPENINGS ARE    30 THOUSANDTHS OF INCH WIDE SLOTS
     THERE ARE  1 ZONES IN THE TUSCALOOSA FORMATION          *BETWEEN   573.0 AND   580.0 FEET BELOW GRADE
                                                                *          .0          .0

PACKING DATA:
     PACKING IS           *(                *)                    *
     BETWEEN       AND       FEET BELOW GRADE

WATER LEVEL DATA:
     ON 10/03/58, DEPTH TO WATER WAS   -126.00 FEET, MEASURED FROM GROUND LEVEL  OF 316.80 FEET ABOVE SEA LEVEL

YIELD DATA:
     DEVELOPMENT WAS BY PUMP          FOR     HOURS
     TEST YIELD ON 10/03/58 WAS    .0 GPM, WITH A DRAW DOWN OF      .0 FEET, SPECIFIC CAPACITY IS    .000
     TEST DURATION WAS     HOURS, USING                *
     PRODUCTION YIELD IS   100 GPM, WITH A DRAW-DOWN OF  17.0 FEET, USING                *
     SPECIFIC CAPACITY IS   5.882

OTHER FILES OF INFORMATION:
     DRILLER'S LOG.............  WATER WELL FILE, PROJECTS
     GEOPHYSICAL LOG...........  NOT ON FILE
     PHYSICAL CORE.............  NOT ON FILE
     CUTTING SAMPLES...........  NOT ON FILE
     WATER LEVEL OBSERVATIONS...  WATER WELL FILE, PROJECTS
     DISSOLVED SOLIDS ANALYSIS..  WATER WELL FILE, PROJECTS
     DISSOLVED GASSES ANALYSIS..  WATER WELL FILE, PROJECTS
     RADIONUCLIDE ANALYSIS.....  NOT ON FILE
     ENGINEERING DRAWING.......  WATER WELL FILE, PROJECTS
```

FIGURE 3. Example of Well Data File Output - One Well per Page

EARTHQUAKE DAMAGE TO UNDERGROUND FACILITIES

D. E. Stephenson and H. R. Pratt*

A recently completed literature study (Pratt, 1978) shows that earthquakes of equal intensity damage underground facilities significantly less than surface facilities. This is a known fact in the mining industry, but because earthquake damage has been minor, the subject had not been intensively studied.

The potential seismic risk to an underground nuclear waste repository must be considered to determine its ultimate location. Thus, a documented study of the effects of underground earthquakes is required for such an evaluation. For this purpose, SRL contracted with a consulting firm to document and assess the damage to underground facilities caused by earthquakes (Pratt, 1978).

DISCUSSION

Earthquake effects were delineated in terms of both displacements and accelerations. For underground facilities, displacements are considered more damaging than accelerations.

Sources of data included both U.S. and foreign experiences of earthquake damage or nondamage. Damage from documented nuclear events was also included where applicable (Pratt, 1978). A study of the seismic stability and behavior of tunnels (Rozen, 1976) provides one of the better sets of data available. The dynamic behavior of 71 tunnels was compared with surface accelerations and damage (Figure 1). Surface peak accelerations of less than 0.2 g did not damage the tunnels. Between 0.2 and 0.5 g, damage was minor; damage only became significant above 0.5 g. Below about 100 m no damage occurred to wells and shafts unless they were crossed by a fault (Pratt, 1978).

An evaluation of these data was made in terms of acceleration, velocity, and displacement as a function of earthquake magnitude, distance, and depth. Damage decreases with distance from the source and with depth below the ground surface. However, extensive damage can occur if the facility is cut by a fault or fault fissure along which a slip can occur during an earthquake. Peak acceleration decreases with depth; however, peak displacements show much less reduction with depth.

* Terra Tek, Salt Lake City, UT.

CONCLUSIONS

- Little data exists on damage in the subsurface due to earthquakes. This paucity of data attests to the lessened effect of earthquakes in the subsurface, because mines exist in areas where strong earthquakes have done extensive surface damage.

- More damage is reported in shallow tunnels near the surface than in deep mines. Data are very sparse below 500 m from the surface.

- In mines and tunnels, large displacements occur primarily along pre-existing faults and fractures or at the surface entrance to these facilities.

- Data indicate vertical structures such as wells and shafts are less susceptible to damage than surface facilities. Even the Alaska earthquake of 1964, which had a magnitude of 8.5 on the Richter scale, damaged few wells in Anchorage except those sheared by landslides.

- Damage tends to decrease with distance from the source and with depth below the ground surface; however, extensive damage can occur if the facility is cut by a fault or fault fissure along which a slip can occur during an earthquake.

- There appears to be a reduction in peak acceleration with depth; however, peak displacements show much less reduction with depth.

- Acceleration and displacement data from nuclear explosions can give close-in upper bound limits for large earthquakes when a facility is very near the epicenter.

REFERENCES

H. R. Pratt, W. A. Hustrulid, and D. E. Stephenson. **Earthquake Damage to Underground Facilities.** Report DP-1513, E. I. du Pont de Nemours & Company, Savannah River Laboratory, Aiken, SC (1978).

A. Rozen. **Response to Rock Tunnels to Earthquake Shaking.** M. S. Thesis, Massachusetts Institute of Technology, Cambridge, MA (1976).

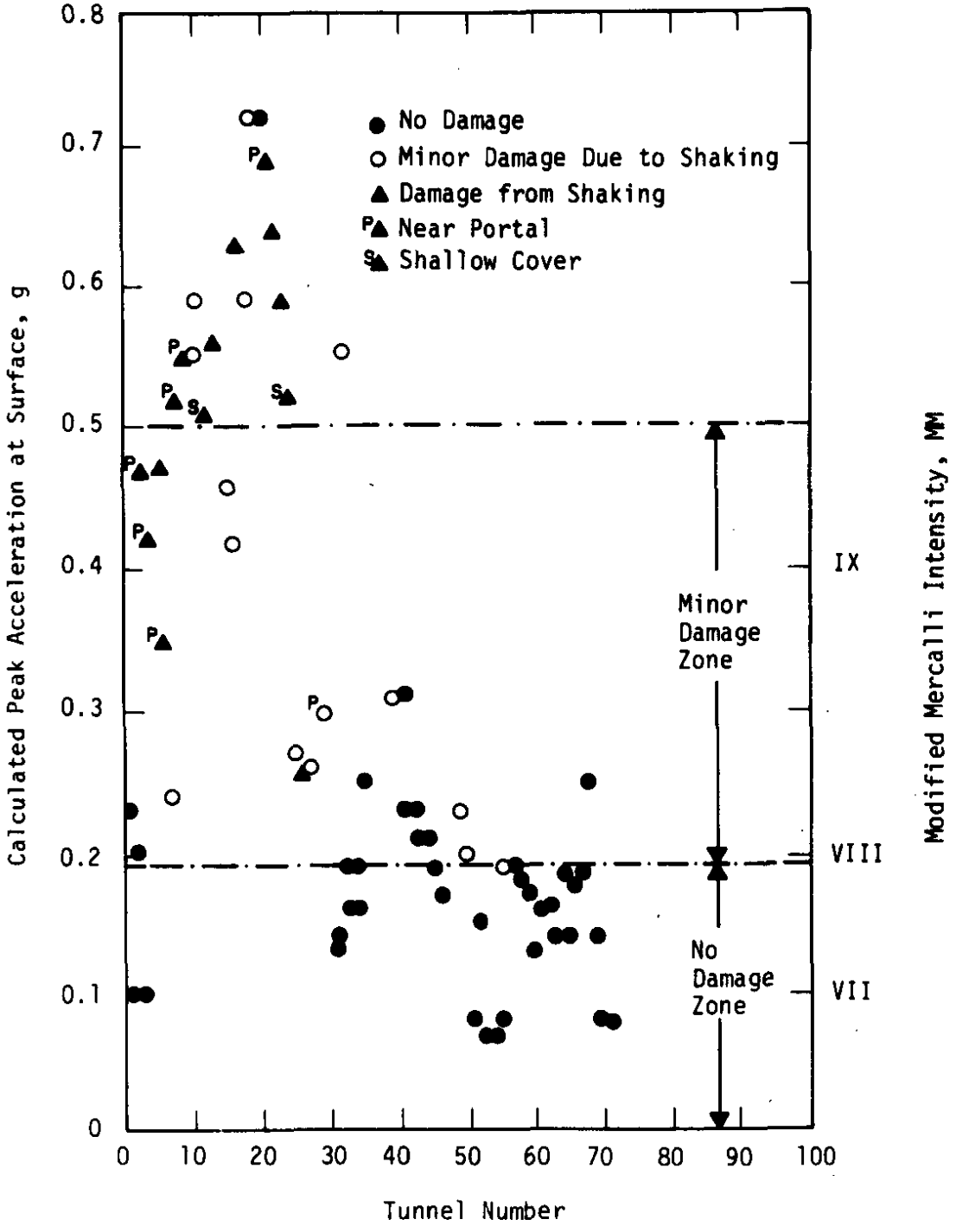

FIGURE 1. Seismic Damage in Tunnels

COMPARISON OF EARTHQUAKE PARAMETERS DERIVED FROM EMPIRICAL RELATIONSHIPS

D. E. Stephenson

A review was made of southeastern seismicity to illustrate the effects of attenuation, recurrence and intensity-acceleration relationships on seismic design. For the attenuation relationships studied, intensity varies by about 25% for a given site. Earthquake recurrence rate varies by a factor of about 2 for the eastern U.S. depending on the data base and the methods of analysis. The largest variation is in the intensity-acceleration relationship, where for a given intensity at a site the acceleration may vary by a factor of about 4. All of these factors will affect the probabilities of occurrence of a specific intensity-acceleration calculated for a site.

BACKGROUND

The owner and operator of certain project developments must prove that there is no undue hazard to the public or the environment, whereas intervenors need only demonstrate that there is a reasonable doubt. When, geology and seismology become points of contention, it is difficult to prove some conclusions beyond a reasonable doubt, even to other geologists and seismologists, since experience and background strongly influence their analysis and none have exactly the same training and experience. Thus, from essentially the same geologic and seismologic data, different results are possible. This study highlights the different results obtainable from the same historical seismic data depending upon the assumptions made and the relationships used.

ATTENUATION

There are numerous attenuation relationships found in the literature. They are of the general form:

$$I_s\ [S,R] = C_1 S + C_2 + C_3\ (R + r_o) + C_4\ \ln\ (R + r_o)$$

where I_s is the intensity at the site of interest and C_1, C_2, C_3, C_4, and r_o are constants, S is the size of the earthquake, in intensity, magnitude or acceleration and R is the epicentral distance. Five commonly used attenuation relationships to determine the site intensity are listed in Table 1.

ACCELERATION-INTENSITY-MAGNITUDE

Since most of the historic data on earthquakes in the eastern U.S. are in terms of intensity, and design is in terms of acceleration at the site, it is necessary to convert intensity to acceleration. Measured accelerations and assigned intensities were first related in the early 1900's. As the number of strong motion seismographs increased in active earthquake zones, empirical correlations of this sort were developed by over 40 investigators. For this study it was decided to give only those that are more common and appear often in the literature. The general form of the equations relating intensity and acceleration is

$$\text{Log}\,\alpha_h = m_1 I_s + m_2$$

where m_1 and m_2 are constants, and α_h is the horizontal acceleration.

By choosing the appropriate intensity level at the site from an attenuation relationship, the corresponding horizontal acceleration can be determined. Various values of acceleration for intensity levels from IV to XMM are presented in Table 2. Table 3 lists the design ground motions for several facilities in the Georgia-South Carolina region.

RECURRENCE

One of the primary uses of seismicity data is to establish the earthquake recurrence rate, for the purpose of deriving risk-associated design information. It has been determined that earthquake recurrence generally follows the relationship:

$$\log N_I = a - bI_e$$

Where N_I is the number of earthquakes occurring in a given time period within the region being investigated with intensity greater than or equal to I_e. In the U.S., the constants a and b vary with the region being investigated.

The effect of the size of the region being investigated and the individual investigator's chosen data base on recurrence relationships are shown in Figure 1.

RISK

As can be seen from the preceding discussions, there are large uncertainties in determining seismic design parameters, and

therefore in any risk assessment, risk values will be dependent upon the parameters chosen for the analysis. To illustrate this, Table 4 shows the results of a risk evaluation in terms of intensity and acceleration for two nuclear power plants in the southeast. The risks were calculated independently by seven experts in the field of seismology using the same basic data. Differences as large as 3 orders of magnitude in the probability of occurrence of earthquakes with intensities VI to IXMM are common.

REFERENCES

S. T. Algermissen and D. M. Perkins. "A Probabilistic Estimate of Maximum Ground Acceleration in the Contiguous United States." **U.S. Geol. Surv. Open-File Rept.** 76-416 (1976).

N. N. Ambraeseys. "The Correlation of Intensity with Ground Motions." **Advancements in Engineering Seismology in Europe,** Trieste, Italy (1974).

G. A. Bollinger. "Reinterpretation of the Intensity Effects of the 1886 Charleston, South Carolina, Earthquake." Geological, Geophysical, and Seismological Studies Related to the Charleston, South Carolina Earthquake of 1886; A Preliminary Report, **U.S. Geol. Surv. Profess. Paper 1028-B,** 17-32 (1977).

H. W. Coulter, H. H. Waldron, and J. F. Devine. "Seismic and Geologic Siting Consideration for Nuclear Facilities." **Proceedings, Fifth World Conference on Earthquake Engineering,** Rome, Paper 302 (1973).

I. N. Gupta and O. W. Nuttli. "Spatial Attenuation of Intensities for Central U.S. Earthquakes." **Bull. Seism. Soc. Am. 66,** 743-751 (1976).

B. Gutenberg and C. F. Richter. "Earthquake Magnitude, Intensity, Energy, and Acceleration (Second Paper)." **Bull. Seism. Soc. Am. 46,** 105-145 (1956).

J. Hershberger. "A Comparison of Earthquake Accelerations with Intensity Ratings." **Bull. Seism. Soc. Am. 46,** 317-320 (1956).

B. F. Howell, Jr. and T. R. Schultz. "Attenuation of Modified Mercalli Intensity with Distance from the Epicenter." **Bull. Seism. Soc. Am. 65,** 651-665 (1975).

E. L. Krinitzsky and F. K. Chang. **State-of-the-Art for Assessing Earthquake Hazards in the United States;** Earthquake Intensity and the Selection of Ground Motions for Seismic Design, Miscellaneous Paper S-73-1, Report 4, U.S. Army Engineer Waterways Experiment Station, Vicksburg, MS (1975).

R. K. McQuire. "Effects of Uncertainty in Seismicity on Estimates of Seismic Hazard for the East Coast of the United States." **Bull. Seis. Soc. Am.** 67 827-848 (1977).

J. R. Murphy and L. J. O'Brien. "The Correlation of Peak Ground Acceleration Amplitude with Seismic Intensity and Other Physical Parameters." **Bull. Seis. Soc. Am.** 67, 877-912 (1977).

F. Neumann. **Earthquake Intensity and Related Ground Motion.** University of Washington Press, Seattle (1954).

D. Okrent. **A Survey of Expert Opinion on Low Probability Earthquakes.** UCLA-ENG-7515, PB 261 864 NTIS,. Springfield, VA (1975).

M. D. Trifunac and A. G. Brady. "On the Correlation of Seismic Intensity Scales with the Peaks of Recorded Strong Ground Motion." **Bull Seism. Soc. Am.** 65, 139-162 (1975).

TABLE 1

Intensity Attenuation with Distance

For Eastern U.S.	
Bollinger (1977)	$I_s(R) = I_e + 3.7 - 0.0052(R) - 2.88 \log R$
McGuire (1977)	$I_s(R) = I_e + 3.1 - 1.34 \ln R$
For Central and Eastern U.S.	
Howell and Schultz (1975)	$I_s(R) = I_e + 3.3 - 0.0029(R) - 0.99 \ln R$
Gupta and Nuttli (1975)	$I_s(R) = I_e + 3.7 - 0.0011(R) - 2.7 \log R$
For California	
Neumann (1954)	$I_s(R) = I_e + 0.15 - 3.17 \log R$

TABLE 2

Horizontal Accelerations as a Function of Intensity Using Eight Relationships

Relationships for Horizontal Acceleration	Ambraseys (1974)	Trifunac & Brady (1975)	Guttenberg & Richter (1942 & 1958)	Hershberger (1956)	Newman (1954) 125 km	Newman (1954) 25 km	Murphy & O'Brien (1973)*	Coulter, Waldron Devine (1973)*	U. S. Army Corps of Engineers (1975 & 1977)† NP	U. S. Army Corps of Engineers (1975 & 1977)† FF	Recorded Charleston, SC November 1974
Intensity											
IV	0.02	0.02	0.01	0.01	0.01	0.02	0.02	0.02		0.07 MR** 0.03 1σ = 0.08	
									1σ = 0.23		
V	0.04	0.03	0.015	0.02	0.01	0.03	0.03	0.03	2σ = 0.40 MR = 0.03 1σ = 0.39	2σ = 0.13 MR = 0.12 1σ = 0.1	
VI	0.10	0.06	0.03	0.05	0.03	0.06	0.06	0.07	2σ = 0.67 MR = 0.42 1σ = 0.45	2σ = 0.15 MR = 0.18 1σ = 0.17	0.01
VII	0.23	0.13	0.07	0.13	0.05	0.13	0.10	0.16	2σ = 0.73 MR = 0.50 1σ = 0.33	2σ = 0.21 MR - 0.24	
VIII	0.54	0.26	0.15	0.35	0.11	0.27	0.18	0.32	2σ = 0.46 MR = 0.28	MR - 0.24	
IX	1.23	0.53	0.32	0.93	0.22	0.54	0.32	0.73			
X	2.80	1.05	0.69	2.5	0.46	1.12	0.57	1.22	MR = 1.24		

* Values taken from curve as mean for average foundation conditions.

** MR maximum recorded data.

† Mean values are like Trifunae and Brady's since data base was the same. Different at high intensity because of separation into near field (NF) and far field (FF). 1σ and 2σ is standard deviations.

TABLE 3

Design Ground Motion for Facilities in Georgia and South Carolina

Facility	Location	Peak Horizontal Acceleration (g)
Nuclear		
SRP	Aiken, SC	0.2
AGNS	Barnwell, SC	0.2
A. W. Vogtle	McBean, GA	0.2
E. I. Hatch	Baxley, GA	0.15
V. C. Summer	Parr, SC	0.15 rock
Oconee	Oconee, SC	0.10
Catawba	Rock Hill, SC	0.15
Westinghouse Fuel Fabrication	Anderson, SC	0.14
Robinson	Hartsville, SC	0.20
VA Hospitals	Atlanta, GA	0.13
	Augusta, GA	0.18
	Charleston, SC	0.25
	Columbia, SC	0.10
Dams		
R. B. Russell	GA-SC Border	0.4 - 0.5
Clark Hill	GA-SC Border	Unknown
Hartwell	GA-SC Border	Unknown

TABLE 4

Probabilities Calculated by Seven Experts for Two Nuclear Facilities in the Southeast

SUMMER (South Carolina) Piedmont

Respondent No.	1	2	3	4	5	6	7
	Probability per Year*						
MM Intensity							
V	10^{-2}		10^{-2}	10^{-1}			10^{-2}
VI	10^{-4}		10^{-3}	3×10^{-2}	3×10^{-3}		10^{-2}
VII	3×10^{-6}		10^{-4}	5×10^{-3}	10^{-3}		10^{-3}
VIII	5×10^{-7}		10^{-6}	5×10^{-3}	10^{-4}	10^{-6}	10^{-4}
IX	10^{-7}			5×10^{-9}	10^{-6}		10^{-7}
X	10^{-8}						10^{-8}
XI	10^{-8}						$<10^{-8}$
XII	10^{-5}						$<10^{-8}$
Peak Horizontal Acceleration (g)							
0.05	10^{-1}		10^{-3}	2×10^{-2}	3×10^{-3}		10^{-2}
0.1	10^{-2}		10^{-6}	4×10^{-3}			10^{-3}
0.13	10^{-3}			10^{-3}	10^{-3}		10^{-3}
0.2	10^{-4}	3×10^{-3}		4×10^{-4}			10^{-4}
0.25	10^{-5}			10^{-4}	10^{-4}	10^{-6}	10^{-4}
0.3	3×10^{-6}			4×10^{-5}			10^{-4}
0.4	4×10^{-7}	2×10^{-5}		8×10^{-7}	10^{-3}		10^{-5}
0.5	10^{-7}				10^{-6}		10^{-6}
0.6	3×10^{-3}	1×10^{-5}					10^{-3}
0.8	10^{-3}	7×10^{-6}					$<10^{-3}$
1.0	10^{-8}	3×10^{-6}					$<10^{-3}$
>1.1	10^{-8}						$<10^{-8}$
Dominant Frequency and Duration for 10^{-6}/year Earthquakes							
Cycles/sec	3	3	5-9	2-5		1/3-15	
Seconds	10		10-15	15		15-20	

* Probabilities per year are accelerations greater than the size indicated.

TABLE 4, Contd

BRUNSWICK (North Carolina) Coastal Plain

Respondent No.	1	2	3	4	5	6	7
	Probability per Year*						
MM Intensity							
V	10^{-2}		10^{-2}	7×10^{-2}			10^{-2}
VI	10^{-2}		10^{-4}	10^{-3}	5×10^{-3}		10^{-3}
VII	10^{-3}		10^{-6}	5×10^{-7}	3×10^{-3}		10^{-3}
VIII	10^{-3}				10^{-3}	10^{-6}	10^{-6}
IX	10^{-7}				10^{-4}		10^{-7}
X	10^{-8}				10^{-5}		10^{-8}
XI	10^{-8}				10^{-6}		$<10^{-8}$
XII	10^{-8}						$<10^{-8}$
Peak Horizontal Acceleration (g)							
0.05	10^{-2}		10^{-4}	8×10^{-3}			10^{-2}
0.1	10^{-3}		10^{-3}	2×10^{-3}			10^{-3}
0.15	10^{-4}		10^{-6}	3×10^{-4}			10^{-5}
0.2	10^{-5}	$<3 \times 10^{-3}$		6×10^{-3}	2×10^{-3}	10^{-6}	10^{-5}
0.25	3×10^{-6}			6×10^{-6}	10^{-3}		10^{-6}
0.3	10^{-6}			8×10^{-7}	5×10^{-4}		10^{-6}
0.4	4×10^{-7}	$<2 \times 10^{-5}$					10^{-7}
0.5	10^{-7}				10^{-4}		10^{-7}
0.6	3×10^{-3}	$<10^{-5}$					10^{-7}
0.8	10^{-8}	7×10^{-6}					$<10^{-7}$
1.0	10^{-8}	$<3 \times 10^{-6}$			10^{-5}		$<10^{-8}$
>1.1	10^{-8}				10^{-6}		$<10^{-8}$

Dominant Frequency and Duration for 10^{-6}/year Earthquakes				
Cycles/sec	2	1-2	2-5	1/3-10
Seconds	10	3	15	20

* Probabilities per year are accelerations greater than the size indicated.

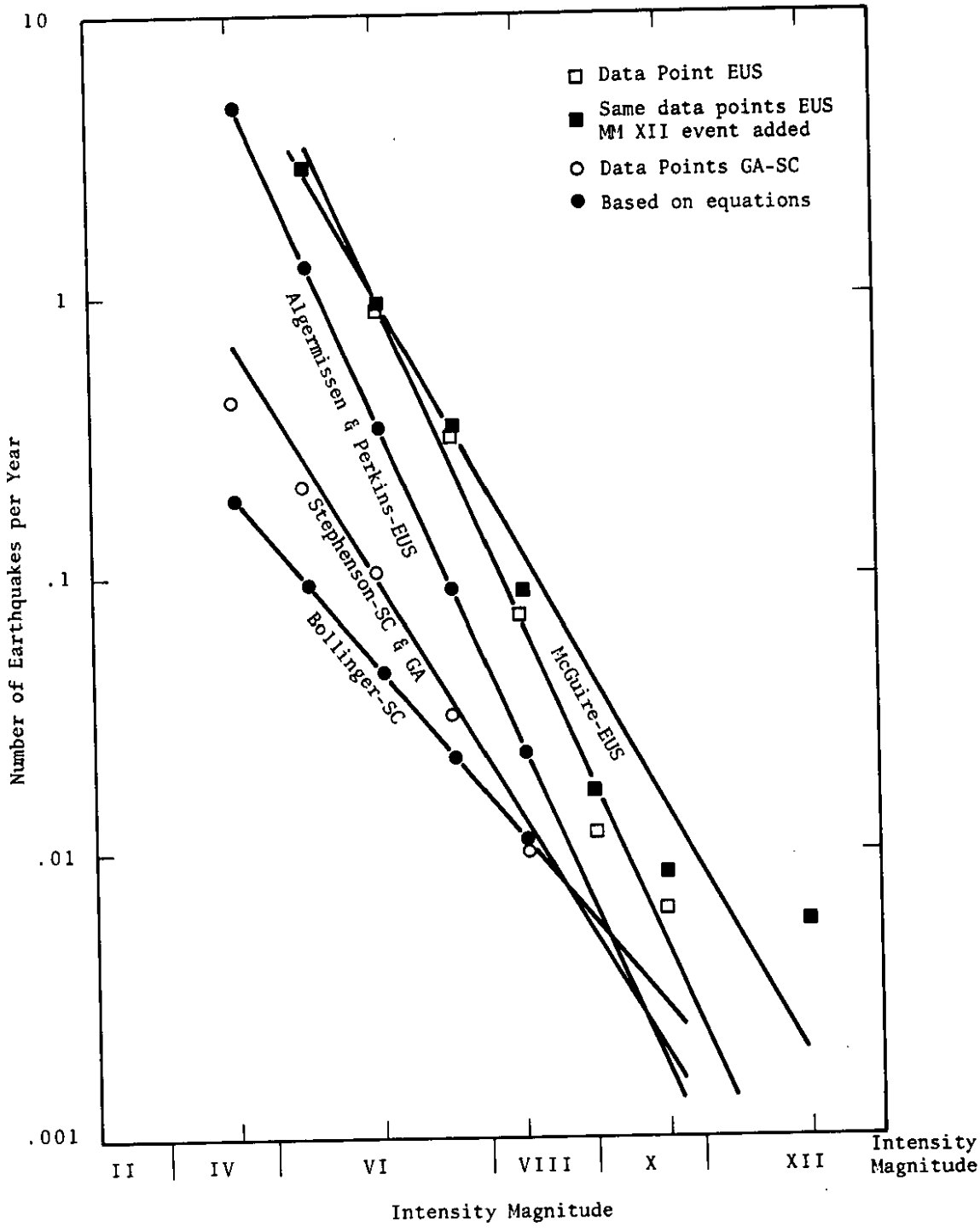

FIGURE 1. Comparison of Selected Recurrence Curves for the Eastern and Southeastern U.S.